Investigations on Particle Dynamics
in a High Intensity Heavy Ion Linac for Inertial Fusion

Dissertation
zur Erlangung des Doktorgrades
der Naturwissenschaften

vorgelegt beim Fachbereich Physik
der Johann Wolfgang Goethe−Universität
in Frankfurt am Main

von
Giovanni Parisi
aus Genua

Frankfurt am Main 1999
DF1

dem Fachbereich Physik der

Johann Wolfgang Goethe−Universität als Dissertation vorgelegt.

Dekan: Prof. Dr. Reinhard Stock

Gutachter: Prof. Dr. Horst Klein

                                    Prof. Dr. Alvin Schempp

Datum der Disputation: November 1999

ZUSAMMENFASSUNG

Die Physik intensiver Ionenstrahlen wird zur Zeit für verschiedene neue Hochstrom- und Hochenergie-Beschleunigeranlagen untersucht. Ein kritischer Punkt ist dabei die Minimierung der Strahlverluste, um die Aktivierung der Beschleunigerstruktur zu verhindern und die Wartung zu ermöglichen. Deshalb müssen sorgfältige Untersuchungen ausgeführt werden, um das Verhalten des Ionenstrahls zu verstehen sowie seine Eigenschaften zu kontrollieren; insbesondere sind das Emittanzwachstum und die Filamentierung zu reduzieren und die Halobildung zu vermeiden. Die internationale HIDIF-Studiengruppe (Heavy Ion Driven Ignition Facility) nahm 1994 unter der Federführung der GSI die Untersuchungen zur Machbarkeit einer Schwerionen-Beschleunigeranlage zur Inertiale Fusion wieder auf, nachdem neue zuverlässigere Daten über Zündung und Abbrennen eines indirekt getriebenen DT-Pellets vorlagen. Es wurde der Entwurf einer Anlage bestehend aus HF-Linacs, Speicherringen und Induktionslinacs zur Erzeugung von Strahlen hoher Intensität, hoher Energie und einer vorgegebenen Zeitstruktur erarbeitet.

Der wesentliche Inhalt der Dissertation befaßt sich mit einem HF-Hauptbeschleuniger (DTL) vom Alvarez-Typ, der einen Strahl von hoher Qualität (niedriges Emittanzwachstum bei hoher Transmission) liefern muß. Das Strahlverhalten im DTL wurde durch numerische Vielteilchen-Strahldynamik-Berechnungen erstmals umfassend untersucht, um sicher zu stellen, daß die HIDIF-Projektanforderungen an die Teilchendynamik erfüllt werden können.

Die Untersuchungen befassen sich mit der Wahl der passenden Beschleuniger-Parameter: ein Strom von 400 mA einfach geladener ^{209}Bi$^+$ Ionen (der aus mehreren Quellen gebildet werden) muß stabil beschleunigt und fokussiert werden, hieraus ergab sich eine Frequenz von 200 MHz, ein 5F5D-Fokussierschema und eine Anfangsenergie von 10 MeV/Ion. Bei einer vorgegebenen Endenergie von 50 MeV/Ion ist bei einer konventionell angenommen beschleunigenden elektrischen Feldstärke von 3 MV/m der Linac 3 km lang. Der Strahl wird dann in einer Transportstrecke "debuncht" und in mehrere Speicherringe eingeschossen, in Induktionlinacs zeitlich komprimiert ("bunching") und mit 500 TW Spitzenleistung auf ein Target transportiert.

Im fehlerfreien Fall ist das Emittanzwachstum des Strahls während der Beschleunigung klein, und es entsteht fast kein Halo. Dadurch können die Eingangsemittanzen ("Waterbag"-Verteilungen) so gewählt werden, daß sie in der Nähe der erlaubten maximalen Ausgangsemittanzen liegen, die von den Forderungen für eine verlustarme Ringinjektion ($\beta\gamma\varepsilon_{full} = 1.26\,\pi$ mm mrad, $dp/p < 10^{-4}$) bestimmt werden. Hierdurch kann das maximal erlaubte Emittanzwachstum zwischen den Ionenquellen und dem DTL im Injektor mit 4 Funnelschritten auf etwa einen Faktor 8 vergrößert werden, unter Annahme einer geringen Filamentierung des belegten Phasenraumvolumens. Im Vergleich zu Protonen hilft die hohe Masse der Ionen dabei, die Raumladungseffekte zu vermindern: Das Strahlverhalten ist nicht raumladungsdominiert, was sich als ein großer Vorteil für das Emittanzwachstum und

die Halobildung erweist. Trotzdem zeigen die Werte der "Tune depression", daß die Raumladung nicht vernachlässigt werden darf.

Zur Überprüfung der Stabilität des Strahls werden die Auswirkungen von statistischen Fehlern und Eingangsfehlanpassungen untersucht. Für das elektrische HF-Feld wurden Fehler von ±1% für die Amplitude und ±1° für die Phase verwendet; das Strahlverhalten entlang des Linacs ist trotzdem sehr stabil. Es werden kleine Schwankungen eines gut eingeschlossenen Bunches um seine Solllage herum beobachtet. Obwohl ein phasen- oder energieverschobener Bunch eine größere Fläche in der longitudinalen Ebene am Linac-Ausgang belegt, spielt das für die Ringinjektion nur eine kleine Rolle, da die nachfolgende Transportstrecke diesen Effekt vermindert. Ein größeres Problem stellt die Justierung der Quadrupole in den Driftröhren und die Stabilität ihrer Felder dar: Wegen ihrer großen Zahl sollen die Gradientenfehler den kleinen Wert von ±0,2% nicht überschreiten. Dies ist ein wichtiges, nicht erwartetes Resultat. Kann ein solcher kleiner Fehler nicht erreicht werden und wird ein konventioneller Wert von ±1% angenommen, muß versucht werden, den Strahl an einigen Positionen entlang des Linacs erneut anzupassen. Da eine realistische Ausgangsemittanz des Injektorteils nicht vorlag, wurden verschiedene Eingangsemittanzen und Verteilungen (mit verschiedenen Verhältnis von Gesamt-zu-rms-Emittanz) für die Rechnungen angenommen: Die Effekte sind unbedeutend, solange der Strahl angepaßt ist. Der Einfluß von Stromschwankungen um ±10% auf die Teilchendynamik ist ebenfalls unkritisch.

Für einen fehlangepaßten Strahl konnte wegen der kleinen Beschleunigungsrate ein Modell für einen periodischen Fokussierungskanal angewandt werden: Die 3 vorhergesagten Eigenmoden wurden gut identifiziert. Das Strahlverhalten ändert sich für eine Fehlanpassung von 20% nur gering; ein höheres Emittanzwachstum und gelegentliche Halobildung werden insbesondere in der longitudinalen Ebene festgestellt. Deshalb soll die Eingangsfehlanpassung ±10% für jeden Eigenmode für die hier angenommene Emittanz nicht überschreiten, sonst sind kleinere rms-Emittanzen am Linac-Eingang (und aufwärts im "Funnel"-Teil) nötig, um ein größeres Wachstum zu erlauben. Eine anfängliche 3 mm-Verschiebung von der Strahlachse weg führt zu stabilen Schwankungen um die Achse herum, wobei der Strahl gut eingeschlossen bleibt. Da der verschobene Bunch eine größere Fläche in der transversalen Ebene am Linac-Ausgang belegt, müssen diese Fehler korrigiert oder kleinere angenommen werden. Im fehlerfreien Fall füllt der Strahlradius etwa die Hälfte der freien 16 mm-Öffnung; für die obengenannten Fehler liegt das äußerste Makroteilchen nie weiter als 12 mm von der Achse entfernt.

Um die Einschränkungen bei der Strahlkomprimierung durch Liouvillesche Satz zu verringern, ist der Einsatz von zwei weiteren Ionensorten mit etwa ±10%-Masse-unterschied (z. B. ^{187}Re$^+$ und ^{232}Th$^+$) und verschiedenen Geschwindigkeiten geplant: Sie überlagern sich auf dem Pellet ohne Emittanzwachstum ("Telescoping"). Es wurde durch Simulationen untersucht, welche Veränderungen an Geometrie und Feldern für das "Telescoping" notwendig werden. Ein wichtiges Resultat ist es, daß diese Option jedoch zu großen technischen Problemen und schlechtem Strahlverhalten führt, selbst wenn man zur kleineren Masseunterschied (±5%) geht. Diese Betriebsart einer HIDIF-Anlage scheint daher für den hier untersuchten DTL nicht möglich zu sein.

Um die Impulsunschärfe des Strahls für eine verlustfreie Ringinjektion zu verringern, ist eine kurze (170 m) Strahltransportstrecke zwischen dem DTL und den Ringen nötig, wobei der Strahl "debuncht" und in der longitudinalen Ebene gedreht wird. Die analytischen Berechnungen und Strahldynamik-Simulationen beweisen, daß auch mit allen angenommen Fehlern die Teilchen innerhalb der geforderten Impulsunschärfe $dp/p < 10^{-4}$
für die Ringinjektion liegen.

Teilchendynamik-Simulationen (inklusive der Raumsladungseffekte) zeigen, daß ein konventioneller DTL vom Alvarez-Typ eine gute Lösung darstellt; der technische Aufbau des Linacs ist jedoch z. B. wegen seiner großen Länge und der zahlreichen Driftröhren noch offen. Die Berechnungen wurden wegen der begrenzten verfügbaren Computerleistung mit höchstens 20.000 Makroteilchen durchgeführt. In jedem Fall (auch für kombinierte Wirkungen von verschiedenen Fehlern) wurde kein Makroteilchen verloren, d. h. Strahlverluste $< 5 \times 10^{-5}$ wurden erreicht. Für eine Zündanlage (niedriger "Duty-cycle") sind diese Ergebnisse eine zuverlässige Richtlinie für einen Hochstrom-DTL: Die Höhe des notwendigen elektrischen HF-Felds und des magnetischen Feldes der Quadrupole sind Stand der Technik, und die Shuntimpedanz ist hoch genug, um eine gute Linac-Effizienz zu erlauben.

Für eine Anlage mit hoher Einschaltdauer, wie z. B. für die Energieproduktion erforderlich, müssen höhere Sicherheitsmargen eingebaut und Rechnungen mit $10^7 \div 10^8$ Teilchen durchgeführt werden, um die erlaubten Verluste von 10^{-7}/m sicher abschätzen zu können. Aufgrund der hier erzielten Ergebnisse erscheint dies jedoch ohne größe Änderungen an der Auslegung des Linearbeschleunigers erreichbar zu sein.

CONTENTS

CHAPTER 1

INTRODUCTION

A strong interest is currently going on in the physics of high intensity and high energy beams: intense <u>proton</u> or <u>deuteron</u> beams are required in various fields of science and industry, including sources of neutrons for research experiments and material processing, nuclear physics experiments, tritium production and nuclear waste transmutation. High current <u>heavy ion beams</u> are envisaged for power production facilities (inertial fusion).

Several projects presently under study are based on rf linacs as driver, sometimes followed by accumulation and/or compressor rings [Acc98]. The critical issue for all of them is to be operated in a low loss regime, because of activation problems in the structure. For this reason careful investigations have to be performed in order to understand and control the beam behaviour, aiming at conserving the beam quality, reducing the emittance growth and filamentation and avoiding the formation of halo. The beam current to be accelerated is actually limited by the amount of beam losses, which depends upon the beam halo: in order to reduce induced radioactivity and to allow for hands-on maintenance, normally losses <1 W/m are considered as acceptable [Sto96].

One of the major facilities under study is the European Spallation Source (**ESS**), a project based on a $\underline{H^=}$ linac accelerating a 107 mA peak current beam (360 ns pulse in the DTL) and on two compressor rings, producing 5 MW average beam power [ESS]. Also the USA are developing a proposal for a Spallation Neutron Source (**SNS**), providing a short pulse $\underline{H^=}$ beam with average power of 1÷2 MW; a 30 mA linac is required [SNS]. The Accelerator for Production of Tritium (**APT**), studied at Los Alamos, requires a 100 mA <u>proton</u> beam current (cw) to produce a power of 130÷170 MW [APT]. A similar but smaller accelerator (40 mA, 40 MW beam power) would serve as driver for the Accelerator Driven Transmutation of Waste (**ADTW**) system [ATW]. The accelerator system for the International Fusion Material Irradiation Facility

(**IFMIF**) will test the behaviour of materials to be used for magnetic fusion (e.g. ITER); it consists of two 125 mA deuteron beams in parallel, to generate a fusion-like neutron spectrum with 10 MW cw [IFM].

In the field of heavy ions, for about 20 years scientists have been working on inertial confinement fusion, as an alternative to magnetic confinement one, to find a practical and cleaner method for producing energy. Nuclear fusion occurs when the nuclei of lighter elements (in a state of matter called "plasma") merge to form heavier elements; the extremely high temperatures and densities needed to get the nuclei to collide in the proper way and release big amounts of energy are obtained in a small "pellet" of fusion fuel, which receives energy from laser or ion beams, implodes and its inertia compresses it hard enough to hold together the plasma until it reaches ignition. Both laser and accelerator facilities have been investigated as drivers, since a demonstration of ignition at low gains is more easily accessible by lasers, whereas the intrinsic properties of accelerators −efficiency and repetition rate− will be essential for a medium-gain power plant.

One study for a fusion power system driven by heavy ion beams (**HIBALL**) was completed in Europe already in 1982 [Bad81]. When the USA declassified essential information on pellet design, "indirect drive" targets have been considered openly, where the pellet is hit by X-rays generated from laser or ion beams rather than directly from the beams. Main progress has been achieved during the latest years in the understanding of pellet dynamics after ignition, i.e. in plasma physics [Sym1][Sym2][Sym3][Bas97][Lut97], imposing also new requirements on the layout of the driver accelerator facilities.

In 1994-95 Frankfurt University and several other European laboratories (leaded by GSI) started a new collaboration called **HIDIF** (Heavy Ion Driven Ignition Facility) in order to simplify the accelerator plant design owing to the new technique of indirectly driven targets and to some technological improvements. First studies were oriented towards the conceptual goal of a facility providing just enough beam energy for the ignition of fusion reactions at very low gain (a "proof of principle") [Hof98]. In a recent phase of the study, it was realized that the proposed concept would make this scheme a more appropriate choice for energy production rather than for ignition; the acronym

HIDIF was therefore intended as Heavy Ion Driven <u>Inertial Fusion</u>, and the parameters are going to be modified accordingly [Hof96][Hof97][Hof98].

The scenario presently discussed by this group proposes the formation and acceleration of an intense beam (400 mA) of singly charged heavy ions of three different atomic species, with mass differences of about 10% (the reference one is $^{209}Bi^+$) in a main rf linac; they are then injected into some storage rings at an energy of 50 MeV/u, bunched in induction linacs and finally transported to a target with different velocities in such a way that the three species merge on the pellet ("telescoping") at 500 TW peak power.

In this thesis the main linac of the HIDIF proposal is extensively investigated as an example of a high intensity heavy ion linac. Results are presented from numerical simulations of multi-particle beam dynamics carried out for the first time in this context.

After a short presentation of the HIDIF reference scenario (<u>Ignition Facility</u>), including a discussion of the motivations for a high current heavy ion linac, some elements of the theory of beam transport and acceleration are recalled [Con91][Hof82][Kap85] [Lap87][Law88][Mit78][Rei94][Str83]. Then the used simulation programs are described, and a particle dynamics layout of a conventional 200 MHz Alvarez DTL is discussed with respect to low emittance growth at high transmission, including large space-charge effects, taking into account the influence of different kinds of statistical errors and of input mismatch on the beam dynamics. The modifications needed for "telescoping" are investigated with simulations for the nominal mass difference (10%) and for a smaller one (5%); finally the transfer line between DTL and rings is discussed and studied both analytically and by numerical calculations.

The large mass number (A= 209) helps to reduce the space-charge effects with respect to protons, therefore the behaviour of the beam is not space-charge dominated. Nevertheless the tune depression values (similar to those of the ESS linac e.g.) indicate that these effects cannot be neglected.

For a linac with low duty cycle, as in the case of an ignition facility, the results from particle dynamics calculations can be considered as a reliable guideline for the DTL

layout, since they indicate that such a high intensity linac can fulfill the requirements on smooth beam behaviour and low losses.

CHAPTER 2
HIDIF REFERENCE SCENARIO

A combination of rf linacs and storage rings has been proposed by the HIDIF study group as an approach of a driver for a Heavy Ion Driven Ignition Facility [Hof97]. This driver should provide the acceleration of an intense beam of single-charged heavy ions, of three different atomic species, up to a final energy of about **10 GeV**.

The mostly discussed fuel for nuclear fusion is a mixture of deuterium and tritium, which is contained in a small spherical capsule (1.2 mm radius). This D-T "pellet" is not directly hit by the heavy ions, but it is put inside a casing: the beam particles are stopped by two converters and generate thermal X-rays which fill this "hohlraum" and drive the implosion of the pellet [Ram97]. The concept of indirectly driven targets has been chosen since it appears nearly impossible to achieve the required high symmetry of irradiation with heavy ion beams in the case of direct drive.

For an ignition driver based on such a two-converter target, it has been agreed that a beam energy of **3 MJ** must be brought to the converters within a pulse length of **6 ns**, focused to spot sizes of about **1.7 mm** radius.

The requirement of 3 MJ beam energy and 6 ns pulse length corresponds to an average pulse power of **500 TW**, then a total current of **50 kA** is needed for a 10 GeV beam.

Since the capability of high current acceleration in a rf linac is limited (by space-charge at the low energy end), an array of rings and bunch compressors will be needed for the necessary current multiplication and pulse compression for the final focus. Consequently, several beams from different ion sources have to be accelerated and merged together in a funnel tree [Bon81] at the low energy front-end. The schematic layout of this facility is shown in Figure 2.1.

By tracking back the parameters needed at the final focus, some limits are determined on the required beam size and emittances at the linac output.
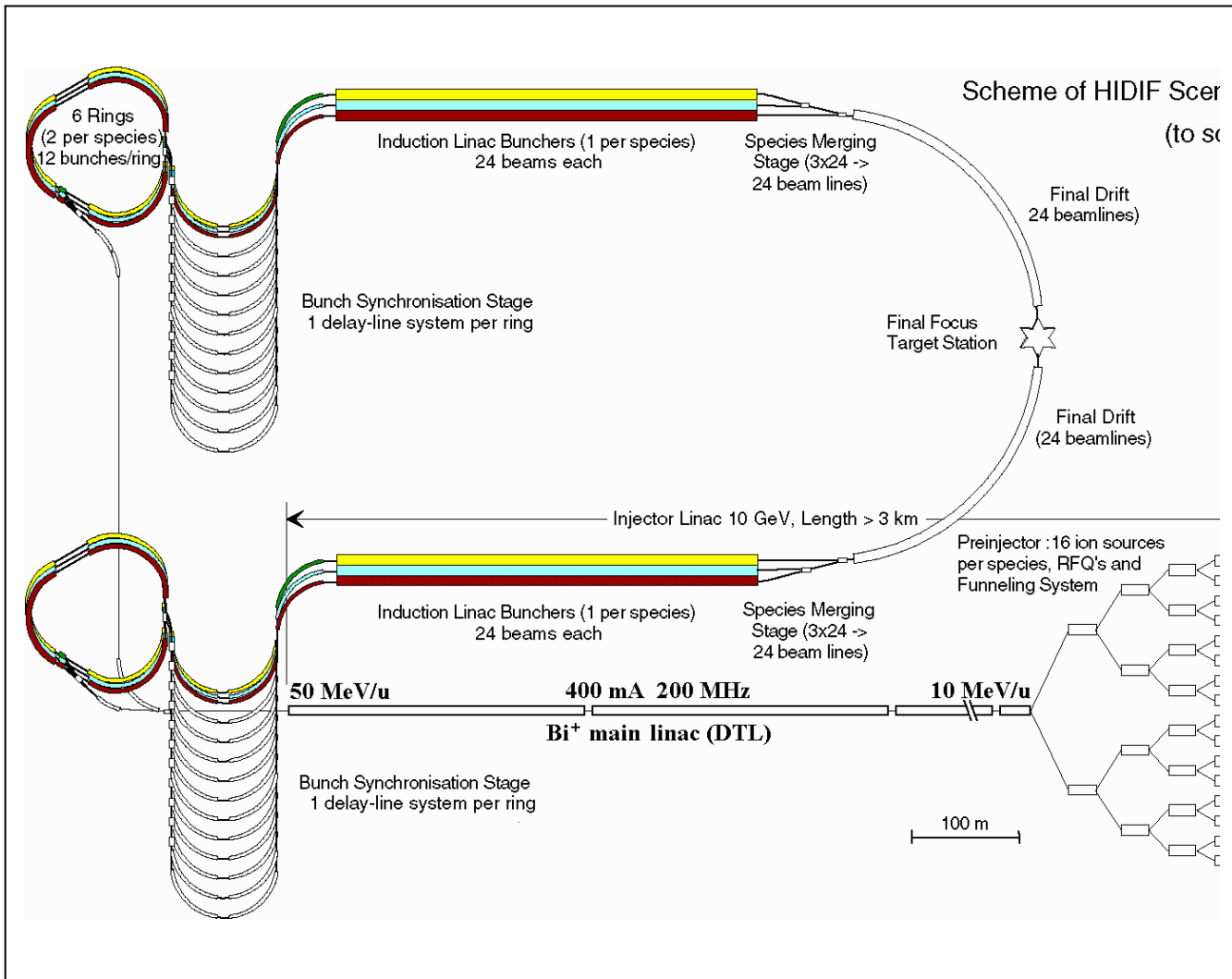
Figure 2.1: Full scenario of the heavy ion driven ignition facility (adapted from [Hof98]).

Final focus and target

The reference parameters required for pellet ignition are: a total current of 50 kA for a 10 GeV beam. Such a formidable amount of current will be transported ballistically to the target through 48 final beam lines in high vacuum: 4 bundles of 6 beam lines are focused on each converter using a 2×3 lens matrix. The focusing of the individual beamlets has been optimized using superconducting quadrupole lenses; it was found that the beam emittance for the allowed momentum spread ($dp/p = 1\%$) at the final lenses is limited to 50 π mm mrad in order to keep aberrations acceptably small at the 1.7 mm focal radius.

Along each beam line, three bunches of different species will be transported (144 bunches in total). The reference species is ^{209}Bi, with the lowest charge state 1+ in order

to reduce the space-charge repulsion. In the present scheme, a mass difference $\Delta m/m \approx \pm 10\%$ is required for the other two species, which would correspond to the ions ^{187}Re$^+$, and ^{232}Th$^+$. They will be accelerated to the same momentum to allow for "telescoping" of the different bunches in the final transport lines, aiming to reduce the space-charge effects until they merge. Telescoping is a non-Liouvillean method: bunches with different ion species but same momentum are started with an appropriate delay time in a single beam line; the delay time and the velocity difference have to be chosen in such a way that the bunches fully overlap in real and momentum space only in the very last part of the final transport, i.e. just when hitting the pellet [Oef97].

Storage rings and induction linac

The necessary current multiplication and bunch compression is achieved through a set of 12 storage rings (4 per species), and some induction linacs. Each ring is filled during a 20-turn injection with a 3 μs long pulse, coming from the main linac. The linac pulse structure is illustrated in Figure 2.2.

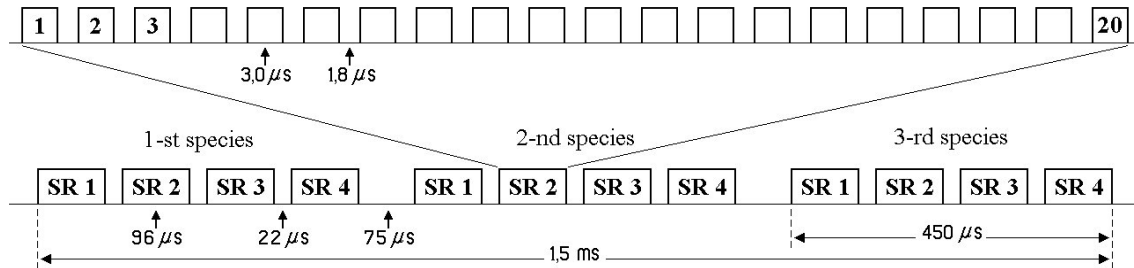Figure 2.2: Scheme of the linac pulse structure.

First of all, in the funnelling section, the beam has to be "chopped" into pulses 3 μs long, leaving a 1.8 μs space between them (62.5% bunching factor). Twenty such pulses fill one ring in successive turns during 96 μs; then a 22 μs pause allows for switching to the next storage ring. Three other rings are filled with the same ion species. When all

6

the four storage rings are full (after 450 μs), the ion species is changed during a 75 μs pause and the procedure is repeated. The filling of all the 12 rings requires then 1.5 ms. As a result, the average linac current is reduced to 48% of its peak value (20 pulses $\times$ 12 rings $\times$ 3 μs = 0.72 ms of beam during a 1.5 ms long macropulse).

A simultaneous two-plane multi-turn injection into the storage rings is chosen to optimize septum losses. The injected beam, coming from the main linac, is captured into rf "barrier buckets" which allow to form 12 bunches starting from the coasting beam; they are then compressed from the initial length of 250 ns (i.e. 3 μs / 12) to a length of 120 ns (adiabatic prebunching).

The 12 bunches of each ring are extracted and transported through a delay line system in such a way to synchronize them (each bunch will travel along a separate transport line with a different length); all the 144 bunches from the 12 rings will arrive therefore simultaneously at the input of the 6 induction linacs (each one housing 24 beams).

These linacs provide a fast bunch rotation along 440 m; the final drift to the target must be 330 m long in order to complete the quarter synchrotron rotation which reduces the pulse length to about 6 ns. The number of final beam lines is 48 (24 per converter).

Since each of the 144 bunches is compressed by a factor 250/6 and transports 20 times the peak linac current, a total current multiplication factor of 144 $\times$ 20 $\times$ 250/6 = 120,000 is obtained; for this reason, the peak beam current envisaged for the main linac is 400 mA. This corresponds to a circulating current of 8 A in the rings, of 17 A for each extracted bunch and of 340 A after final compression (which for 144 bunches gives the required 50 kA on the target).

Injector linac and funnel tree

In order to get a peak current of 400 mA in the main linac (the average current being 192 mA), a total number of 48 ion sources is assumed (16 $\times$ 3 species), each one producing 35 mA current with an extraction voltage of 50 kV, that corresponds to a kinetic energy of 0.24 keV/u for the reference Bi$^+$ species. With a dc post-acceleration of 250$\div$ 300 kV after extraction, the energy can be increased to about 1.2$\div$1.5 keV/u.

The low energy beams are transported from each source to the first accelerator using a magnetic LEBT with space-charge compensation. The estimated transmission is larger than 80% (28 mA) and the emittance growth smaller than 40% [Poz98].

The first accelerating structure is a low frequency RFQ, which can capture, focus and bunch the beam even at high space-charge forces. It operates at 12.5 MHz and accelerates the 28 mA beam to 60 keV/u, delivering a current of 25 mA (90% transmission). The total number of required RFQs is 16 [Sch97].

Two beams can then be merged provided that their energy is high enough to inject them into the following structure by doubling the frequency. In such a "funnelling" step, the beam current is therefore doubled as well as the frequency. The first funnelling stage merges two 25 mA beams into a 50 mA beam by increasing the frequency to 25 MHz.

The next accelerating structures can be RFQs, then Wideröe or IH linacs and finally Drift Tube Linacs; their frequency is doubled at each step (25, 50 and 100 MHz) as well as the transported current (50, 100 and 200 mA), as soon as the proper output energy is reached (0.2, 2 and 10 MeV/u). No more particles will be lost in these structures [Sch98].

The last accelerating structure is the main Drift Tube Linac which is discussed in detail in this thesis; it is about 3.4 km long and has a frequency of 200 MHz; it accelerates the 400 mA Bi^+ beam to its final energy of 50 MeV/u.

The basic parameters of driver emittances and momentum spread can be derived largely from the final focusing requirements, once the general layout of the driver is determined. At the end of the main linac, after bunch rotation, the requirements for tolerable losses ($< 3\%$) at ring injection are: a maximum total transverse emittance of $4\,\pi$ mm mrad (i.e. $1.26\,\pi$ mm mrad, norm.) and a maximum longitudinal momentum spread of $\pm 2 \times 10^{-4}$ for 99% of the particles.

In all the funnelling process losses will be avoided by having short enough bunches. A more severe problem is that the transverse emittance of the beam is assumed to be increased by not more than a factor of seven, from 0.15 to $1.05\,\pi$ mm mrad (full norm.), which is the nominal input for the main linac. On the other hand the values measured so far in Frankfurt at the ion source with a 7-hole extraction system are: $0.21\,\pi$ mm mrad (80% norm.) for a current of 10 mA and $0.27\,\pi$ mm mrad for 21 mA; no measurements

up to now were made for the maximum current of 38.5 mA (expected: 0.33 π mm mrad) [Web97].

A more detailed description of the HIDIF scenario, as well as an exhaustive list of all the parameters, can be found in [Hof98].

CHAPTER 3

BASICS OF BEAM TRANSPORT AND ACCELERATION

3.1 Definitions and main equations

A beam of charged particles can be conveniently represented by means of a distribution function f of the charge in six-dimensional phase space $x\, p_x\, y\, p_y\, z\, p_z$.

Owing to the Coulomb repulsion between particles, there are defocusing forces inside the beam, which depend on the spatial density distribution itself ("space-charge" forces). The motion of the set of particles, depending on some external forces and on space-charge forces, can be described as that of a set of points in 6-dim phase space: $f = f(x\, p_x\, y\, p_y\, z\, p_z\, t)$.

When only the particle trajectories are of interest ("transverse dynamics"), and the angles between these trajectories and the axis are small ("paraxial approximation"), then the transverse momenta can be divided by the longitudinal one and the $x\, x'\, y\, y'$ space can be used, with $x' = p_x/p_z$ and $y' = p_y/p_z$.

The motion of the centre of mass of the beam is described by the first moments $\langle x \rangle$, $\langle x' \rangle$, $\langle y \rangle$, $\langle y' \rangle$ of the particle distribution $f(x, x', y, y')$, which are defined statistically as:

$$\langle x \rangle = \iiiint x f(x, x', y, y')\, dx\, dx'\, dy\, dy' \qquad (f \text{ normalized to 1})$$

and similarly for the other three.

Other important information is contained in the second moments $\langle x^2 \rangle$, $\langle xx' \rangle$, $\langle xy \rangle$, $\langle xy' \rangle$, $\langle x'^2 \rangle$, $\langle x'y \rangle$, $\langle x'y' \rangle$, $\langle y^2 \rangle$, $\langle yy' \rangle$, $\langle y'^2 \rangle$ of the particle distribution, which are defined statistically in a similar way:

$$\langle x^2 \rangle = \iiiint (x-\langle x \rangle)^2 f(x, x', y, y')\, dx\, dx'\, dy\, dy'$$

$$\langle xx' \rangle = \iiiint (x-\langle x \rangle)(x'-\langle x' \rangle) f(x, x', y, y')\, dx\, dx'\, dy\, dy'$$

and so on for the other eight. The <u>root-mean-square</u> (rms) values of such quantities are defined as:

$$x_{\text{rms}} = \langle x^2 \rangle^{1/2}$$

The quality of a beam may be quantitatively described by its <u>emittance</u>, which is closely related to the area of the 2-dim projections of the hyper-ellipsoidal volume occupied by the particles in the 6-dim phase space on the xp_x, yp_y and zp_z planes (area = $\pi \times$ emittance). The transverse emittance is normally expressed in [mm mrad], since x' and y' are preferred to p_x and p_y; the longitudinal emittance, defined only for bunched beams, is normally expressed in [ns keV] or [deg keV].

In many cases, as for instance in an optic system with alternating focusing, an ellipse can roughly approximate the emittance boundary. The area of such an ellipse represents the <u>full emittance</u> $\varepsilon_{\text{full}}$ of the beam in that plane, and its size is in fact determined by the outermost particle of the distribution.

If the nonlinear components of the forces (space-charge or external) are not sufficiently small, then the projections of the phase space of a real beam may have a complex shape and a poorly defined boundary; a few particles may go very distant from the beam core and form a so-called "halo". In such cases, the emittance can be defined as $1/\pi$ times the area delimited by an isodensity contour containing some large fraction of the particles, e.g. 95% or 99%. In some other cases it is simpler to consider the area of the smallest ellipse which includes a large fraction of the particles, e.g. 95% or 99%; this definition will be used in this thesis. Such emittances, respectively indicated as $\varepsilon_{\text{full},95\%}$ and $\varepsilon_{\text{full},99\%}$, can be much smaller than the full one, in the presence of halo.

The equation of the emittance ellipse, for example on the xx'-plane, is given by:

$$\gamma_x x^2 + 2\alpha_x xx' + \beta_x x'^2 = \varepsilon_{x,\text{full}}$$

where α_x, β_x and γ_x (which are related as $\beta_x \gamma_x - \alpha_x^2 = 1$) are called <u>Courant-Snyder invariants</u> or <u>Twiss parameters</u> [Cou58]. The meaning of these quantities is illustrated in Figure 3.1; notice that the maximum beam size can be expressed as $(\beta_x \varepsilon_{x,\text{full}})^{1/2}$. A similar equation holds for the yy'-plane and for the longitudinal one.
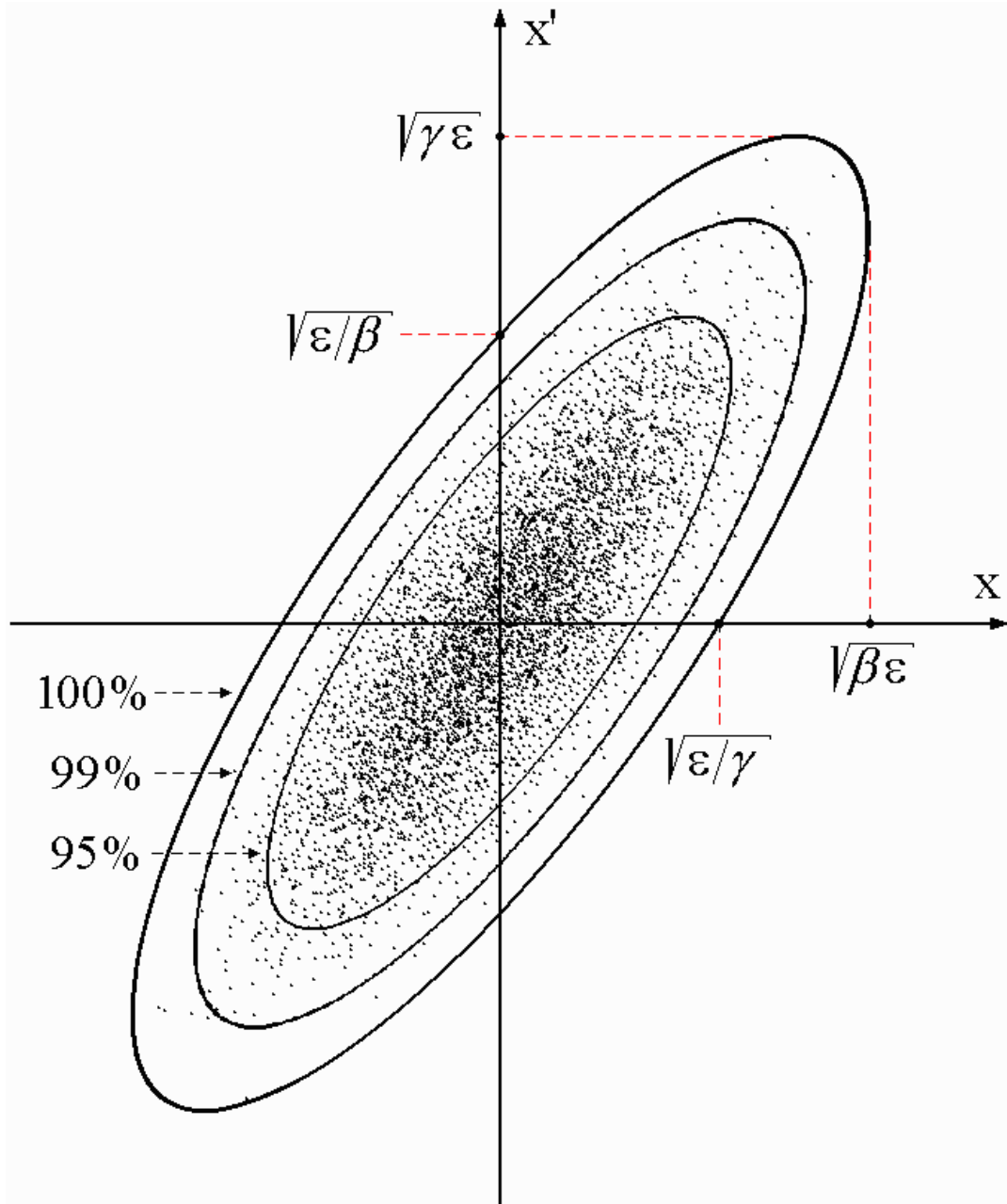
Figure 3.1: Full emittance ellipse in the *xx'* plane, showing the geometrical interpretation of the Twiss parameters; the smallest ellipses which include 100%, 99% and 95% of the particles are shown.

The mostly used quantity to characterize a distribution, and to compare a beam with another one, is the rms emittance, defined by Sacherer from the second moments of the distribution function [Sac71][Lap71]: the horizontal and vertical rms emittance can be statistically defined from the relations:

$$\varepsilon_{x,rms} = (\langle x^2 \rangle \langle x'^2 \rangle - \langle xx' \rangle^2)^{1/2}$$
$$\varepsilon_{y,rms} = (\langle y^2 \rangle \langle y'^2 \rangle - \langle yy' \rangle^2)^{1/2}$$

The ratio between full and rms emittance depends on the chosen distribution f. The quantity $(\beta_x \, \varepsilon_{x,rms})^{1/2}$ corresponds now to the variance of the distribution f in the xx'-plane, i.e. to the rms beam size, and similarly in the yy'-plane.

Particle distributions

A convenient distribution function of charge in the 4-dimensional phase space $x \, x' \, y \, y'$ was introduced by Kapchinskij and Vladimirskij [Kap59]; it will be referred to as the "K-V distribution". All the two-dimensional projections of this distribution are uniform, i.e. it projects to a uniform elliptical distribution on the xx', yy', xy, $x'y'$, xy' and $x'y$ planes (see Fig. 3.2a). Therefore this distribution has the property that the charge density across the beam is constant and the transverse space-charge forces associated with the self-fields are linear functions of the particles' positions in the beam, i.e. they vary linearly with radius.

Where the axes of the hyper-ellipsoid are parallel to the co-ordinate axes, the K-V distribution has the simple form of a delta function of the transverse emittances ε_x and ε_y:

$$f(x,x',y,y') = \delta\,(x^2/a_x^2 + y^2/a_y^2 + a_x^2 x'^2/\varepsilon_x^2 + a_y^2 y'^2/\varepsilon_y^2 - 1)$$

The particles fill uniformly only the surface of a hyper-ellipsoid in a 4-dimensional phase space, therefore the 4-dimensional volume is zero. Such a distribution is physically unrealistic, nevertheless the spatial uniformity of charge density in the K-V distribution provides a very practical model to handle analytically space-charge forces. Moreover it should be noticed that, over short distances, K-V equations are satisfied

with good approximation by rms dimensions (size and emittances) also for other non-K-V distributions.

On the other hand, realistic distributions tend to have a spatial density which decreases with radius. For computer simulations the <u>waterbag distribution</u> is often used as an input, where the 4-dim hyper-ellipsoidal volume is populated with uniform density (like an elastic bag filled with water); therefore the particle density decreases parabolically with radius in all the 2-dim projections (see Fig. 3.2b). The longitudinal phase space zp_z is also populated with uniform density and therefore this longitudinal distribution is indicated as a 2-dim waterbag one.

Using a 4-dim waterbag distribution for the transverse planes and a 2-dim waterbag distribution for the longitudinal one (later referred to as "4d+2d" waterbag) implies that the particle density is parabolic in xx' and yy', but uniform in zp_z. Therefore in this thesis a 6-dim waterbag distribution has also been tested as an input, where the particles fill uniformly a 6-dim hyper-ellipsoid; this has the advantage that the density decreases with radius in all the 2-dim projections (see Fig. 3.2c). In the real 3-dim space, a "4d+2d" waterbag distribution has a cylindrical shape, while a 6-dim one is ellipsoidal.

In the <u>Gaussian distribution</u>, the 4-dim hyper-ellipsoidal volume is populated with a Gaussian density; therefore the particle density is also Gaussian in all the 2-dim projections (see Fig. 3.2d). This is true also for the 2-dim longitudinal distribution.
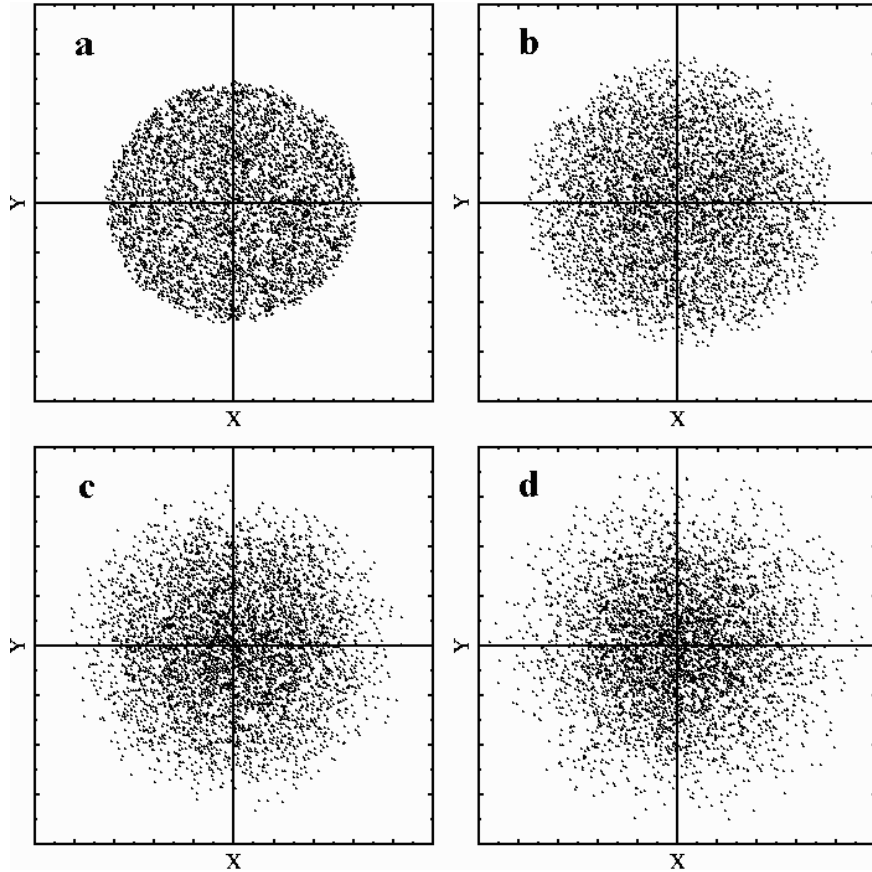
Figure 3.2: Two-dimensional projections (for instance on the *xy* plane) of different particle distributions: a) 4-dim K-V or 2-dim waterbag; b) 4-dim waterbag; c) 6-dim waterbag; d) 4-dim Gaussian, cut at 3σ.

In both the above non-K-V distributions (4-dim waterbag and Gaussian), the transverse space-charge forces associated with the self-fields are nonlinear functions of the particles' positions in the beam. In the presence of space-charge forces, these distributions therefore cannot be matched exactly to a uniform focusing channel and they do not retain their initial mathematical form, i.e. they are not "self-consistent" distributions. They are however often used to represent the initial state of a beam in particle simulation studies.

The ratio between full and rms emittance is equal to 4 for a 4-dim K-V distribution, while it is equal to $m+2$ for a m-dim waterbag distribution (i.e. $\varepsilon_{full}/\varepsilon_{rms} = 4$ for a 2-dim

14

one, 6 for a 4-dim one and 8 for a 6-dim one). For a 2-dim and 4-dim Gaussian distribution truncated at n times the variance, this ratio is given respectively by:

$$\varepsilon_{full}/\varepsilon_{rms} = n^2 (1 - e^{n^2/2}) / (1 - e^{n^2/2} + n^2/2)$$

$$\varepsilon_{full}/\varepsilon_{rms} = n^2 (1 - e^{n^2/2} + n^2/2) / (1 - e^{n^2/2} + n^2/2 + n^4/8)$$

which tend to n^2 for $n > 4$ [Mar71]. This ratio can be used as a measure of the tails in a given distribution, i.e. to estimate the amount of halo.

Tables 3.1 and 3.2 give a survey on the properties of the different particle distributions discussed above.

Table 3.1: Features of different particle distributions.

Distribution	dimensions	space-charge	$\varepsilon_{full}/\varepsilon_{rms}$	$f(r)$	Figure
K-V	4	linear	4.00	constant	3.2 a
Waterbag	2	linear	4.00	constant	3.2 a
Waterbag	4	nonlinear	6.00	parabolic	3.2 b
Waterbag	6	nonlinear	8.00	cubic	3.2 c
Gaussian	2 or 4	nonlinear	$> n^2$	Gaussian	3.2 d

Table 3.2: Ratio $\varepsilon_{full}/\varepsilon_{rms}$ for a Gaussian distribution truncated at $n\sigma$.

n	0.5	1.0	1.5	2.0	2.5	3.0	4.0	5.0
2-dim	4.08508	4.36199	4.89992	5.82272	7.29810	9.47919	16.0431	25.0012
4-dim	6.06368	6.26953	6.66628	7.34860	8.46912	10.2249	16.1742	25.0073

From the rms emittances $\varepsilon_{x,rms}$ $\varepsilon_{y,rms}$, bunch sizes a_x a_y, beam energy W_{rms} and particle mass $m = Am_o$ one can define the <u>temperature</u> of the beam in a given direction:

$$T_x = mc^2(\beta\gamma\varepsilon_{x,rms})^2/a_x \qquad T_y = mc^2(\beta\gamma\varepsilon_{y,rms})^2/a_y \qquad T_z = W_{rms}^2/\beta^2\gamma^2mc^2$$

which are expressed in [keV]. An average transverse temperature can also be defined, as $T_\perp = (T_xT_y)^{1/2}$; the longitudinal one is then denoted as $T_\parallel$.

Liouville's theorem

According to Liouville's theorem, the 6-dim density of <u>non-interacting particles</u> in a conservative system is invariant. If the density is not uniform, then the volume enclosed by an isodensity surface is conserved. This property derives from the fact that position and momentum are canonically conjugate variables and from the continuity equation.

For <u>interacting particles</u>, the theorem remains a good approximation under the condition that a single particle interacts more strongly with the collective fields of the other particles rather than with its nearest neighbour, since this implies that the space-charge fields can be treated as a smooth "external" potential and that particle collisions can be ignored. Quantitatively this happens if the so-called Debye length $\lambda_D = (\varepsilon_o T / n_o q^2)^{1/2}$ is much larger than the average distance between particles $\langle d \rangle = (8\pi n_o/3)^{-1/3}$, where ε_o is the dielectric constant of free space, $T = \frac{1}{2}(T_\perp + T_\parallel)$ the average beam temperature, n_o and q the density and charge of the particles [Rei94]. In this case, scattering can be neglected and Liouville's theorem is a good approximation.

When defining the transverse emittance in terms of $x' = p_x/p_z$ and $y' = p_y/p_z$, its value will depend on the energy of the beam, since p_z increases with acceleration as $\beta\gamma$. For this reason an invariant <u>normalized emittance</u> is often used, which is obtained by multiplication with the relativistic factor $\beta\gamma$; this is also expressed in [mm mrad]. Liouville's theorem applies therefore to the normalized emittance only.

The quantities $\varepsilon_{x,n} = \beta\gamma \, \varepsilon_x$ and $\varepsilon_{y,n} = \beta\gamma \, \varepsilon_y$ are independent and constant during acceleration only if there is no coupling between the horizontal and vertical motion, and in absence of particle losses, nonlinear forces, instabilities, collisions and misalignments. Some of these effects, which cause emittance growth, will be discussed in Chapter 6.

When defining the longitudinal emittance in terms of [ns keV], Liouville's theorem still applies, because time and energy are canonically conjugate variables. If the emittance is expressed in [deg keV], the theorem remains valid only for a constant rf frequency f_{rf}, since 1 [ns] $\leftrightarrow$ $(360 \times f_{rf})$ [deg], with f_{rf} in [GHz]. If the energy spread is used rather than the energy, then the phase space area decreases with increasing energy.

3.2 Transverse beam dynamics

The **F0D0** quadrupole channel is a periodic-focusing system, where a period is defined by a quadrupole **F** of length L_q that is focusing in x and defocusing in y, a drift section **0** of length L_d, a quadrupole **D** of length L_q that is defocusing in x and focusing in y (i.e. rotated by 90°), and another drift section **0** of length L_d (<u>alternating gradient</u> lattice).

In paraxial approximation, the equations of motion for a single particle in this <u>strong focusing</u> transport channel as functions of the distance s along the z-axis are:

$$x'' - k(s)\, x = 0$$
$$y'' + k(s)\, y = 0$$

where $k(s)$ represents the applied (external) focusing force. For $k(s) > 0$, the particle is horizontally focused and vertically defocused; for $k(s) = 0$ it just drifts.

For an ideal quadrupole lens $k(s)$ is constant; the focusing strength of a quadrupole of length L_q is then $k^{1/2}L_q$. The value of k is related to the magnetic field gradient G by the relation $k = qG/p$, where q is the particle charge and p its momentum.

The solution of the equations of motion can be written by means of <u>transfer matrices</u>; for a quadrupole lens (focusing and defocusing) and a drift section, they are respectively:

$$M_F = \begin{pmatrix} \cos\sqrt{k}\,L_q & \frac{1}{\sqrt{k}}\sin\sqrt{k}\,L_q \\ -\sqrt{k}\sin\sqrt{k}\,L_q & \cos\sqrt{k}\,L_q \end{pmatrix} \quad M_D = \begin{pmatrix} \cosh\sqrt{k}\,L_q & \frac{1}{\sqrt{k}}\sinh\sqrt{k}\,L_q \\ \sqrt{k}\sinh\sqrt{k}\,L_q & \cosh\sqrt{k}\,L_q \end{pmatrix} \quad M_0 = \begin{pmatrix} 1 & L_d \\ 0 & 1 \end{pmatrix}$$

The alternation of focusing and defocusing elements may produce a net focusing effect; this happens if the half-trace of the resulting transfer matrix for a period of the F0D0 channel is $\frac{1}{2}\mathrm{Tr}\,(M_{F0D0}) = \frac{1}{2}\,(m_{11}+m_{22}) < 1$. Such a transfer matrix can be calculated by multiplicating the transfer matrices of the four sections, i.e. $M_{F0D0} = M_F \times M_0 \times M_D \times M_0$.

Since $k(s)$ is piecewise constant, with period S equal to the structure period length, then the equations of motion for a single particle are known as Mathieu-Hill's equations and the solution can be written, for instance in the x-plane, by means of the following transfer matrix:

$$M_{F0D0,\,x} = \begin{pmatrix} \cos \sigma_t + \alpha_x \sin \sigma_t & \beta_x \sin \sigma_t \\ -\gamma_x \sin \sigma_t & \cos \sigma_t - \alpha_x \sin \sigma_t \end{pmatrix}$$

where α_x, β_x and γ_x are the Courant-Snyder parameters [Cou58]. This turns out to be equivalent to the form [Rei94]:

$$x(s) = [\varepsilon_x \beta_x(s)]^{\frac{1}{2}} \cos \left(\sigma_t(s) + \delta \right) \tag{3.1}$$

where the amplitude ε_x and the phase δ depend from the initial conditions, while $\beta_x(s)$ and $\sigma_t(s)$ are linked as $\sigma_t'(s) = 1/\beta_x(s)$; the quantity $\sigma_t(s)$ is therefore given by:

$$\sigma_t(s) = S \int_z^{z+S} \frac{du}{\beta_x(u)} = \int [\varepsilon / X^2(u)] \, du$$

and, since it measures the fraction of the particle oscillation in one focusing period, it is called phase advance per period (or tune) of the particle in the transverse direction. For instance, $\sigma_t = 40^o$ means that a single particle requires 9 periods to perform a complete oscillation. The tune is related to the trace of the transfer matrix of one lattice period as $\cos \sigma_t = \frac{1}{2}\text{Tr} (M_{F0D0})$; then a condition for stable motion is: $\sigma_t < 180^o$. From the unitarian determinant of the M_{F0D0} matrix, one derives again that $\beta_x(s) \, \gamma_x(s) - \alpha_x^2(s) = 1$; similarly for the y-plane (notice that there is a σ_t only, owing to the same periodicity in x and y).

The cosine term in Eq. (3.1) may assume any value between -1 and $+1$; the maximum amplitude of the transverse oscillation is therefore given by $X(s) = [\varepsilon_x \beta_x(s)]^{\frac{1}{2}}$, which defines the envelope of a beam constituted by several particles (see Fig. 3.1).

In a periodic array of quadrupoles (F0D0 channel) particles trajectories are not sinusoidal, but there is a well-defined wavelength $2\pi S / \sigma_t$, where S is the period length and σ_t is the tune. Particle trajectories are in general not even periodic, but the envelope may be: when the envelope periodicity is equal to the focusing system one, the beam is said to be "matched".

The function $\beta_x(s)$, called betatron function, has then the same period S as the focusing function $k(s)$; it has usually its maximum in the centre of a focusing magnet

and its minimum in the centre of a defocusing one. The ratio $\Psi = (\beta_{max} / \beta_{min})^{1/2}$ is called "flutter factor".

Particles move in the xx'-plane inside an ellipse, which shape at any point s is given by the Twiss parameters $\alpha_x(s)$, $\beta_x(s)$ and $\gamma_x(s)$; in particular, the ellipse is upright at the positions of maximum and minimum envelope (middle of a focusing and defocusing magnet respectively), where $\alpha_x = 0$ and $\beta_x = 1/\gamma_x$.

The particle motion is restricted by the aperture size r_o of the quadrupoles ("bore" radius). The maximum allowed transverse emittance of a matched beam which the channel is still capable of transmitting is called <u>acceptance</u> α_t. Since $r_o = X_{max} = (\alpha_t \beta_{max})^{1/2}$, the acceptance is given by:

$$\alpha_t = r_o^2 / \beta_{max}$$

The transverse dynamics of charged particles must be analysed keeping into account not only the alternating gradient focusing due to the magnetic quadrupoles but also the defocusing due to the space-charge forces. The former effect is alternatively focusing in one direction and defocusing in the other, while the latter acts simultaneously on both transverse directions.

For large beam intensities, the space-charge forces play then an important role on the beam behaviour, since the beam properties are not only determined by the external focusing fields. As a result, there is no solution for the differential equations of motion in a general case.

Well-known equations exist however for the beam envelopes $X(s)$ and $Y(s)$ in the two transverse directions for the <u>self-consistent K-V distribution</u>, with the same unnormalized emittance ε in both transverse directions, considered to be constant during the motion [Kap59]:

$$X'' + k(s)\,X - 2K / (X + Y) - \varepsilon^2 / X^3 = 0$$
$$Y'' - k(s)\,Y - 2K / (X + Y) - \varepsilon^2 / Y^3 = 0$$

where the dimensionless parameter K is called the <u>generalized perveance</u> and is defined (for a homogeneous, monoenergetic and unneutralized ion beam) as [Law58]:

$$K = 2I / \beta^2 \gamma^2 I_A = 2I / \beta^3 \gamma^3 I_o$$

where I is the beam current, $I_A = \beta\gamma I_o$ is called Alfvén current [Alf39] and $I_o = 4\pi\varepsilon_o mc^3/q$ is the characteristic current ($\cong 31 \times 10^6$ A/Z [Amp] for mass $m = Am_o$ and charge $q = Ze$).

The focusing term $+k(s)X$ (respectively $-k(s)Y$) has to act against the space-charge term $-2K/(X+Y)$ and against the emittance term $-\varepsilon^2/X^3$ (respectively $-\varepsilon^2/Y^3$). If the first defocusing term is larger than the second one, then the beam is said to be "emittance dominated"; if the opposite is true, then it is said to be "space-charge dominated".

In the so-called "smooth approximation" theory, small envelope oscillations are assumed, i.e. small variations of the beam radius in one focusing period compared to the average value; the envelope equations are then solved for the average values of the quantity involved.

Having assumed the same emittance in both transverse directions, the envelopes for a matched beam can be written in terms of the average radius R, which is constant, and a modulation function $\delta(s)$, with $|\delta(s)|«1$:

$$X(s) = R\,[1+\delta(s)] \qquad \text{and} \qquad Y(s) = R\,[1-\delta(s)]$$

In this case, averaging over one period the above differential equations of motion for the beam envelopes, one gets the following algebraic equation for the constant radius R [Str83]:

$$(\sigma_{to}^2/S^2)R - K/R - \varepsilon^2/R^3 = 0$$

The zero-current tune σ_{to} has been introduced, which depends only on the average strength of the external focusing forces. For $K = 0$ (no space-charge) the above relation gives the average (full) radius of the beam:

$$R_o = (\varepsilon S/\sigma_{to})^{½}$$

Introducing now the depressed tune σ_t, by combining the $(\sigma_{to}^2/S^2)R$ term representing the external forces with the K/R term representing the space-charge forces, i.e.:

$$\sigma_t^2/S^2 = \sigma_{to}^2/S^2 - K/R^2 \qquad \text{or} \qquad \sigma_t = (\sigma_{to}^2 - K\,S^2/R^2)^{½} \tag{3.2}$$

one obtains the average (full) radius of the beam in the presence of space-charge:

$$R = (\varepsilon S/\sigma_t)^{\frac{1}{2}}$$

This means that the transverse tunes may also be defined as $\sigma_{to} = \varepsilon S/R_o^2$ and $\sigma_t = \varepsilon S/R^2$, with ε the full unnormalized transverse emittance, S the period length, R_o and R the full transverse beam size without and with space-charge.

The zero-current tune σ_{to}, which depends only on the strength of the external focusing forces, is always larger than the corresponding depressed tune σ_t in the presence of space-charge forces (from Eq. (3.2) one gets $\sigma_t < \sigma_{to}$). This means that the defocusing effect of space-charge reduces the phase advance in one lattice period.

In the region where $\sigma_{to} < 90^o$ the "smooth approximation" results are sufficiently accurate. In particular, an essential result of the theory is the following [Rei78][Jun83]:

$$\sigma_t/\sigma_{to} = \varepsilon/\alpha = (1 + u^2)^{\frac{1}{2}} - u$$

where $u = KS/2\varepsilon\sigma_{to}$ is called the space-charge parameter, and having defined the acceptance α as the maximum emittance without space-charge.

For a given focusing channel the beam physics is largely determined by the <u>tune depression</u> σ_t/σ_{to}, which may have any value between 0 and 1. From the above relations one finds that the before mentioned condition defining a space-charge dominated beam ($K/R > \varepsilon^2/R^3$) is equivalent to the condition $\sigma_t/\sigma_{to} < 0.7$ [Rei94]; furthermore, $\sigma_t/\sigma_{to} > 0.4$ is demanded to avoid instabilities [Glu70].

Actually it has been proved that the above envelope equations are valid not only for the K-V distribution but for any **non**-self-consistent distribution with elliptical symmetry in the *xy* real space, provided that the beam is matched and that its boundary R (respectively X and Y) and full emittance ε_{full} are substituted by the rms value of the beam size a (respectively a_x and a_y) and of the emittance ε_{rms} [Glu70][Lap71]. This result can even be extended to bunched beams with ellipsoid shape [Sac71].

In the special case of a spatially uniform distribution, the physical boundaries and their rms values are related by $X/a_x = 2$ and $Y/a_y = 2$. In general, for other simple distributions, the ratio between the envelope and the rms size is equal to $(\varepsilon_{full}/\varepsilon_{rms})^{\frac{1}{2}}$, i.e. for instance $(m+2)^{\frac{1}{2}}$ for a *m*-dim waterbag distribution (see Tab. 3.1 and 3.2).

The relations found above as a consequence of the envelope equations remain valid for rms quantities. All beams with the same perveance and rms emittance have then the same rms transverse size, since $a^2 = \varepsilon_{rms} S/\sigma_t$.

In a position where the beam is not symmetric, the transverse emittance ε_{rms} and the beam size a are defined by the geometrical average of the respective horizontal and vertical quantities:

$$\varepsilon_{rms} = (\varepsilon_{x,rms}\,\varepsilon_{y,rms})^{\frac{1}{2}} \qquad \text{and} \qquad a = (a_x\,a_y)^{\frac{1}{2}}$$

Notice however that the design and matching of high intensity accelerators should be made considering not only rms but also full quantities, since beam losses −which are of fundamental interest− come from a very small fraction of particles which lie far outside the beam core. The effect of different distributions is discussed in Chapter 5.

Another interesting result is obtained by re-writing Eq. (3.2) as $K = R^2/S^2\,(\sigma_{to}^{\,2} - \sigma_t^{\,2})$ for $R = R_{max} = (\alpha S/\sigma_t)^{\frac{1}{2}}$ and comparing it to the definition of perveance given above, which allows to find the transverse current limit [Rei78]:

$$I_{max,t} = \tfrac{1}{2} I_o\,\beta^3\gamma^3\,\alpha\,(1-\sigma_t^{\,2}/\sigma_{to}^{\,2})\,\sigma_{to}/S = \tfrac{1}{2} I_o\,\beta^3\gamma^3\,\alpha\,(1-\varepsilon^2/\alpha^2)\,\sigma_{to}/S$$

The amount of beam current that can be transported through a periodic focusing channel is a maximum $I_{max,t}$ when the beam is perfectly matched to the acceptance of the channel (provided that the tunes σ_{to} and σ_t are chosen to avoid instabilities) and depends on the energy of the beam and on the ratio of the transverse emittance to the carrying capacity of the focusing channel, that is the acceptance. It can be increased by increasing the acceptance, for instance by reducing the frequency of the accelerating rf field. in this case, however, the dimensions (and the cost) of the linac increase [Kap85].

Since in practice the maximum beam radius $R_{max} = R\,(1+\delta_{max})$ has to be smaller than the aperture r_o, and since $R/R_{max} \cong (1-1.2\,\sigma_{to}/\pi)^{\frac{1}{2}}$ [Rei81], one can write [Rei94]:

$$I_{max,t} = \tfrac{1}{2} I_o\,\beta^3\gamma^3\,\sigma_{to}^{\,2}\,(1-1.2\,\sigma_{to}/\pi)(r_o/S)^2$$

Up to this point a perfectly matched beam has been considered and longitudinal dynamics issues are not treated. In Chapter 3.3 the external rf electric field is applied, i.e. the energy of the beam and the focusing period are not constant and there is a

transverse defocusing in the gap due to the acceleration; in Chapter 3.4 mismatch will be discussed.

3.3 Longitudinal beam dynamics

In order to provide acceleration, a longitudinal time-varying (rf) electric field is required, $E_z = E_o \sin(\omega t - kz)$, having the same phase velocity ω/k as the particles to be accelerated: thus a "synchronous" particle with charge q always meets this travelling wave
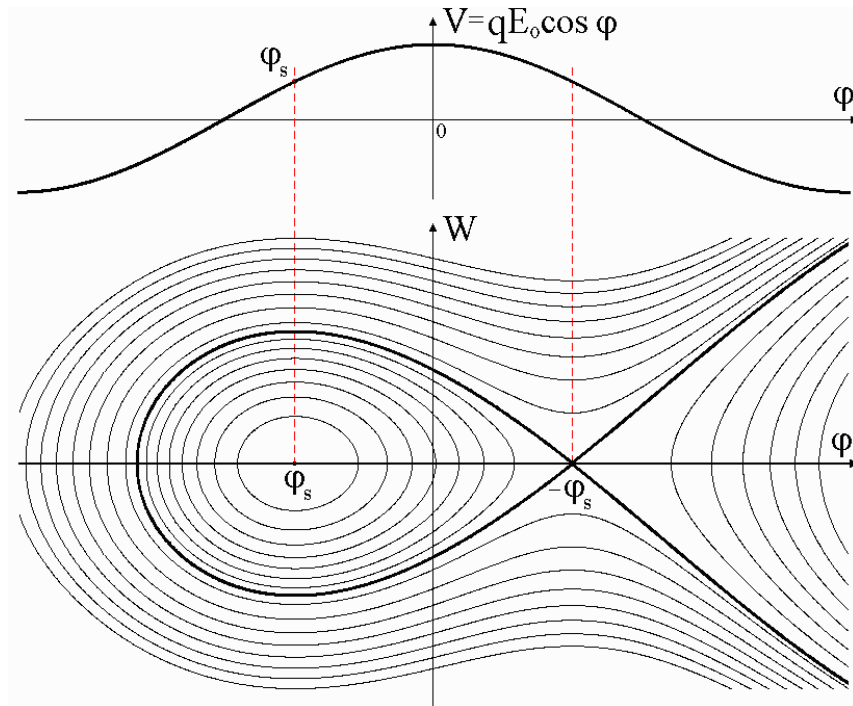

Figure 3.3: Rf trajectories in the longitudinal phase-plane, with graphical definition of bucket and bunch.

with the same phase ϕ_s and it will experience an accelerating voltage $V_s = qE_o \cos \phi_s$, with $\phi = 0$ corresponding to maximum amplitude E_o or crest (see Fig. 3.3).

If ϕ_s is chosen in the negative range $-90^o < \phi_s < 0^o$ (in the time regime), then the phase-stability principle applies. The synchronous phase ϕ_s is in fact stable when the

electric field is rising, since a particle arriving too early will be less accelerated and slip slightly in phase, while the opposite happens for a late particle. Particles will therefore oscillate about the position of ϕ_s. Phase stability accounts for the fact that the beam forms into longitudinally focused "bunches", i.e. that particles stably group themselves in the vicinity of the equilibrium phase of the rf field.

The phase oscillations which are created for a generic particle with respect to the synchronous one are described by the following equation:

$$d^2\phi / dt^2 = (\Omega_s^2 / \cos \phi_s)\,(\sin \phi - \sin \phi_s) \qquad \text{with} \qquad \Omega_s^2 = (\omega q E_z / \beta \gamma^3\, m_o c)\, \cos \phi_s$$

which may be integrated to give:

$$(d\phi / dt)^2 - (d\phi / dt)_o^2 = (2\,\Omega_s^2 / \cos \phi_s)\, [\cos \phi - \cos \phi_s - (\phi_o - \phi)\, \sin \phi_s]$$

where ϕ_o and $(d\phi / dt)_o$ denote the initial values of phase and of phase variation.

The energy difference ΔW between the synchronous particle and any other particle is proportional to $d\phi / dt$, then the longitudinal motion of particles can be represented in the phase plane ϕ-ΔW. For small values of ϕ, the particles orbit around the point $(\phi_s, 0)$ in a stable region called bucket (see Fig. 3.3) with revolution frequency Ω_s (synchrotron oscillation frequency); as the amplitude increases, the frequency decreases, becoming zero when the maximum value of ϕ reaches the separatrix.

The longitudinal acceptance is the area in the ϕ-ΔW phase space where particle motion is stable. Without space-charge, the maximum amplitudes $\Delta\phi$ and ΔW can be calculated exactly using analytical equations; in the presence of space-charge, they can be calculated in an approximate way, provided one has calculated the ratio μ_l of the defocusing space-charge force to the restoring force of the rf field [Mit78]:

$$2\,\phi_s(1-\mu_l) \le \phi \le -\phi_s(1-\mu_l) \quad \text{with} \quad \phi_s \le 0 \quad \Rightarrow \quad \Delta\phi_{\max} = 3\,|\phi_s|(1-\mu_l)/2$$

$$\Delta W_{\max} = [2\,\lambda q E_o T mc^2 \beta_s^3 \gamma_s^3\, |\phi_s|^3\, (1-\mu_l)^3 / 3\pi]^{\frac{1}{2}}$$

with

$$\mu_l = (3\,I\,\lambda^2\, M_z\, \beta) / (8\pi^2\, a_x a_y b\, \varepsilon_o c\, E_o T \sin \phi_s)$$

$$M_z \approx (a_x a_y)^{\frac{1}{2}} / 3b \qquad \text{valid for} \quad 0.8 < b / (a_x a_y)^{\frac{1}{2}} < 5$$

The maximum amplitudes without space-charge can be obtained for $\mu_l = 0$. Approximating the acceptance area α_l in the longitudinal phase space by that of an ellipse, the maximum current $I_{max,l}$ which can be accelerated in the longitudinal direction is [Mit78]:

$$\alpha_l \approx \pi \, \Delta\phi_{max} \, \Delta W_{max}$$

$$I_{max,l} \leq (\pi \, a_x a_y \, \varepsilon_o c \, E_o T \, \phi_s \sin \phi_s) \, (1-\mu_l) \, \mu_l / (M_z \, \lambda)$$

Optimizing $I_{max,l}$ as a function of μ_l yields $\mu_l = 1/3$; in such a case, the longitudinal phase space can accept at most a current $I_{max,l}$ given by:

$$I_{max,l} = (8/9) \, \pi^2 \, a_x a_y b \, \varepsilon_o c \, E_o T \sin |\phi_s| / (M_z \, \beta\lambda^2) = 211 \, \phi_s^2 \sin |\phi_s| \, E_o T \, \beta^2 \lambda / \Psi^{1/2} \quad (3.3)$$

having used the relation $b = \frac{1}{2} \, (\phi_s/2\pi) \, \beta\lambda$ and a numerical value for some constants.

The limit on the current imposed by longitudinal repulsion is therefore roughly proportional to the cube of the equilibrium phase; its absolute value should then be made large enough to eliminate the restriction imposed by longitudinal repulsion on the beam current, in particular at lower energies [Kap85].

The longitudinal phase advance (or tune) may be defined in "smooth approximation", in a similar way to the transverse one, as $\sigma_l = \varepsilon \, S / b^2$, where ε denotes now the rms longitudinal emittance and b is the rms longitudinal size of the bunch.

The tune of single particle oscillations in one channel period without space-charge σ_{lo} is related to the synchrotron oscillation frequency Ω_s.

The rf field in an accelerating gap is not perfectly parallel to the beam axis, but has some radial component which cause a transverse force. Since the amplitude of the electric field is increasing while particles cross the gap (for longitudinal stability), then the focusing effect in the first half of the gap is smaller than the defocusing effect in the second half. In a linac, the effect of this "rf defocusing" on transverse motion is not negligible; this effect will be discussed quantitatively in Chapter 3.6.

The longitudinal motion is weakly coupled with the transverse one, even in linear approximation, because the transverse rf defocusing force for a generic particle depends upon its longitudinal phase. A parametric resonance occurs when the average transverse oscillation frequency of the particle moving in an equilibrium phase is close to the half-

integer frequency of the small longitudinal oscillations. i.e. $\sigma_l = (n/2)\,\sigma_t$ with $n = 1, 2, 3...$

These resonances can force particles to leave the beam core. They are excited by mismatch, as described in the next paragraph; a correlation between halo production and parametric resonances in a bunched beam has been verified by numerical simulations in the DTL for ESS (European Spallation Source) [Bon98].

The most critical part is the low energy end of the linac, because the region of allowed values of cos σ_t (bandwidth) will be mainly reduced [Kap85].

Finally notice that, from the definitions of energy and momentum, $W = (\gamma - 1)\,mc^2$ and $p = \beta\gamma mc$, and using simple relativistic relations, one finds:

$$dp/p = [\gamma / (\gamma + 1)]\,dW/W \cong \tfrac{1}{2}\,dW/W \qquad \text{for } \gamma \cong 1$$

For this reason, one can switch between "energy spread" and "momentum spread" just including or removing a factor $\tfrac{1}{2}$ (see Chapter 8).

3.4 Beam matching and mismatched beams

For a <u>matched</u> K-V beam, with identical emittances and depressed tunes in both transverse planes, the average beam radius remains constant along a F0D0 focusing channel, and the beam envelope is a function which has the same period as the external focusing force (see Chapter 3.2). This result was found neglecting acceleration and bunching (coasting beam).

Under the same assumptions, the small oscillations $x_o \cos ks$ and $y_o \cos ks$ of the mean radius along the average value R for a slightly <u>mismatched</u> beam ($|x_o|,|y_o| \ll R$) can be described in terms of the superposition of two pure eigenmodes, in which the amplitudes in the x- and y-plane are respectively "in phase" and "180º out-of-phase" [Str83]. The phase advances ϕ_1 and ϕ_2 of these oscillation modes in one focusing period S are:

$$\phi_1 = k_1 S = (\sigma_{to}^2 + 3\sigma_t^2)^{\frac{1}{2}} \qquad \text{and} \qquad \phi_2 = k_2 S = (2\sigma_{to}^2 + 2\sigma_t^2)^{\frac{1}{2}}$$

Envelope instabilities exist when $\sigma_{to} > 90^o$, since the smooth approximation is no longer adequate. A more accurate analysis [Str83] reveals that resonances between envelope oscillations and periodic focusing structure occur when ϕ_1 or ϕ_2 is equal to 180° and when $\phi_1 = \phi_2$; depending on beam intensity (i.e. on σ_{to} and σ_t), also this resonances can lead to instabilities.

A non-K-V beam is always mismatched, due to the nonlinear space-charge forces; for a real beam matching is possible only in an approximate sense. If space-charge forces are important, the problem becomes very complicated and sophisticated computer programs have to be used in order to deal with it numerically. This is however a highly specialized art: for this purpose one can, for instance, repeatedly modify the Twiss parameters at the input of a period until the same parameters are found again at its end.

In the design of a high intensity linac instabilities should be avoided, as even a slight mismatch may lead to exponential growth of the beam radius. On the other hand, in practice one deals with bunched beams, where space-charge forces are not only nonlinear, but also have intensity variation along the pulse; therefore another (more general) model has to be used.

For <u>mismatched</u> <u>bunched</u> beams with identical emittances and tunes in both transverse planes, a possible approach was proposed by Bongardt and Pabst [Pab97][Pab98], who observed that the beam envelope in a transport channel can be described by means of 3 pure eigenmodes of oscillation, whose frequencies are approximated by analytical functions of the four tunes σ_t, σ_{to}, σ_l, σ_{lo} only (transverse, longitudinal, with and without current). Also the ratio between different amplitudes can be approximated analytically in terms of these four tunes.

- The so-called "<u>quadrupolar</u>" mode is excited by increasing the rms horizontal bunch size a_x and simultaneously decreasing the rms vertical bunch size a_y by the same amount (or the opposite), while the rms bunch length b is not changed:

$$\Delta a_x/a_x = -\Delta a_y/a_y \quad \text{and} \quad \Delta b/b = 0$$

  The corresponding eigenvector is $\delta_o = 2^{-\frac{1}{2}} (+1, -1, 0)$, therefore this mode is schematically indicated as $(+ - 0)$. The mismatches in x and y oscillate with opposite

phases, while b is constant (see Fig. 3.4-left). The phase advance for the quadrupolar mode is:

$$\sigma_Q = 2\,\sigma_t$$

- In the "<u>high</u>" mode, a_x, a_y and b are all increased, according to:

$$\Delta a_x/a_x = \Delta a_y/a_y \quad \text{and} \quad \Delta b/b = f_H\,\Delta a_x/a_x$$

with

$$f_H = [\sigma^2_H - 2\,(\sigma^2_{to} + \sigma^2_t)]\,/\,(\sigma^2_{to} - \sigma^2_t)$$
$$\sigma_H^{\,2} = A + B^{\frac{1}{2}}$$
$$A = \sigma^2_{to} + \sigma^2_t + \tfrac{1}{2}(\sigma^2_{lo} + 3\sigma^2_l)$$
$$B = [\sigma^2_{to} + \sigma^2_t - \tfrac{1}{2}(\sigma^2_{lo} + 3\sigma^2_l)]^2 + 2(\sigma^2_{to} - \sigma^2_t)(\sigma^2_{lo} - \sigma^2_l)$$

The corresponding eigenvector is $\delta_+ = (2 + f_H^{\,2})^{-\frac{1}{2}}\,(+1, +1, f_H)$; since $f_H > 0$, this mode is schematically indicated as $(+ + +)$. The mismatches in x, y and z are all in phase (see Fig. 3.4-middle). The phase advance of the high mode is:

$$\sigma_H = (A + B^{\frac{1}{2}})^{\frac{1}{2}}.$$

- In the "<u>low</u>" mode, a_x and a_y are decreased, while b is increased, according to:

$$\Delta a_x/a_x = \Delta a_y/a_y = (1/f_L)\,\Delta b/b$$

with

$$f_L = [\sigma^2_L - 2\,(\sigma^2_{to} + \sigma^2_t)]\,/\,(\sigma^2_{to} - \sigma^2_t)$$
$$\sigma_L^{\,2} = A - B^{\frac{1}{2}}$$

The corresponding eigenvector is $\delta_- = (2/f_L^{\,2} + 1)^{-\frac{1}{2}}\,(1/f_L, 1/f_L, +1)$; since $1/f_L < 0$, this mode is schematically indicated as $(- - +)$. The mismatches in x and y are in phase, while the mismatch in z has opposite phase (see Fig. 3.4-right). The phase advance of the low mode is:

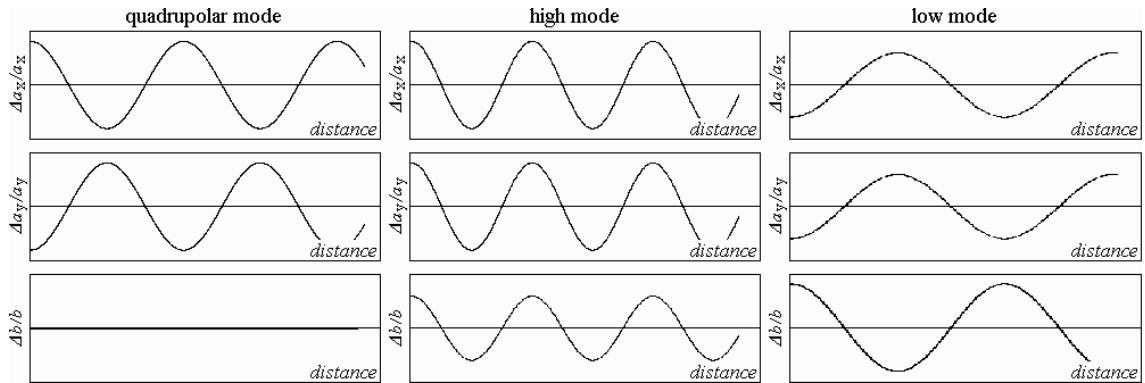$$\sigma_L = (A - B^{\frac{1}{2}})^{\frac{1}{2}}.$$

Figure 3.4: Rms bunch size with respect to the nominal one at the end of each period, for excitation of the "quadrupolar", "high" and "low" eigenmodes through initial mismatch (arbitrary units).

This model has the advantage that, for small initial mismatch amplitudes of the beam, the envelope is a superposition of the 3 above described eigenmodes. In fact, any mismatched input condition can be expressed as a linear combination of these three modes.

If either the beam centre is displaced transversally (due to misalignments) or longitudinally (due to rf amplitude and phase errors), the above given statements are correct for the oscillation of the beam envelope relative to the shifted bunch centre. For small displacements, in fact, the external forces are in first approximation linear and therefore they act in the same way on all the particles.

These relations have been derived for a F0D0 channel without any acceleration. Nevertheless, if the acceleration rate is low (e.g. in the case of heavy ions), the effect still exists and can clearly be seen in the linac, at least in the beginning. However, due to the fact that beam acceleration and non-homogeneous space-charge cause nonlinear forces, the motion along x, y and z will couple to each other after a certain number of periods, as will be observed by multiparticle calculations (see Chapter 6.5).

29

3.5 Emittance growth and halo formation

Emittance

Liouville's theorem states that the emittance is a constant for a conservative system; several mechanisms may however contribute to its growth and lead to <u>filamentation</u> of the distribution in the phase-space. From a thermodynamic point of view the emittance is correlated with the entropy of the particle distribution, therefore a growth is always an irreversible process. The control and the reduction of the emittance growth is one of the most fundamental issues in beam physics.

The main causes of emittance growth are: nonlinear forces (both "external" rf field and magnetic focusing and "internal" space-charge for spatially non-homogeneous distributions), beam mismatch and instabilities, nonlinear coupling and single particle resonances, statistical errors on the rf field and magnetic focusing, misalignments of the accelerating and focusing elements, chromatic aberrations...

The external rf electric field which acts upon the particles determines a nonlinear accelerating force, since its amplitude is not a linear function of the phase ($F \propto \sin \phi$); this intrinsic effect can be reduced by shortening the bunch but cannot be eliminated. On the other hand the magnetic field gradient of the quadrupoles can, in principle, be made linear.

Also the internal electric field due to the charged particles themselves determines nonlinear space-charge forces, when a spatially non-homogeneous distribution is used; in dilute beams this effect is virtually absent, but in high intensity beams it becomes important and adds to the external nonlinearities. To evaluate separately the emittance growth due to the external and internal forces, one can for instance compare the results obtained for two bunches having the same rms longitudinal size but different length: while the effect of the space-charge repulsion is equivalent, the longer bunch has its tails in a region where the nonlinear part of the rf electric field is higher (see an example in Chapter 5.3).

If the injected beam is mismatched, the initial distributions is not in thermodynamic equilibrium but has some "free energy" which can be "thermalized" by nonlinear space-charge forces, instabilities or collisions, and can produce emittance growth [Rei91]. The

envelope oscillation modes and the instabilities of mismatched beams (see Chapter 3.4) are therefore another mechanism that can lead to emittance growth [Rei94]. This effect is stronger in a space-charge dominated regime (tune depression < 0.7).

Another mechanism leading to emittance growth is the nonlinear coupling between different directions; it may be due to the space-charge (especially for high currents) or to other effects, as the rf defocusing in the gap of a DTL or some statistical "tilt" errors in the focusing magnets (rotations around the quadrupole axis). Nonlinear resonances are a further source of emittance growth.

Halo

For high current accelerators some of these effects, induced by the nonlinear character of the space-charge forces, may lead to the formation of a low density "halo" surrounding the central core of the beam: experiments and numerical simulations show that such a halo can develop radially at several core radii beyond the beam centre and reappears when scraped [Sym4].

An increase of the beam size entails a risk of particle losses from halo. Even if it contains less than 1% of the particles, halo can be a serious problem for high intensity machines: their dominating design feature is in fact to bring particle losses at high energy below an extremely low threshold, in order to avoid radiation damages in the structures and to allow hands-on maintenance of the accelerator, by limiting the induced radioactivity.

The maximum tolerable losses for a proton beam (producing a γ-dose of 2.8 mrem/h at 1 m distance, 1 hour after shutdown) range from ≈200 nA/m at 10 MeV to ≈2.5 nA/m at 50 MeV; this corresponds to loss rates < 1 W/m, or $< 10^{-7}$/m for 100 mA [Lag96]. For the <u>HIDIF main linac</u> the same value of 10^{-7}/m was assumed, corresponding to allowed losses of 80÷400 W/m ($W = 2 \div 10$ GeV, $I = 400$ mA); for a cross section Bi-Fe of ≈3.5 barn, the induced radiation is 2×10^{-5} Sv/h for γ-rays and 10 cm^{-1}s^{-1} neutron flux [Str96].

A universally agreed definition of halo does not exist; for some purposes one can say that a particle lays in the halo when its distance from the bunch centre is larger than 3, or maybe 4, times the rms size of the bunch (a_x, a_y, b). Also the formation of the halo is largely unexplained in theory; as it follows from recent investigations, the main

reason of the beam halo formation are the nonlinear interactions of the single particles with the collective density oscillations and fluctuations of the beam core, which can lead to a net increase of the transverse energy and amplitude of the particle oscillation [Jam94].

If a particle travels through an oscillating beam core when the core density is increasing, it will gain energy; on the contrary, the particle will lose energy if travelling through the core when the core density is decreasing [Bnd93][Bnd94]. Since the linac is a periodic system, this may happen several times during the acceleration. If a particle falls into a parametric resonance with the core frequency, then repeated energy transfer can move it far outside into the halo. There its tune changes, so the particle will later traverse the core with opposite phase, lose its excess energy and return into the core.

Beam halo formation can therefore be caused by a mismatched initial distribution, and in particular to particle-core coupling resonances, which are enhanced by the strong influence of the nonlinear space-charge forces. This mechanism may also lead to a redistribution of energy between the transverse and longitudinal planes, with an emittance exchange between them.

Due to the nonlinear part of the space-charge forces, the oscillation frequency of the single particle σ^j is limited between the depressed and the zero current tune either in the transverse or in the longitudinal plane ($\sigma_t < \sigma^j < \sigma_{to}$ or $\sigma_l < \sigma^j < \sigma_{lo}$). The excitation at the beginning of the linac of one of the three bunched beam eigenmodes, described in Chapter 3.4, will then lead either to radial or to axial halo formation only, according to the corresponding mode frequency [Bon98][Pab98].

In the HIDIF main linac discussed in this thesis, the observed either radial or axial halo formation when exciting one of the pure beam eigenmodes (see Chapter 6.5) will be explained in terms of a 1:2 parametric resonance excitation between single particle and oscillating mismatched core. The worst case is the "mixed" mode, where the input conditions are not matched in all planes ($\Delta a_x/a_x = -\Delta a_y/a_y = \Delta b/b$); since this mode is a superposition of the quadrupolar and of the low eigenmodes, it leads simultaneously to radial and axial halo formation.

Equipartitioning

It has been demonstrated that space-charge interactions in high intensity linear accelerators can lead to a redistribution of energy between the transverse and

longitudinal planes, owing to the strong coupling between them. This process can lead not only to emittance transfer from one plane to another, but also to emittance growth (the total emittance tends to increase) and to halo formation. However, it was shown that no emittance exchange occurs if the transverse and the longitudinal temperatures of the beam are equal ($T_\perp = T_\parallel$); this condition is fulfilled when a linac is designed according to the so-called <u>equipartitioning</u> rule [Jam81]:

$$\varepsilon_t / \varepsilon_l = \sigma_l / \sigma_t = a / \gamma b$$

where ε_t and ε_l are the transverse and longitudinal rms emittances, σ_l and σ_t the depressed tunes, a is the rms bunch radius and b the rms bunch length.

Normally equipartitioning has a positive effect on beam dynamics and it is helpful in the reduction of halo; quite good results have been found even if the above relations are not perfectly fulfilled, but within a tolerance of about 50% [Hof81]. This is therefore considered as a good starting condition for the design of a high intensity linac.

Most beams have different longitudinal and transverse temperatures; various effect tend then to drive the particle distribution toward a 3-dim thermal equilibrium, particularly at high currents. Generally in the design of a linac the transverse tune at zero current σ_{to} is kept constant during acceleration, then the transverse beam size a becomes smaller with the increase of the energy; moreover, the longitudinal focusing is often fixed, then the bunch length b becomes larger: such a beam is not equipartitioned.

Another way to reduce the generation of halo particles outside the dense beam core is to design the linac in a non-space-charge-dominated regime [Pab96]. All the accelerator sectors have to be designed to be far away from the space-charge limit, by increasing the external focusing in order to have a tune depression > 0.7. A disadvantage is that one needs more power for both the transverse and the longitudinal focusing (cost increases).

Nevertheless, it was preferred to follow this kind of approach to the problem, also trying to avoid strong mismatches and limiting the external errors, rather than to deal with a space-charge-dominated accelerator, because the beam behaviour is less critical.

3.6 The Drift Tube Linac (DTL)

The Drift Tube Linac (DTL) is a machine where the acceleration is achieved via successive energy kicks, generated in the gaps between some tubes by a row of rf cavities settled along a straight line. When drifting inside a tube, the particles do not see any external electric field but can be focused by magnetic lenses (quadrupoles) [Con91].

The early examples were ion machines, where particles remained very well non-relativistic. In the Wideröe type [Wid28], for example, an rf generator feeds a series of tubes with such a timing that ions experience an accelerating voltage each time they cross the gap between two neighbouring tubes. The external electric fields is almost zero inside any tube, and it has opposite phases in two adjacent gaps ("π-type" standing wave); since half period of the rf generator has to elapse while the ion is crossing any drift tube, the synchronism condition is given by:

$$L_{cell} = v\tau_{rf}/2 = \beta c/(2f_{rf}) = \beta\lambda_{rf}/2$$

With a constant frequency f_{rf}, the drift tube lengths must increase according with the velocity β of the particles. The limitation of this structure is that relativistic particles would require either too long drift tubes or too high frequencies, which wavelength must not exceed the dimension of the circuit. The obvious improvement consists of including the walls of the vacuum tank into the circuit, building up a series of cavities whose resonant frequency is equal to the frequency of a rf generator (see Fig. 3.5). This structure, named Alvarez type [Alv46], can work at much higher frequencies.
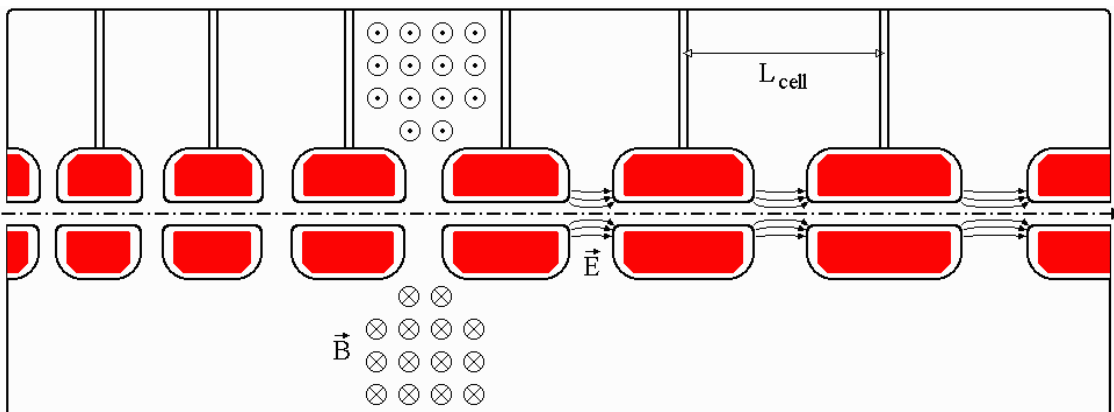
Figure 3.5: Scheme of a Drift Tube Linac of Alvarez type.

In an Alvarez structure, the fields of all the accelerating gaps have the same phase ("0-type" standing wave). Since a full period of the rf generator has now to elapse while the particles are crossing any drift tube, the synchronism condition is given by:

$$L = v\,\tau_{\mathrm{rf}} = \beta c/f_{\mathrm{rf}} = \beta\lambda_{\mathrm{rf}}$$

This determines the minimum input energy of the DTL, since the first drift tube must be long enough to house a quadrupole. In fact the beam is transversally defocused, while longitudinally the phase-stability principle applies. This effect is compensated by an array of magnetic lenses: a quadrupole is therefore put inside each drift tube.

Since horizontal focusing produces vertical defocusing (and vice-versa), then quadrupoles must be arranged in such a way to have an alternating gradient (AG) focusing in these two planes as discussed in Chapter 3.2. The shortest repetition of the focusing structure is called period. It may consist of different combinations of lenses; the most conventional period is the F0D0 channel, where F and D denote respectively a focusing and defocusing magnet, while 0 denotes the accelerating gap in between.

If more focusing and/or smoother oscillations are required, a longer period may be used instead of a F0D0, as for example F0F0D0D0 or F0F0F0D0D0D0 and so on (see Fig. 3.6). In some cases, the only way to achieve magnetic quadrupole focusing of low-charge heavy ions is to increase the number of lenses having the same sign in the focusing period.
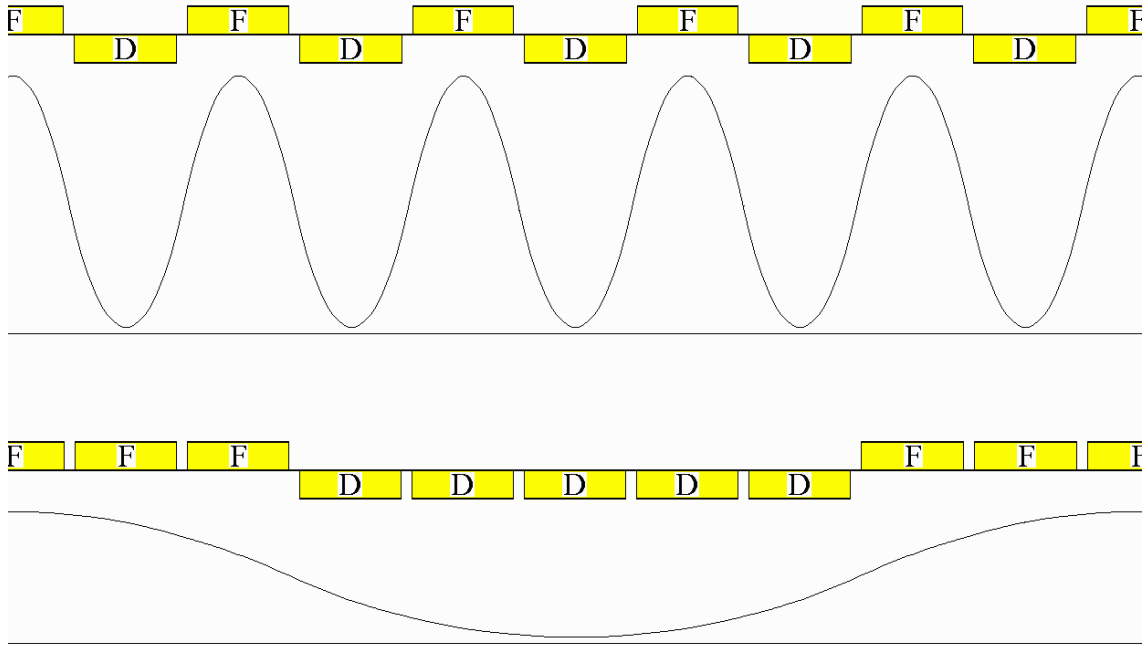
Figure 3.6: Comparison between a conventional F0D0 lattice and a 5F05D0 one.

If the number of lenses of the same sign in the period is increased to n, while the length L_q of each lens is held constant and the length of the period S is increased accordingly, then the situation is the following [Kap85]:

- the field gradient of the lenses falls off in proportion to $1/n^2$; consequently the power needed for focusing is significantly reduced;
- the defocusing factor and the phase oscillation swing increase in proportion to n^2; the stability region is therefore contracted;
- the current carrying capacity of the channel falls off in proportion to $1/n$.

The electric field in the gap is not spatially uniform; on the contrary, it penetrates inside the open holes of the tubes and the longitudinal component has a distribution as shown in Figure 3.7; moreover it is not constant in time.

36
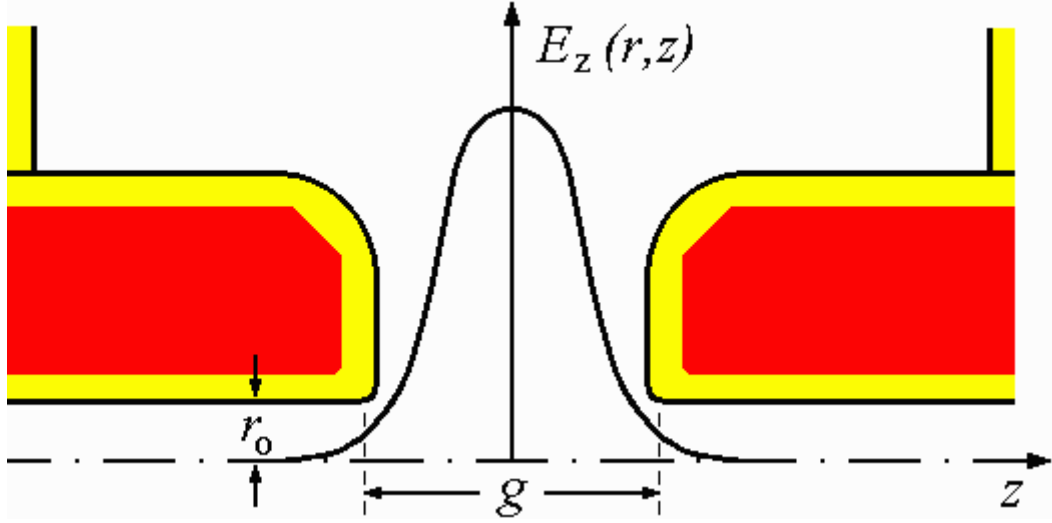
Figure 3.7: Longitudinal component of the electric field in the gap of a DTL cell.

Assuming circular symmetry, the amplitude of the field $E_z(r,z)$ at a small distance r from the axis at a given instant t can be expressed by a Fourier integral, as the sum of an infinite set of travelling waves:

$$E_z(r,z) = \int A(k_z) \, I_0(k_r r) \cos k_z z \, dk_z$$

where $k_z = \omega / v_p$ is the wave number, I_0 is the modified Bessel function of order zero, and $k_r = [k_z^2 - (\omega/c)^2]^{1/2}$ (dispersion relation). The complete distribution of each $A(k_z)$ can be known by inversion of the Fourier integral:

$$A(k_z) = (Eg/2\pi) \, [\sin (k_z g/2) / (k_z g/2)] / I_0(k_r r_0) = (Eg/2\pi) \, T(k_z)$$

where E is the field $E_z(r_0,z)$ at a distance r_0 (bore radius) from the axis, assumed to be constant, and g is the effective gap length (approximated by the real gap length +85% of the drift tube radius of curvature at the bore end). The <u>transit time factor</u> $T(k_z)$ has been introduced, which is defined on the axis of the cavity as:

$$T(k_z) = 1/(E_0 L) \int E_z(z) \cos k_z z \, dz = [\sin (k_z g/2) / (k_z g/2)] / I_0(k_r r_0)$$

where E_0 is the average longitudinal field in a cell and L is the cell length.

In this way the complete field distributions throughout the gap has been derived inside of a cylinder of radius r_o, the hole radius:

$$E_z(r,z) = (Eg/2\pi) \int T(k_z) \, I_o(k_r r) \cos k_z z \, dk_z$$

Including now the time factor $\cos(\omega t + \phi)$, a particle which crosses the mid gap at a constant distance r from the axis, with a constant velocity $v_p = z/t$ and a phase ϕ, gains in a cell an energy:

$$\delta W = q \int E_z(r,z) \cos(\omega z/v_p + \phi) \, dz =$$

$$= q \, Eg \, [\sin(k_z g/2) / (k_z g/2)] \, [I_o(k_r r)] / I_o(k_r r_o)] \cos \phi$$

Substituting Eg by $E_o L$ and introducing the transit time factor one gets:

$$\delta W = qE_o L \, T(k_z) \, I_o(k_r r) \cos \phi$$

It is also possible to compute the phase change across the gap, accounting for the change in velocity, and to consider the transverse component of the motion (i.e. the slope of the trajectory) at mid gap. The resulting expressions involve the additional field integral:

$$S(k_z) = 2/(E_o L) \int E_z(z) \sin k_z z \, dz$$

similar to the transit time factor, but calculated on half cell because of the odd sinus function, and the first and second derivatives of $T(k_z)$ and $S(k_z)$ with respect to k_z. With this correction, the variables W and ϕ are canonically conjugate and they fulfil Liouville's theorem [Lap87][Lap99].

The Drift Tube Linac structure of Alvarez type is world-wide used nowadays, for protons and ions with $0.03 < \beta < 0.40$, in the range of frequencies between 100 and 400 MHz.

For higher values of β, side-coupled cavities (SCC) are used, with frequencies ranging between 600 and 1200 MHz; focusing is installed in between sections. For electrons ($\beta=1$), iris-loaded cavities are used, with 3 or 4 cells per wavelength; frequency is usually above 1 GHz; transverse defocusing is very weak, since particles

see a much shorter linac, because of the relativistic contraction of lengths. For very small values of β, Radio Frequency Quadrupoles (RFQ) are the best choice [Kap70].

H-mode cavities may allow significantly higher beam intensities (around 2 A) and relax the complexity of beam accumulation; the possibility of basing the driver design on an Interdigital H-mode DTL, using the "Combined 0° Structure" beam dynamics, has been discussed [Rat97].

CHAPTER 4

DESCRIPTION OF THE USED CODES

4.1 General remarks

An analytic description of particle motion is possible only for the self-consistent K-V distribution. For non-consistent distributions, computer codes allow to simulate particle motion. Both PARMILA [Str88] and MAPRO [Mar71] codes are multi-particle simulation programs which transport a 6-dim distribution in the phase space through a user-defined generated structure.

The total charge Q of a single bunch is given by the ratio between the current and the frequency, i.e. $Q = I / f_{rf} = 400$ mA $/ 200$ MHz $= 2$ nC for the HIDIF main linac. The number of singly charged particles in a bunch is given by $N_p = Q/e = 2$ nC $/ 1.6 \times 10^{-19}$ C $= 1.25 \times 10^{10}$. Even the most modern computers are not powerful enough to cope with such a big number of particles, therefore for a realistic simulation of an intense beam "macroparticles" will be used, each one equivalent in mass and charge to a few million "real" particles. The motion along the structure is then simulated by thousands of macroparticles (for instance 1000, 5000, or 20,000). The reliability of this approximation is discussed in Chapter 4.3.

The tracking program has to calculate the motion of such a set of macroparticles, under the effect of some "external" forces (accelerating rf electric field, focusing magnetic field) and of "internal" space-charge forces. To evaluate space-charge forces, several routines may be used, which are based on different models, for instance:

- a numerical integration using analytical expressions valid for an ellipsoidal bunch;
- a Fast Fourier Transform (FFT) routine to solve Poisson's law in a 2-dim mesh, assuming circular symmetry for the bunch;
- a general 3-dim series expansion (for instance of Hermite polynomials) of the charge;

- a point-to-point computation (single-particle solver) with no assumption on the geometry.

For investigating the emittance growth and the halo formation process in an intense heavy ion beam, a 3-dim single-particle solver (which impose therefore no constraints on the shape of the bunch) seems to be the most appropriate choice. For this reason it was decided to use the program MAPRO, which moreover allows to use the first two of the above mentioned possibilities.

The linac is divided into many short cells and the particle distribution is transported from one cell to another, up to the end of the system.

The external forces due to the magnetic focusing are calculated in the middle of a drift tube (i.e. of a quadrupole lens); those due to the electric rf field are calculated in the middle of the gap; space-charge forces are computed in both positions, i.e. twice per cell.

The information needed to compute the external forces is contained in some files normally provided by the programs ADAPT and GENLIN; the latter, on its turn, interpolates the output files generated by another program named CLAS [Mar68].

Unfortunately the program ADAPT cannot deal with the 5F05D0 focusing scheme chosen for the HIDIF linac, therefore a new Fortran routine had to be written.

The procedure to be followed in order to perform a numerical simulation of beam transport along a DTL is the following (see Fig. 4.1):

- at first CLAS must be run a few times for different values of β (corresponding at different energies) to find the proper geometry of some cells of the linac at the given frequency and to calculate the electric field distribution inside them;
- then GENLIN interpolates the output files from CLAS code to generate the needed parameters for all the intermediate cells, according to a given phase law;
- then ADAPT (in our case the self-written routine) generates all the quadrupole gradients, according to a given tune or focusing law;
- finally MAPRO tracks the particles through the linac, with space-charge calculation; it computes all the quantities which are relevant in the design of the linac and produces several output files.
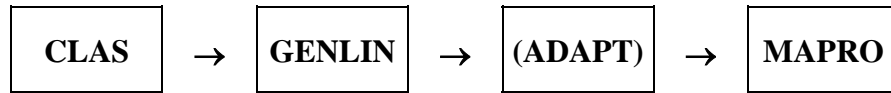
| CLAS | → | GENLIN | → | (ADAPT) | → | MAPRO |

Figure 4.1: Scheme of the program chain

4.2 The program chain

The Program CLAS

The program CLAS [Mar68] allows to define the geometry of a DTL cell for a given particle velocity β. In particular, after having found the dimensions that give the chosen resonant frequency, it computes the distribution of the electromagnetic fields inside the cell and the complete set of required transit time factors (see Chapter 3.6) from solving Maxwell's equations. It must be run to generate a proper number of cells along the linac, corresponding to different energies, for further interpolation.

The cell length $\beta\lambda$ is determined by the frequency; all the other geometrical parameters (gap length, tank diameter, aperture of the drift tube, radii of curvature...) have to be varied manually until the pre-given frequency is obtained.

This program was running on a VM environment at KFA-Jülich; it has been moved into a Unix system at IAP-Frankfurt and successfully installed. A major effort was requested on the implementation of the Bessel's functions, since the internal functions (based on an assembler routine) were not working, and some of them were not existing in the standard library of the cluster [Par96].

The Program GENLIN

The program GENLIN interpolates the output files from CLAS code and it generates the linac parameters for a given phase law. In particular, it computes the cell and the gap lengths, the transit-time-factor integrals which are needed to solve the equations of motion [Pro71], the amplitude and synchronous phase of the accelerating electric field for all the intermediate cells. These results are written in four output files.

This allows to know the total number of cells which are needed (and therefore the overall linac length) as well as information on the power (transferred into the beam and dissipated in the cavity walls) and on the average shunt impedance.

Also this program has been moved from a VM environment at KFA-Jülich into a Unix system at IAP-Frankfurt and successfully installed, requiring only small modifications [Par96].

The routine which replaces the program ADAPT

Since the program ADAPT cannot deal with the 5F05D0 focusing scheme, it could not be used for our purposes. Three of the four files which it should produce have been generated by means of a self-written Fortran routine which imposes a fixed bore radius, a quadrupole length equal to 80% of the drift tube length and a constant product between quadrupole length and gradient. The fourth file, which contains the Twiss parameters and the emittances at injection, had to be written by hand (the proper values were found running MAPRO until the beam was well matched).

The Program MAPRO

The program MAPRO [Mar71] tracks the particle distribution through the linac including space-charge calculation. The required input data are read (subroutine INPUT) from a command file, from the four output files generated by GENLIN and from the four output files generated by ADAPT or, in our case, from the self-made code. The requested data are prepared according to these values (subroutine GENLIN).

The input distribution is user-defined. A 4-dim input distribution (waterbag or Gaussian) may be generated by MAPRO code for the transverse planes; a 2-dim one for the longitudinal plane (subroutine INFILL and WBACK or GAUSS). For allowing the generation of a 6-dim waterbag input distribution a new algorithm had to be written and included into the code.

The full emittances and the Twiss parameters $\alpha_{x,y,z}$ and $\beta_{x,y,z}$ in all the three planes are required; in case of a Gaussian distribution, a cut-off radius should be given in terms of the variance of the distribution (i.e. how many σ). There is also a possibility to start the simulation reading from a file some given (previously generated) distribution.

The random number generation routine used to produce the co-ordinates of the particles in the 6-dim space (function RANF) has been copied from PARMILA code and properly adapted.

Each cell is sub-divided into four segments: from the middle of the quadrupole to its end, from here to the middle of the gap, from here to the beginning of the following quadrupole and from here to the its middle. At the beginning of each segment the forces acting on the particles along it are calculated; the beam is then transported up to the beginning of the next segment. The tracking procedure is illustrated in Figure 4.2.
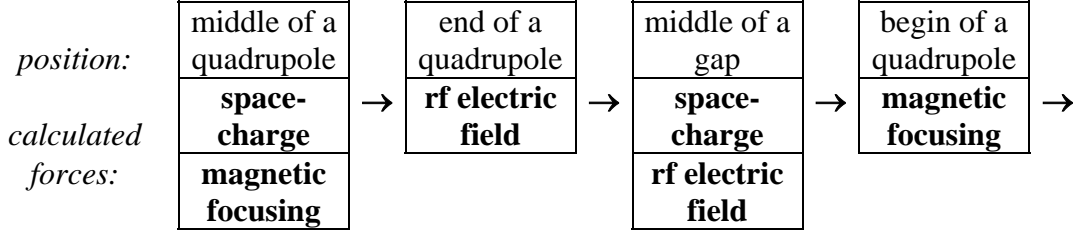
position:	middle of a quadrupole		end of a quadrupole		middle of a gap		begin of a quadrupole	
calculated forces:	**space-charge**	→	**rf electric field**	→	**space-charge**	→	**magnetic focusing**	→
	magnetic focusing				**rf electric field**			

Figure 4.2: Scheme of the tracking procedure.

1. The calculations start in the middle of a drift tube, which is also the middle of a quadrupole. In this position only the effects of internal space-charge forces and of external (linear) forces due to the magnetic focusing are considered.

   Space-charge (subroutines CHARGE and CHARG2): for each pair of particles, the distance vector $\mathbf{d}_{ij} = \mathbf{r}_i - \mathbf{r}_j$ is calculated, where $\mathbf{r}_i$ and $\mathbf{r}_j$ are the position vectors of the i-th and j-th macroparticle in xyz Cartesian co-ordinates. The force vector is given by $\mathbf{F}_{ij} = (q^2 / 4\pi\varepsilon_0)\,\mathbf{d}_{ij}\,/\,|\mathbf{d}_{ij}|^3$ for the i-th macroparticle, and $\mathbf{F}_{ji} = -\mathbf{F}_{ij}$ for the j-th one. The variation of momentum $\mathbf{dp}_i$ for the i-th macroparticle is obtained from $\mathbf{F}_{ij}$ multiplying it for a proper coefficient, depending upon the time step. The time step is related to the distance between two consecutive calls of the space-charge routine, which in our case is half cell.

   If the time step is too large, two macroparticles might become very close to each other, while in reality this would not happen; as a consequence, the huge resulting force might "kick" them away from the beam. In order to avoid this numerical effect, a cut-off distance d_{cut} is introduced, equal to the average distance between macroparticles: if $|\mathbf{d}_{ij}| < d_{cut}$ then the cut-off distance is used to compute the force. The reliability of this approximation is discussed in Chapter 4.3.

   Magnetic focusing (subroutine QG): for each macroparticle, the transfer matrices M_F and M_D are built, where the strength $k = eG/p_i$ is not the average one, but depends on

the momentum p_i of the actual macroparticle; then the 4 co-ordinates x_i, x'_i, y_i, y'_i are transported by means of such matrices up to the end of the quadrupole.

2. In the next segment only the external forces due to the rf electric field are considered (subroutine DG1). The amplitude $E_z(z,r)$ of the electric field in the gap is expressed by a Fourier integral (see Chapter 3.6), where the complete set of required transit time factors was calculated by CLAS and GENLIN codes. With MAPRO code the energy gain of a particle is calculated keeping into account the transverse component of the motion and the phase change across the gap, owing to the change in velocity.

3. In the middle of the gap, the effect of space-charge is considered again (subroutines CHARGE and CHARG2).

4. In the next segment only the external forces due to the rf electric field are considered (subroutine DG2): in analogy to subroutine DG1, the particles are transported by means of matrices up to the beginning of the following quadrupole.

5. In this position only the external forces due to the magnetic focusing are considered (subroutine GQ): in analogy to subroutine QG, the particles are transported by means of matrices up to the middle of the quadrupole. Here, the simulation continues from step 1 for the following cell.

Along the linac several quantities are calculated in the middle of each drift tube and of each gap (subroutine CHAS); among the others, the first and second moments (see Chapter 3.1) of the discrete particle distributions:

$$\langle x \rangle = (1/N) \sum_i x_i \qquad \text{with } i = 1, 2, ..., N$$
$$\langle x^2 \rangle = (1/N) \sum_i (x_i - \langle x \rangle)^2 \qquad \text{with } i = 1, 2, ..., N$$

which allow to define several average quantities as: position of the bunch center, rms beam sizes (a_x, a_y and b), rms emittances (normalized and not), Courant-Snyder parameters ($\alpha_{x,y,z}$, $\beta_{x,y,z}$, $\gamma_{x,y,z}$), beam temperatures ($T_\perp$ and $T_\parallel$), full current tunes (σ_t and σ_l), average particle distance $\langle d \rangle$, Debye length λ_D, and so on.

Lost particles, if any, are detected (subroutine NEWLOS) and information on the reason of the loss are given.

An alpha-numeric graphic output is available (subroutine GRAPH), which has a quite poor resolution; for this reason some interesting values (as rms emittance growth, rms radius, tunes along the linac, input and output distributions) were written into new output files, in order to be presented later in a better graphic form.

Furthermore, a new routine had to be written (subroutine FULL) in order to compute the full (100%, 99% and 95%) emittances and the full beam radius, and to write them into further new output files. The used algorithm finds the smallest ellipse which includes the given fraction of the particles and has the same shape and orientation as the rms one.

The program MAPRO was running on a VM environment at KFA-Jülich; it has been moved into a Unix system at IAP-Frankfurt and successfully installed [Par96]. In addition to the changes and improvements above mentioned, some further modifications were needed:

- the maximum allowed number of cells has been increased from 250 to 9999;
- the maximum allowed number of particles has been increased from 2000 to 20,000;
- the possibility of subtracting the oscillation of the bunch centre has been added;
- the possibility of using a DTL cavity as buncher ($\varphi = -90^o$) has been added.

4.3 Discussion of the space-charge model

Number of macroparticles

Since the single-particle solver considers the Coulomb interactions between each pair of macroparticles, the computing time required for space-charge calculations scales as the square of the particles' number. On a dedicated Sun-workstation, a run with 1000 macroparticles requires about 2 hours; increasing the particles' number to 10,000 brings the required time to more than one week... Then a good compromise between speed and precision must be found.

As a first guess, it was tried running with 1000 macroparticles, as the maximum value allowed by MAPRO was 2000. Looking at the plot of the rms emittance along the linac, big oscillations were observed. After modifying the code to increase the limit of 2000, it was tried running with 5000 macroparticles. The simulation required about 2 days, but the oscillations of the curves resulted much smoother. Finally 20,000 macroparticles were tracked and, after about 5 weeks, an almost monotonous curve was obtained, without major changes (see Fig. 5.5 in next Chapter).

The slope of the curves is however the same for the three cases, as well as the final value of the rms emittance growth. Then it was concluded that 1000 macroparticles are already sufficient for a fast check (for example to test a new configuration), while 20,000 macroparticles yield to a precise result. A good compromise between computing time needed and loss of information can therefore be fixed around 5000 macroparticles; most of the results presented in this thesis have been obtained with such a number of macroparticles, unless explicitly declared.

It should be noticed that a single macroparticle represents 1/5000 of the beam current and power, i.e. 80 μA and 800 kW for 400 mA at 10 GeV (linac end), whereas the maximum allowed losses (1 W/m) correspond to a small fraction of a macroparticle. For a final beam dynamics check, at least one million macroparticles would then be needed!

Cut-off radius

If the distance between two dimensionless macroparticles becomes very small ($d_{ij} \rightarrow$ 0), then the Coulomb force ($F_{ij} \rightarrow \infty$) kicks them away with such an energy that they are lost; this cannot happen in reality, because the trajectories are bent before the distance vanishes. To prevent this <u>numerical</u> effect, one assumes that macroparticles cannot get closer than a minimum given distance d_{cut}; each macroparticle is therefore considered as a sphere which may experience elastic collisions, rather than as a point; the radius of this sphere is called "cut-off radius".

MAPRO allows three possible definitions of a cut-off radius d_{cut}: the average distance $\langle d \rangle$ between macroparticles, the Debye length λ_D or the radius $r_{1\%}$ of a sphere having 1% of the bunch volume. At the beginning of the linac, with a nominal "4d+2d"

waterbag distribution for 5000 macroparticles, one has $\langle d \rangle = 0.52$ mm, $\lambda_D = 3.65$ mm and $r_{1\%} = 1.92$ mm; these values remain almost constant during acceleration.[*]

Since the maximum angle x' or y' of a macroparticle trajectory never exceeds 1.0 mrad and the single-particle solver is called every half-cell, i.e. always less than 24 cm, then a macroparticle cannot move transversally by more than 0.24 mm between two space-charge calculations. For this reason, the average distance between macroparticles was chosen, i.e. $d_{cut} = \langle d \rangle$, because this definition leads to the smallest cut-off radius, which is nevertheless large enough to avoid the singularity.

[*] As it was mentioned in Chapter 3.1, the relation $\lambda_D \gg \langle d \rangle$ implies that Liouville's theorem remains valid with a good approximation even for interacting particles, i.e. the rms normalized emittance is conserved.

CHAPTER 5

PARTICLE DYNAMICS DESIGN OF A BI$^+$-ION DTL

In the scenario presently discussed by the HIDIF group for a Heavy Ion Driven Inertial Fusion facility, a Drift Tube Linac of Alvarez type is proposed as main linac for the acceleration of intense beams of singly charged heavy ions up to an energy of 10 GeV (see Chapter 2). The ion species selected as reference is ^{209}Bi$^+$; the requested beam intensity has been fixed to 400 mA, after our preliminary results confirmed that it was feasible [Dei97][Dei97b][Par97]. The main linac has therefore to accelerate and focus such an intense beam to a final specific energy of about 50 MeV/u.

The choice of the other linac parameters is mainly determined by the requirements of the HIDIF facility. Using well known analytical formulae, given in Chapter 3, a study has been performed to find a range of beam and structure parameters (e.g. frequency, shunt impedance, energy, emittances and focusing scheme), in which the requirements on a DTL for a Heavy Ion Driven Inertial Fusion facility can be well fulfilled [Par98b]. Beam dynamics aspects have been checked by numerical simulations [Dei98][Dei98b].

5.1 Parameter choice

The existing ion sources are not able to produce a current of 400 mA Bi$^+$: for a 7-hole extraction with high voltage, values up to 70 mA have been recently reported; with a lower extraction voltage a 38.5 mA beam has been achieved in Frankfurt. An emittance of $0.27\,\pi$ mm mrad (80% norm.) was measured at 21 mA [Web97]. Moreover, low energy accelerators (RFQ) could not accept 400 mA current, as space-charge forces would be too large. The beams from several ion sources must then be extracted, accelerated and merged together in a funnel tree [Bon81], as indicated in Figure 2.1 and 2.2 of Chapter 2.

Following the scheme of funnelling, already proposed for HIBALL, and taking the above measured values of ion source currents and emittances, there are only a few degrees of freedom for the choice of frequency and injection energy for the main linac. In fact, the properties of the injection system have a large influence on the linac parameters.

In each funnel step the frequency of the linac and the current are doubled. Assuming three funnel steps and including some 20% losses at beam formation, an ion source current of 60 mA is required; this current might be lowered to 30÷35 mA, assuming four funnel steps.

The first accelerator is an RFQ, which is able to capture, focus and bunch the beam even at high space-charge forces. Its frequency must be chosen with respect to the input ion velocity; for a Bi^+ ion source with an energy of about 1.2÷1.5 keV/u (obtained with a dc post-acceleration of 250÷300 kV after extraction) an appropriate choice is 12.5 MHz. At this frequency, a beam intensity of 30 mA can be easily accepted by the RFQ, whereas 60 mA are still accepted but already close to the RFQ current limit.

During acceleration in the RFQ, the dc current from the ion source is formed to bunches of about $\pm 30^o$ phase width. Owing to the high space-charge forces in the beam, the initial bunch length will stay nearly constant, i.e. the ion energy should be increased by a factor of $2^{8/3} \cong 6.4$ before the frequency can be doubled in the next funnel step, to avoid dilution in the longitudinal phase space [Kle68]. With these assumptions and after 3 funnel steps, one ends up with a frequency of 100 MHz and an injection energy of about 2÷3 MeV/u for the main linac; alternatively, after 4 funnel steps, with a frequency of 200 MHz and an injection energy of about 10÷12 MeV/u.

In both cases the standard formulae of Mittag [Mit78] show that the longitudinal acceptance of the main linac is large enough to capture a beam with an rms emittance of 25 π deg MeV without filamentation.

In order to choose between the two possibilities, it was decided to maximize the effective shunt impedance Z_{eff}, which is a measure of the linac efficiency:

$$Z_{eff} = (E_o T \cos \phi_s)^2 \, L / P_s \qquad \text{in } [M\Omega/m]$$

where P_s is the rf power dissipated in the walls of an accelerating structure of length L.

For a 100 MHz DTL structure of Alvarez type, the effective shunt impedance drops in the high energy end of the linac: to improve the efficiency, a frequency jump in the main linac would be necessary, leading to a higher peak current (800 mA) and empty rf buckets. For a 200 MHz structure, on the contrary, Z_{eff} changes only slightly in the whole velocity range. For all these reasons the frequency of 200 MHz was preferred, for which the technology is well proven in different laboratories. As seen above, this choice yields to four funnel steps (starting with 30÷35 mA from 16 ion sources) and to an injection energy of 10÷12 MeV/u, which also helps in overcoming the longitudinal phase space filamentation.

5.2 Reference layout

A particle dynamics layout of a conventional 200 MHz Alvarez Drift Tube Linac has been investigated, with respect to low emittance growth and high transmission, trying to avoid the space-charge-dominated regime. Beam dynamics calculations have been performed for a reference 400 mA ^{209}Bi$^+$ ion beam accelerated from 10 MeV/u (β = 14.5%) to 50 MeV/u (β = 31.4%).

The geometry of the linac has been generated using the two codes named CLAS and GENLIN, then the beam behaviour along the linac has been examined running beam dynamics calculations with the code named MAPRO (see Chapter 4).

The average electric field amplitude E_o was set to a rather conventional 3.0 MV/m. A scaling law for the synchronous phase was determined keeping into account that:

- the longitudinal current limit increases as $\phi_s^2 \sin|\phi_s|$, as shown by Eq. (3.3);
- the effective rate of acceleration decreases as $\cos \phi_s$ (since $E_{eff} = E_o T \cos \phi_s$);
- the transverse space-charge effects decrease as $1/\phi_s$ [Mit78];
- the rf defocusing effect scales as $\sin \phi_s$ [Mit78].

Therefore a reasonable choice for ϕ_s seems to be -40° at input, to increase the longitudinal acceptance; the synchronous phase is then exponentially decreased to -30° in a few periods (about 130 m of length) and then kept constant up to the end of the linac, to gain acceleration rate.

With an average electric field amplitude $E_o = 3.0$ MV/m and the above scaling law for the synchronous phase, the linac results to be made of 9775 cells, corresponding to a length of 3.38 km. The calculated shunt impedance has a quite reasonable average value of 26 MΩ/m, which gives an overall linac efficiency of nearly 30% [Bon98b]. The total ac-

accelerating field E_oT (including the transit time factor T) is 2.80÷2.88 MV/m; the total voltage gain of 8.4 GV gives an average effective accelerating field (including now also the cosine term) of 2.5 MV/m.

When generating the geometry of the linac, a drift tube aperture (bore radius) of about 1.6 cm came up, in order to limit the maximum magnetic field at the pole tip to about 1÷1.2 Tesla. Consequently, the transverse focusing turned out to be too weak for the conventional F0D0 or F0F0D0D0 quadrupole configuration normally used.

Schemes from 3F03D0 to 7F07D0 have been studied, in order to limit the maximum field in the quadrupoles; all of them seem to be possible solutions. A 5F05D0 focusing scheme (that is F0F0F0F0F0D0D0D0D0D0) was then adopted, as proposed in [Kos96] [Dei96], and no optimisation has been done for the other cases. Going to this longer period resulted in a smoother focusing and a maximum pole tip field of 1.15 Tesla at linac input, corresponding to a maximum gradient of about 72 T/m.

The main linac parameters are summarized in Table 5.1.

Table 5.1: Linac parameters.

Mass number A	209 (Bi$^+$)	
Current I	400	mA
Frequency f_{rf}	200.0	MHz
Injection Energy W_{in}/A ($\beta = 0.145$)	10.0	MeV/u
Extraction Energy W_{out}/A ($\beta = 0.314$)	50.0	MeV/u
Total energy gain $W_{out} - W_{in}$	8.36	GeV
Number of cells N_c	9775	
Cell length $\beta\lambda$	21.8 ... 47.1	cm
Total linac length L_{tot}	3383	m
Average electric field amplitude E_o	3.00	MV/m
Total electric field amplitude E_oT	2.80 ... 2.88	MV/m
Average electric field $(W_{out} - W_{in})/L_{tot}$	2.47	MV/m
Synchronous phase ϕ_s	−40 ... −30	deg
Aperture radius r_o	1.6	cm
Max. magnetic gradient G_{max}	72.2	T/m
Max. pole tip field $G_{max} r_o$	1.15	Tesla

Average shunt impedance $\langle Z_{\mathrm{eff}} \rangle$	26	MΩ/m
Peak beam power P_b (62.5% chopping)	690	kW/m
Peak dissipated power P_s	320	kW/m
Total power needed $P_b + P_s$	1.0	MW/m

For proper injection into the following storage rings, a small transverse emittance is required for 99% of the beam, namely $\varepsilon_{\mathrm{full,99\%}} < 4\,\pi$ mm mrad (i.e. $1.26\,\pi$ mm mrad, normalized). The requirement on momentum spread for 99% of the beam is $dp/p < \pm 2 \times 10^{-4}$; this corresponds to an energy spread $dW/W < \pm 4 \times 10^{-4}$, since $dW/W \cong 2\,dp/p$, i.e. $\Delta W < \pm 4$ MeV, since $W_{\mathrm{out}} = 10$ GeV.

The full unnormalized input emittance was set to $7.2\,\pi$ mm mrad in both transverse planes (corresponding to a normalized value of $1.05\,\pi$ mm mrad) thus allowing only a 15% emittance growth along the linac; the full input emittance in the longitudinal plane was set to $100\,\pi$ deg MeV (or $6.7\,\pi$ ns keV/u). It has been assumed that these small values can be obtained by the funnelling tree: although they are within the feasibility range for a conventional injector, in this case the beams from 16 ion sources must be captured, accelerated and merged, to produce a high current beam.

A 4-dim waterbag distribution was used as an input for the transverse planes, which means the rms emittance is 6 times smaller: $1.2\,\pi$ mm mrad, unnormalized (and $0.176\,\pi$ mm mrad, norm.). A 2-dim waterbag distribution was used as a longitudinal input, which means a 4 times smaller rms emittance of $25\,\pi$ deg MeV (or $1.66\,\pi$ ns keV/u).

It is practical to begin the focusing channel in the middle of the third lens of the same kind, since the initial conditions for the matched beam in this case can be simplified because the beam must have a crossover ($\alpha_x = \alpha_y = 0$) at the channel entrance and the emittance ellipse is in upright position. The input matching conditions can be satisfied just by selecting the proper beam cross section at this point.

For the above emittance values, the best matching conditions have been found when the transverse betatron amplitudes are $\beta_x = 9.0$ m and $\beta_y = 6.3$ m, corresponding to transverse beam sizes of ± 7.3 and ± 6.1 mm. In Figure 5.1 the focusing scheme and the betatron functions are plotted, showing a low flutter factor ($\Psi^2 = \beta_{\mathrm{max}}/\beta_{\mathrm{min}} = 1.43$).

The best longitudinal matching has been obtained for an initial betatron amplitude $\beta_z = 11.37$ m, corresponding to an input bunch length of $\pm 21.5^\circ$ and to an energy spread

$dW/W = \pm 0.23\%$ (i.e. $\varDelta W = \pm 4.8$ MeV, since $W_{in} = 2.1$ GeV); these seem realistic values.

The zero current tunes σ_{to} and σ_{lo} have been calculated analytically, by multiplicating the proper transfer matrices; the full current ones come from simulation results using the smooth approximation rules $\sigma_t = \varepsilon_{t,rms}S/a^2$ and $\sigma_l = \varepsilon_{l,rms}S/b^2$, with S the period length (10 $\beta\lambda$), a and b the rms bunch sizes (see Chapter 3). The tune depression values indicate that the reference design is **not** space-charge dominated.
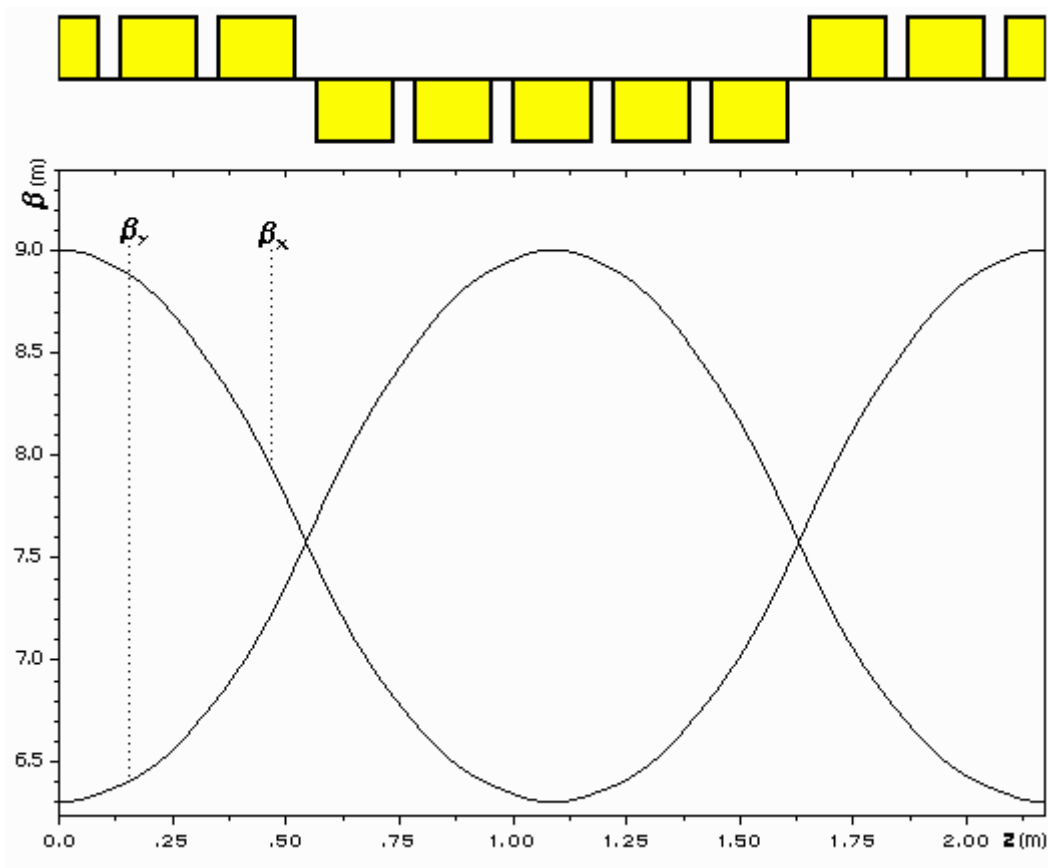
Figure 5.1: Chosen focusing scheme: plot of β_x and β_y.

The beam behaviour has been examined in the DTL generated by the CLAS and GENLIN codes, running beam dynamics calculations with the MAPRO code. To save computation time, at first only 1000 macroparticles were tracked along the linac, which was enough to deliver guidelines for optimizing the input beam parameters until, after a few iterations, good results in terms of emittance growth were reached [Dei97]. In this process, also the linac geometry has been slightly adjusted (Tab. 5.1 shows the final reference parameters).

A tracking with 5000 fully interacting macroparticles gave better symmetry and slightly smaller rms emittance growth. From this point on, this will be considered as the reference layout. The nominal values of the beam parameters for this case are shown in Table 5.2.

It can be observed that the requirements on the output transverse emittance are fulfilled, since $e_{full,99\%} = 1.15 < 1.26\,\pi$ mm mrad (normalized). No particles have been lost (100% transmission).

Table 5.2: Beam parameters.

	input	*output*	
Number of particles	5000	5000	
Trans. rms norm. emittance	0.176	0.183	π mm mrad
Trans. full (*in* 100%, *out* 99%) norm. emittance	1.05	1.15	π mm mrad
Trans. rms unnorm. emittance	1.20	0.583	π mm mrad
Trans. full (*in* 100%, *out* 99%) unnorm. emittance	7.20	3.66	π mm mrad
Long. rms emittance	1.66	1.83	π ns keV/u
id. *	25.0	27.5	π deg MeV
Long. full (*in* 100%, *out* 99%) emittance	6.7	10.6	π ns keV/u
id. *	100	160	π deg MeV
Full current transverse tune σ_t	17	28	deg/period
Zero current transverse tune σ_{to}	22	31	deg/period
Transverse tune depression σ_t / σ_{to}	0.77	0.90	
Full current longitudinal tune σ_l	11	6	deg/period
Zero current longitudinal tune σ_{lo}	13	10	deg/period
Longitudinal tune depression σ_l / σ_{lo}	0.85	0.60	
Trans./long. temperature $T_\perp / T_z$	0.7 / 1.3	1.3 / 0.8	keV
Trans./long. rms bunch size a / b	3.0 / 6.4	2.3 / 8.7	mm

* 1 [ns keV/u] $\leftrightarrow$ 15 [deg MeV] for f_{rf} = 200 MHz and A = 209.

Figure 5.2 shows the input distribution for 5000 macroparticles (4-dim waterbag transversally, 2-dim waterbag longitudinally) and the resulting output distribution at the end of the nominal linac. As can be seen, the bunch remains quite compact in all phase space planes and only a small halo develops; the slight asymmetry in the longitudinal distribution is due to the nonlinear part of the rf field on the long bunch tails.

The requirement on momentum spread for 99% of the beam is not fulfilled at the linac end, since the energy spread for 99% of the beam is about $\pm 8 \times 10^{-4}$ (i.e. $dp/p = \pm 4 \times 10^{-4}$); however, it is still possible to obtain $dp/p < \pm 2 \times 10^{-4}$ by adding a bunch rotation system after a drift at the end of the linac, as described in Chapter 8.

Figure 5.3 shows the total emittance along the linac for 100%, 99% and 95% of the beam. It can be observed that the ratio full-to-rms emittance stays below 10 for 99% of the beam (in fact, $\varepsilon_{rms} = 0.18$ and $\varepsilon_{full,99\%} = 1.00 \div 1.15\ \pi$ mm mrad); then constraints on full emittance are respected and a reserve is left for additional growth due to errors [Par97].

Figure 5.4 shows the full radius along the linac for 100%, 99% and 95% of the beam. It can be seen that the maximum radius (8.5 mm) fills only a half of the 16 mm aperture.
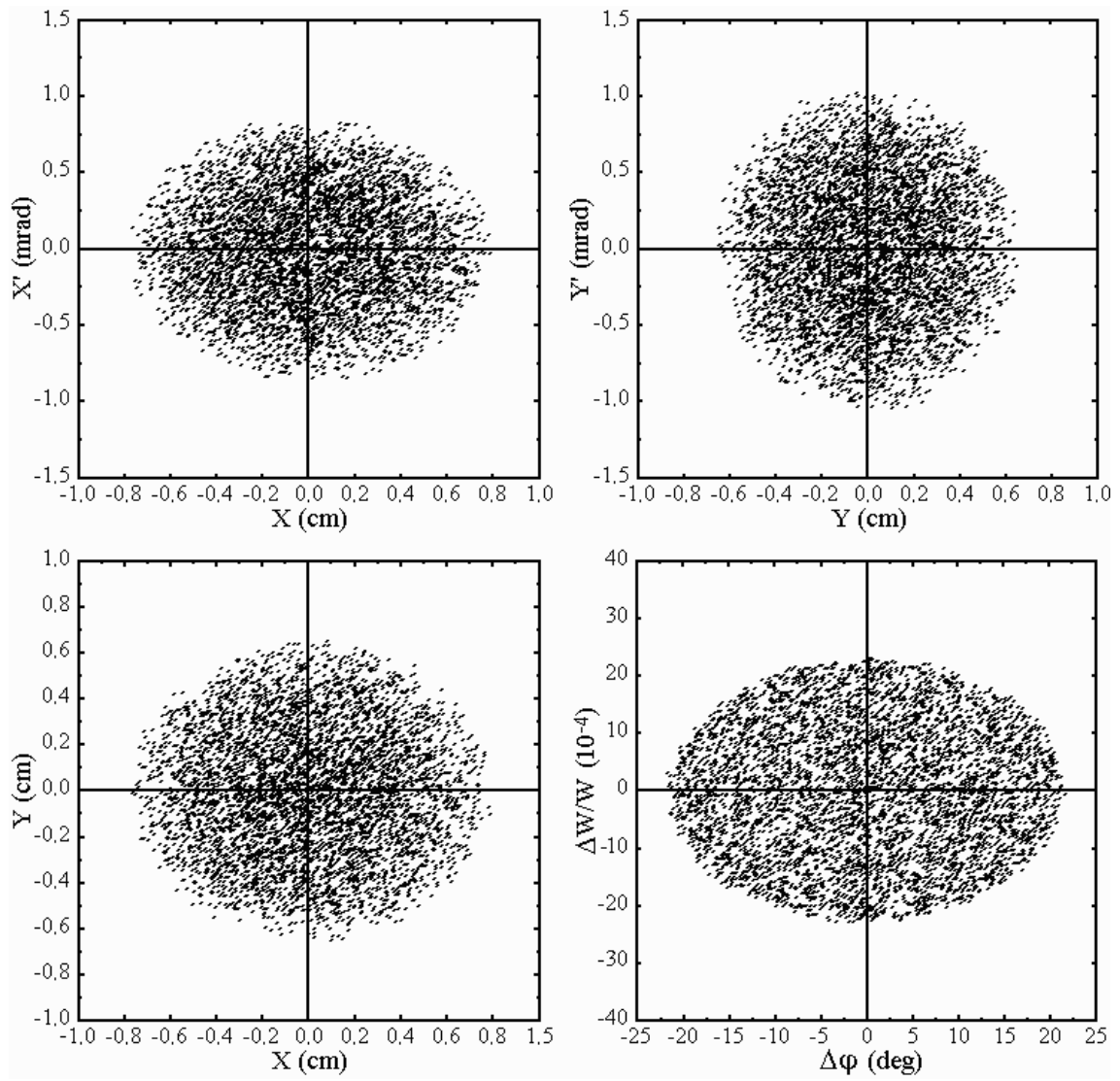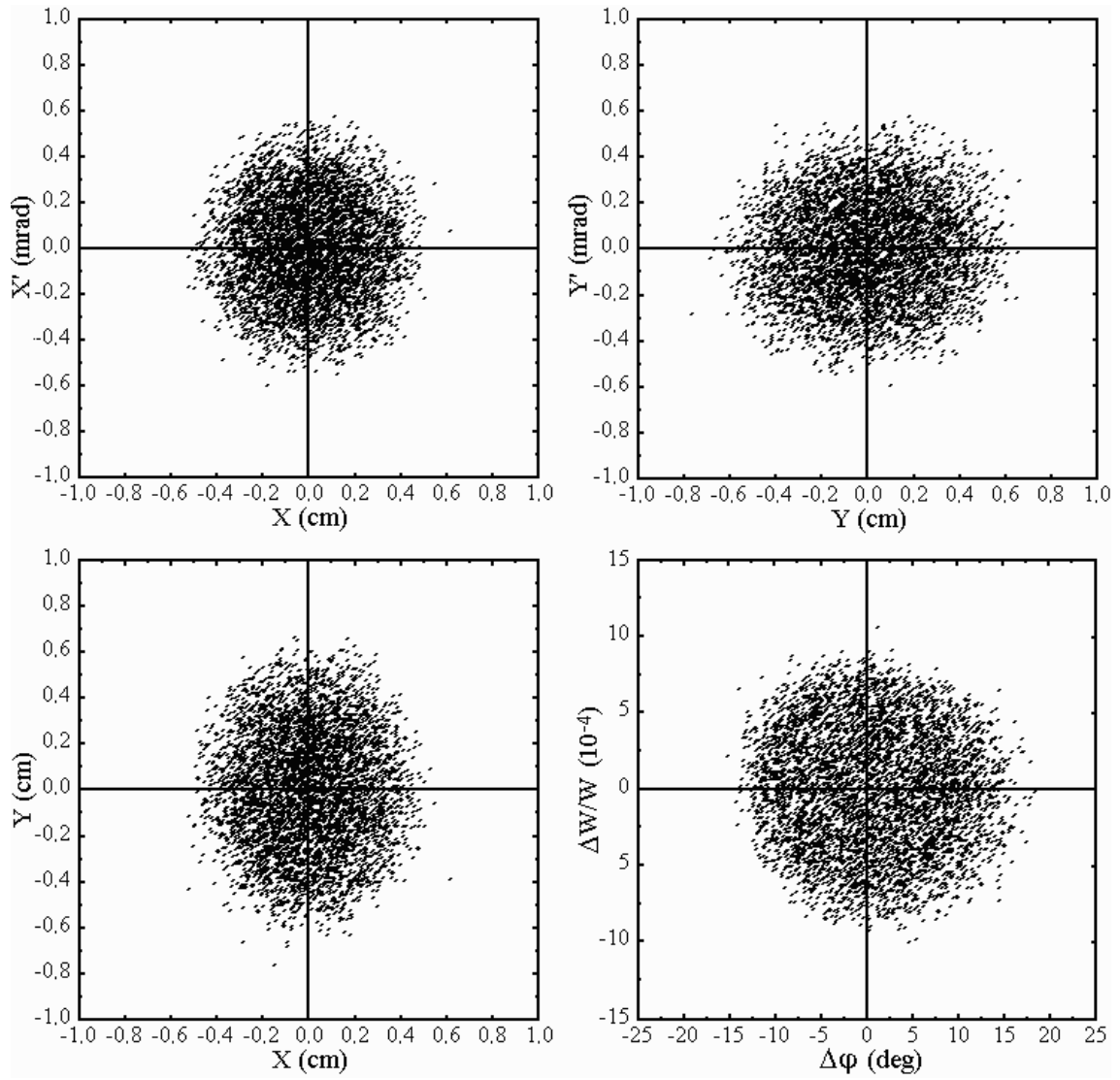
Figure 5.2: The "4d+2d" waterbag input distribution for 5000 macroparticles (upper) and the corresponding output distribution at the end of the nominal linac (lower).
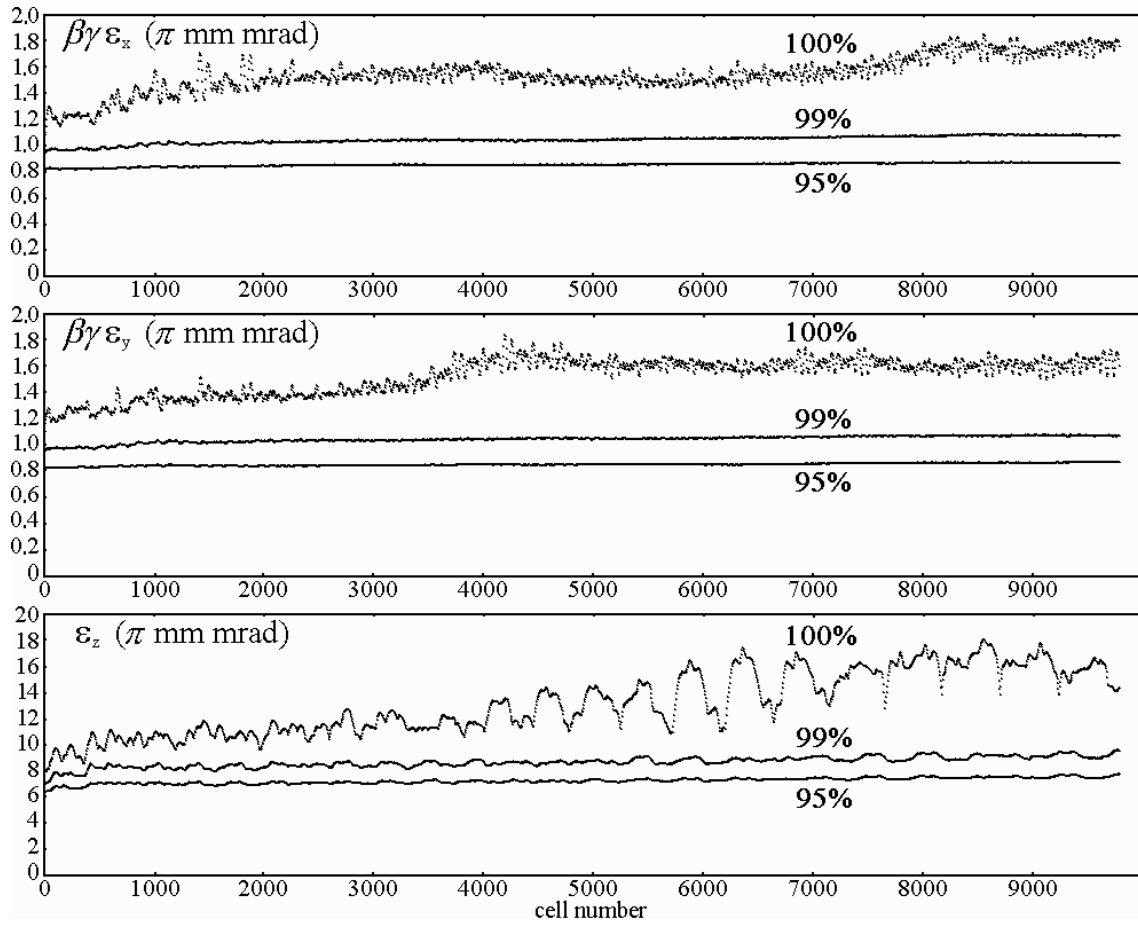
Figure 5.3: Development of the full (100%, 99% and 95%) emittance with 5000 macroparticles along the nominal linac with nominal input.
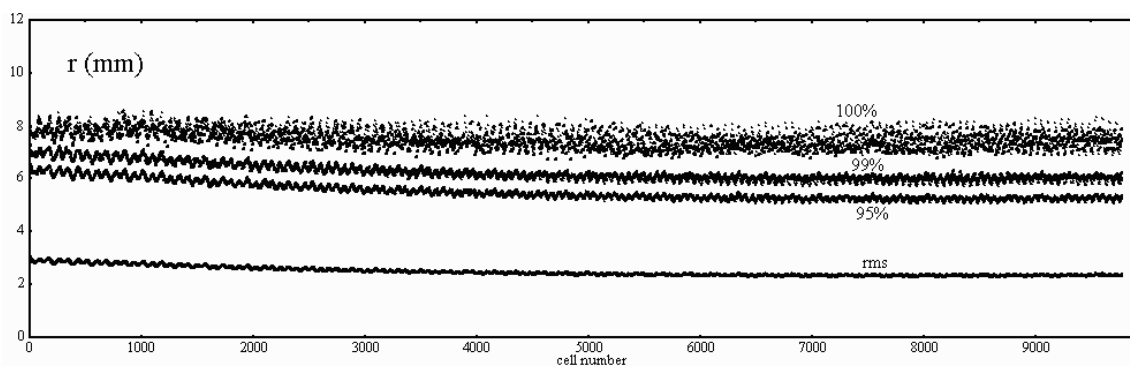
Figure 5.4: Development of the full (100%, 99% and 95%) radius with 5000 macroparticles along the nominal linac with nominal input.

For a final control, the number of macroparticles was increased to 20,000, to improve space-charge calculations; this was quite time consuming, since the computation time grows as the square of the number of macroparticles: the job run several weeks on a dedicated SUN-workstation.

The plot of the rms emittance growth along the DTL (Fig. 5.5) shows that a higher number of particles leads to a smoother behaviour, but no major changes can be observed. As can be seen also from Table 5.2, the output rms emittance growths were $\Delta\varepsilon_x/\varepsilon_x \approx \Delta\varepsilon_y/\varepsilon_y \approx 4\%$ and $\Delta\varepsilon_z/\varepsilon_z \approx 10\%$.
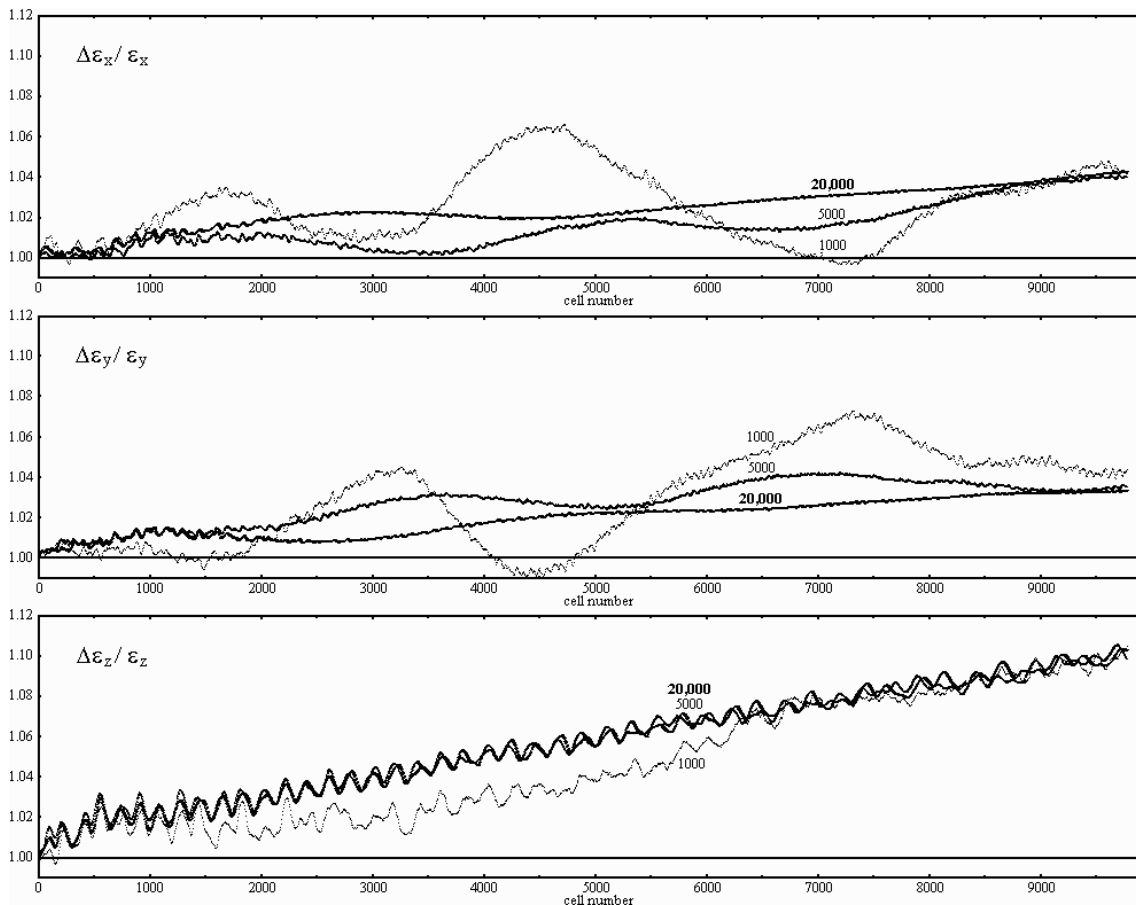
Figure 5.5: Behaviour of the rms emittance with 1000, 5000 and 20,000 macroparticles along the nominal linac with nominal input.

These results are considered as a solid starting basis for the design of a conventional DTL, accelerating 400 mA of Bi^+ from 10 to 50 MeV/u in 3.38 km, with 100% transmission and small emittance growth.

Nevertheless, as mentioned in Chapter 2, the transverse emittance of $1.05\,\pi$ mm mrad (full, norm.) assumed as an input is rather small, particularly if compared to the value of $0.27\,\pi$ mm mrad (4 rms, norm.) measured at the ion source: the unavoidable emittance growth along the whole linac complex should not exceed a factor of 4.

Moreover, assuming a safety factor of 10 between full and rms emittance (which is sometimes felt as necessary to reduce the risk of particle losses and structure activation), the required rms emittance would be pushed down to $0.13\,\pi$ mm mrad! Then a growth factor of 2 only would be allowed and all the upstream emittances should be reviewed.

Next, the effects of different input distributions and of errors on the emittance have also to be investigated. Therefore in Chapter 5.3 results of particle dynamics calculations are presented for a 6-dim waterbag and for a "4d+2d" Gaussian input distribution (4-dim Gaussian transversely and 2-dim one longitudinally); in Chapter 6 the effects of statistical errors and mismatch are discussed, when they are added into the nominal linac design.

5.3 Impact of different input distributions

As mentioned in Chapter 3, the matched state of any beam with a distribution having an ellipsoidal shape in the real space is specified exactly by the K-V equations, provided that the beam boundaries and emittances are defined by rms values [Lap71][Glu70][Sac71].

In general, the ratio between the physical boundary (envelope) and the rms size is the square root of the full-to-rms emittance ratio; it depends on the chosen distribution, therefore it is preferable to avoid defining a beam boundary for each distribution and simply use rms values.

Up to here a 4-dim waterbag distribution has been used for the transverse planes and a 2-dim waterbag distribution for the longitudinal one (nominal design), which is an

idealized case, henceforth indicated as <u>case #0</u>. This implies a ratio $\varepsilon_{full}/\varepsilon_{rms} = 6$ in the transverse planes and 4 in the longitudinal one, while $X/a_x = Y/a_y = 6^{\frac{1}{2}}$ and $Z/b = 2$.

In order to check the stability of the reference layout against other input distributions, different values of this ratio and/or different rms emittances have been considered: namely a 6-dim waterbag distribution, where $\varepsilon_{full}/\varepsilon_{rms} = 8$ in all the three planes (cases #1, #2 and #3), and a "4d+2d" Gaussian distribution (cases #4, #5 and #6).

<u>Case #1</u>

As a first example a <u>6-dim waterbag</u> distribution was used, having in all three planes the <u>same rms input emittance</u> as in the nominal case. As a consequence of the equivalence of ellipsoidal bunches with the same rms emittances, this allows to keep the nominal focusing and the input Twiss parameters and to have still a matched beam. With respect to case #0, the input full emittance is however larger by a factor 8/6 transversally (+33%) and by a factor 8/4 longitudinally (+100%).

The effects on the <u>transverse planes</u> are small: although the input full beam radius is increased by a factor $(8/6)^{\frac{1}{2}}$, that is about 15%, the maximum full radius along the linac is however 9.2 mm, well below the beam pipe radius (16 mm). The full emittance $\varepsilon_{full,100\%}$, which was initially about 33% larger than in the nominal case, reaches approximately the same value than in the nominal case, with a ratio $\varepsilon_{full}/\varepsilon_{rms} = 9.2$ at the end of the linac (it was 9.0 in the nominal case). The ratio $\varepsilon_{full,99\%}/\varepsilon_{rms}$ is about 6.8 at the end of the linac (it was 6.3 in the nominal case); this corresponds to $\varepsilon_{full,99\%} = 1.24\,\pi$ mm mrad, which is just below the limit for proper ring injection. As expected, the rms beam size and the rms emittance growth are about the same as in the nominal case.

The effects on the <u>longitudinal plane</u> are larger, since both the full bunch length and the momentum spread are increased by a factor $(8/4)^{\frac{1}{2}}$, that is about 41%. The full emittance $\varepsilon_{full,100\%}$, which was initially double than in the nominal case, has a sudden growth at the beginning (it reaches a ratio $\varepsilon_{full}/\varepsilon_{rms} = 15$) but it decreases then to a value which is approximately only 30% larger than in the nominal case, with $\varepsilon_{full}/\varepsilon_{rms} = 9.5$ at the end of the linac (it was 7.6 in the nominal case). The full emittance $\varepsilon_{full,99\%}$, which was also initially about double than in the nominal case, is rather flat and reaches a value which is approximately only 20% larger than in the old case, with a ratio $\varepsilon_{full}/\varepsilon_{rms}$

= 7.1 at the end of the linac (it was 5.8 in the nominal case). The output distribution in the longitudinal plane is shown in Figure 5.6-left.

The rms longitudinal emittance grows by about 12% (it was 10% in the nominal case). In this situation it is worth to notice that, since the longitudinal rms emittance is almost preserved, the effects of the space-charge repulsion between particles are the same as in the nominal case. On the other hand, the bunch is now 41% longer and therefore its tails are in a region where the nonlinear part of the rf electric field is higher. A comparison with the results obtained for the nominal case allows then to separate the nonlinear effects due to the space-charge from those due to the rf electric field: the observed emittance increase is therefore mainly due to the nonlinear electric field.

Case #2

As a second example a 6-dim waterbag distribution has been assumed, keeping the same rms input emittance as in the nominal case for the transverse planes, while the longitudinal rms emittance was reduced by 50% in order to have the same full emittance as in the nominal case (i.e. $\varepsilon_{rms} = 12.5 \, \pi$ deg MeV). In all the three planes it is $\varepsilon_{full} / \varepsilon_{rms}$ = 8, and transversally nothing has changed; but longitudinally the beam is now mismatched, since no other modifications have been made apart from the rms emittance.

As expected, the effects on the transverse planes are again small: the maximum full radius, the full emittances and the rms beam size are about the same as in the previous case #1. The rms emittance growth is even smaller (about 2%).

The effects on the longitudinal plane are again larger. The rms emittance grows now by 25% (it was 10% in the nominal case) due to the increased particle density and space-charge forces; nevertheless, since the initial value was 50% smaller, the absolute rms emittance at the linac end ($\varepsilon_{rms} = 15.6 \, \pi$ deg MeV) is much smaller than in the nominal case ($\varepsilon_{rms} = 27.5 \, \pi$ deg MeV). The full emittance $\varepsilon_{full,100\%}$, which was initially the same as in the nominal case, starts growing and then explodes after half of the linac, reaching a value 4 times larger than in the nominal case, with a maximum ratio $\varepsilon_{full} / \varepsilon_{rms}$ = 38 around the end of the linac (it was 7.6 in the nominal case). The full emittance $\varepsilon_{full,99\%}$, which was initially smaller than in the nominal case, is however rather flat and reaches a value which is approximately 20% smaller than in the nominal case, with a ratio $\varepsilon_{full} / \varepsilon_{rms}$ = 8.5 at the end of the linac (it was 5.8 in the nominal case). This means

59

that the core is much denser, but a few macroparticles are very distant from it (that is a halo has been formed), as confirmed from Figure 5.6-middle.

Case #3

As a third example a 6-dim waterbag distribution was used, with intermediate parameters between case #1 and #2: the longitudinal rms emittance was reduced only by a factor 9/7, that is about −22%, with respect to the nominal case (i.e. $\varepsilon_{rms} = 19.4\,\pi$ deg MeV), always keeping the same rms input emittances in the transverse planes. The beam mismatch in the longitudinal plane is now reduced with respect to case #2.

The effects on the transverse planes are always small: the maximum full radius, the full emittances and the rms beam size are about the same as in both previous cases; the rms emittance growth is somehow intermediate (about 3%).

The effects on the longitudinal plane are also intermediate. The rms emittance grows now by 16% (it was 12% in case #1 and 25% in case #2); nevertheless, since the initial value was 22% smaller than in case #0, the absolute rms emittance at the linac end ($\varepsilon_{rms} = 22.6\,\pi$ deg MeV) is still smaller than in the nominal case. The full emittance $\varepsilon_{full,100\%}$, which was initially about 55% larger than in the nominal case, exhibits a bump in the beginning and a growth in the end; nevertheless, the final ratio $\varepsilon_{full}/\varepsilon_{rms}$ is about 14.5 (it was 7.6 in the nominal case). This means that the halo is still present, but it has been significantly reduced with respect to the previous case. The full emittance $\varepsilon_{full,99\%}$, which was initially higher than in the nominal case, is rather flat and reaches the same value than in the nominal case, with a ratio $\varepsilon_{full}/\varepsilon_{rms} = 7.2$ at the end of the linac. The output distribution in the longitudinal plane is shown in Figure 5.6-right.

Case #4

As a fourth example a "4d+2d" Gaussian distribution (4-dim transversally, 2-dim longitudinally) has been assumed; the same rms input emittances as in case #3 were taken, i.e. the nominal transverse one ($\varepsilon_{rms} = 0.176\,\pi$ mm mrad) and the reduced longitudinal one ($\varepsilon_{rms} = 19.4\,\pi$ deg MeV). The transverse and longitudinal distributions were truncated at 2.32 σ and at 2.68 σ respectively, in order to have $\varepsilon_{full}/\varepsilon_{rms} = 8$ in both the transverse and the longitudinal planes, according to the relations seen on Chapter 3.1.

Therefore such a distribution can be directly compared to the 6-dim waterbag distribution having the same ε_{rms} in all the three planes, i.e. to case #3. The only difference is that the beam has been now longitudinally re-matched.

In the <u>transverse planes</u> there is almost no effect on rms quantities: the rms beam size is the same as in the nominal case and the rms emittance grows by about 2.5% as in case #3. The maximum beam full radius along the linac is however 9.7 mm, slightly larger than using a 6-dim waterbag distribution, although always well below the beam pipe radius (16 mm); the full emittances reach a ratio $\varepsilon_{full,100\%} / \varepsilon_{rms} = 11.5$ and $\varepsilon_{full,99\%} / \varepsilon_{rms} = 7.2$ at the end of the linac, corresponding to $\varepsilon_{full,99\%} = 1.30 \pi$ mm mrad, just above the limit for proper ring injection. This increase of the full radius and emittances is due to the fact that the input distributions of case #3 and #4 are equivalent (same rms quantities and ratio $\varepsilon_{full} / \varepsilon_{rms}$) but not identical, and therefore they behave in a slightly different way.

In the <u>longitudinal plane</u>, the rms emittance grows by about 17%; the full one grows until it reaches a ratio $\varepsilon_{full,100\%} / \varepsilon_{rms} = 15$ at the end of the linac, while $\varepsilon_{full,99\%} / \varepsilon_{rms} = 7.6$. These values are similar to those obtained in case #3. The output distribution in the longitudinal plane is shown in Fig. 5.7-left.

Case #5

As a fifth example a <u>"4d+2d" Gaussian</u> distribution was used, having in all three planes the <u>same rms input emittances</u> as in case #3 and #4, but <u>cutting the distribution at 2.00 σ and 2.50 σ</u> in the transverse and in the longitudinal planes respectively. This beam is still equivalent to the previous one, but the input ratio between full and rms emittances has been decreased from 8 to 7.35 in the transverse planes and to 7.30 in the longitudinal one, according to the relations seen on Chapter 3.1; these values are however larger than for the reference "4d+2d" waterbag distribution ($\varepsilon_{full}/\varepsilon_{rms} = 6$ and 4 respectively). The nominal Twiss parameters for case #0 have been used, which means that the beam is again longitudinally mismatched as in case #3.

In the <u>transverse planes</u> there is almost no effect on rms quantities: the rms beam size is the same as in the nominal case and the rms emittance grows by about 3% as in case #3. Owing to the smaller cut radii of the Gaussian distribution, the maximum beam full radius along the linac is now reduced to 9.2 mm, still larger than using a 6-dim

waterbag distribution, but still well below the beam pipe radius (16 mm); the full emittances are also reduced, with $\varepsilon_{full,100\%} / \varepsilon_{rms} = 10.9$ and $\varepsilon_{full,99\%} / \varepsilon_{rms} = 7.0$ at the end of the linac, corresponding to $\varepsilon_{full,99\%} = 1.27\ \pi$ mm mrad, just at the limit for proper ring injection.

In the <u>longitudinal plane</u>, the rms emittance grows by about 19%; the full one grows until it reaches an unacceptable ratio $\varepsilon_{full,100\%} / \varepsilon_{rms} > 24$ at the end of the linac, where $\varepsilon_{full,99\%} / \varepsilon_{rms} = 7.7$; this means that a halo has been formed, as can be clearly seen in Figure 5.7-middle. Since the smaller cut radius of the Gaussian distribution is supposed to reduce the full emittance as in the transverse planes, one can conclude that the observed filamentation is due to the input mismatch rather than to the used distribution.

Case #6

As a last example a <u>"4d+2d" Gaussian</u> distribution was assumed, having the <u>transverse input emittances reduced by 1/6</u>, that is $\varepsilon_{rms} = 0.147\ \pi$ mm mrad, while the same longitudinal rms input emittance as in cases #4 and #5 was taken, but <u>cutting the distribution at 2.00 σ</u> rather than at 2.50 σ. According to the relations seen in Chapter 3.1, this implies a reduction of the input ratio between full and rms longitudinal emittances ($\varepsilon_{full} / \varepsilon_{rms} = 5.82$), while the ratio stays constant for the transverse planes ($\varepsilon_{full} / \varepsilon_{rms} = 7.35$); these values are however still larger than for the reference "4d+2d" waterbag distribution. The beam is not equivalent to the previous ones and is now mismatched also transversally; a <u>new matching</u> of the beam had then to be found at the input of the linac, by adjusting the Twiss parameters $\beta_{x,y,z}$ (but keeping $\alpha_{x,y,z} = 0$).

In the <u>transverse planes</u> the situation is quite improved, owing to the reduced input rms emittance and in spite of the slightly increased space-charge forces: the rms beam size is about 7÷8% smaller than in all previous cases and the rms emittance still grows by about 3% as before. The maximum beam full radius along the linac is 8.7 mm, slightly larger than in the nominal "4d+2d" waterbag distribution and well below the beam pipe radius (16 mm); the full emittances reach a ratio $\varepsilon_{full,100\%} / \varepsilon_{rms} = 10.8$ and $\varepsilon_{full,99\%} / \varepsilon_{rms} = 7.2$ at the linac end, similar to the previous one but corresponding now to $\varepsilon_{full,99\%} = 1.09\ \pi$ mm mrad, which is alright for proper ring injection.

In the <u>longitudinal plane</u> the situation is also improved, due to the the smaller cut radius of the Gaussian distribution and to the re-matching: the rms emittance growth

decreases to 16% and the ratio $\varepsilon_{full,100\%} / \varepsilon_{rms}$ at the linac end is reduced, not only with respect to the mismatched case #5 (by almost a factor two, from 24 to 12.7), but also relative to the matched case #4. The ratio $\varepsilon_{full,99\%} / \varepsilon_{rms}$ is is also reduced (to 6.7), which means that a halo reduction has been achieved. The output distribution in the longitudinal plane is shown in Figure 5.7-right.

All the results from case #1 to #6 are summarized, together with case #0, in Tables 5.3 and 5.4, where the transverse values are calculated as the arithmetic average of the horizontal and vertical emittance, while the indetermination ($\pm x$) has been estimated from the width of the oscillation in the last few periods.
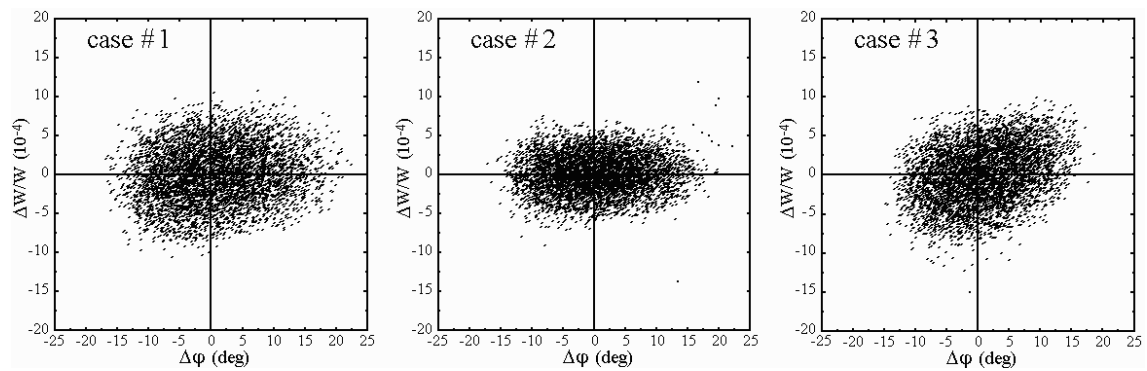
Figure 5.6: Output distribution in the longitudinal plane at the end of the nominal linac, with 6-dim waterbag input distribution for 5000 macroparticles. *Left*: case #1. *Middle*: case #2. *Right*: case #3.
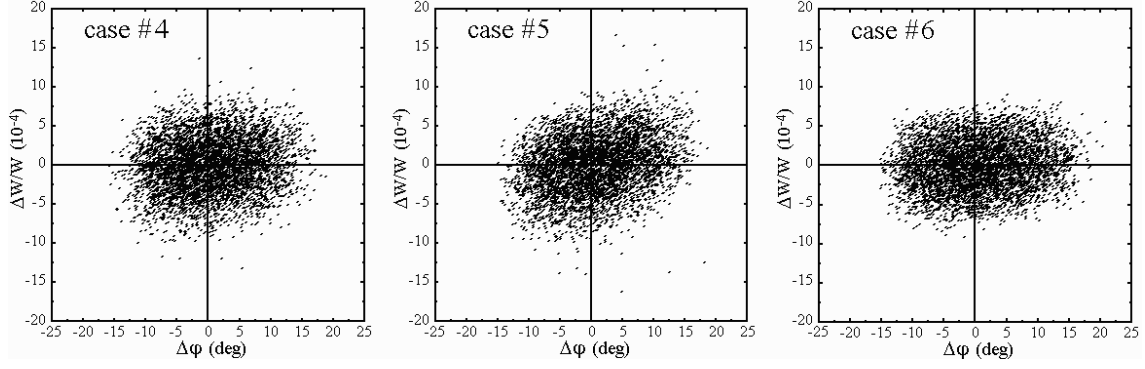
Figure 5.7: Output distribution in the longitudinal plane at the end of the nominal linac, with "4d+2d" Gaussian input distribution for 5000 macroparticles. *Left*: case #4. *Middle*: case #5. *Right*: case #6.

Table 5.3: Summary of normalized emittances at the beginning of the linac.

case	transverse planes			longitudinal plane		
	$\varepsilon_{full,100\%}$ (π mm mrad)	ε_{rms} (π mm mrad)	$\varepsilon_{full,100\%}/\varepsilon_{rms}$	$\varepsilon_{full,100\%}$ (π deg MeV)	ε_{rms} (π deg MeV)	$\varepsilon_{full,100\%}/\varepsilon_{rms}$
# 0	1.06	0.176	6.00	100	25.0	4.00
# 1	1.41	0.176	8.00	200	25.0	8.00
# 2	1.41	0.176	8.00	100	12.5	8.00
# 3	1.41	0.176	8.00	156	19.4	8.00
# 4	1.41	0.176	8.00	156	19.4	8.00
# 5	1.29	0.176	7.35	142	19.4	7.30
# 6	1.08	0.147	7.35	113	19.4	5.82

Table 5.4: Summary of emittances at the end of the linac.

case	transverse planes			longitudinal plane		
	$\varepsilon_{full,100\%}/\varepsilon_{rms}$	$\varepsilon_{full,99\%}/\varepsilon_{rms}$	$\Delta\varepsilon_{rms}/\varepsilon_{rms}$	$\varepsilon_{full,100\%}/\varepsilon_{rms}$	$\varepsilon_{full,99\%}/\varepsilon_{rms}$	$\Delta\varepsilon_{rms}/\varepsilon_{rms}$
# 0	9.0 ±0.5	6.3 ±0.2	≈4 %	7.6 ±0.5	5.8 ±0.2	≈10 %
# 1	9.2 ±0.5	6.8 ±0.2	≈4 %	9.5 ±0.5	7.1 ±0.2	≈12 %
# 2	9.4 ±0.3	6.6 ±0.1	≈2 %	29 ±9	8.5 ±0.2	≈25 %
# 3	8.9 ±0.3	6.5 ±0.1	≈3 %	14.5 ±3.0	7.2 ±0.2	≈16 %
# 4	11.5 ±0.8	7.2 ±0.1	≈2.5 %	15.0 ±1.8	7.6 ±0.1	≈17 %
# 5	10.9 ±0.8	7.0 ±0.1	≈3 %	24 ±4	7.7 ±0.2	≈19 %
# 6	10.8 ±0.8	7.2 ±0.1	≈3 %	12.7 ±1.3	6.7 ±0.1	≈16 %

These tables show that, from the point of view of beam dynamics in the linac, results are quite acceptable for all the input distributions considered above. Going from

a cylindrical distribution ("4d+2d" waterbag) to an ellipsoidal one (6-dim waterbag) is not a problem for the linac: in all cases the beam can be transported without major blow-up up to the end of the DTL; it is worth to point out that no particles have been lost in any simulation. Nevertheless, the crucial point is the ring acceptance for proper injection.

In the transverse planes the situation does not change dramatically with respect to the nominal case; the full emittance for 99% of the beam is generally within the requested acceptance for loss-free injection into the rings (only case #4 slightly exceeds the requirements) even if sometimes the new full emittance is larger than the acceptance for ring injection already at the beginning of the linac ($\varepsilon_{full,100\%} = 1.41\ \pi$ mm mrad for cases #1 to #4, while $\alpha_t = 1.26\ \pi$ mm mrad)!

In the longitudinal plane the situation is always more complicated than in the transverse ones, both with an ellipsoidal 6-dim waterbag and with a cylindrical "4d+2d" Gaussian input; case #1 showed however that the main reason for halo formation is the nonlinear part of the rf field and not the used distribution. Cases #2 and #5 are the worst ones because they are not matched, as confirmed for instance from the comparison of case #5 (not matched) with case #6 (same rms emittance, but matched).

Altogether, from the point of view of ring injection, case #3 is the best one, because transversally $\varepsilon_{full,100\%}$ and ε_{rms} are even smaller than in the nominal case, while $\varepsilon_{full,99\%}$ is only slightly increased but still fulfils the requirements; longitudinally this is a good compromise between case #1 and #2 and it will be found that, after the transfer line and bunch rotation, it is the best one in terms of halo formation and momentum spread, since the resulting *dp/p* for 99% of the beam becomes small enough for proper injection into the rings (see Chapter 8).

The computations will be repeated in Chapter 6.6 for case #3, adding rf field errors ($\pm1\%$ in amplitude and $\pm1^{\circ}$ in phase), with 5000 and with 20,000 macroparticles.

The result of this comparison study is that the impact of an input distribution with a larger ratio $\varepsilon_{full} / \varepsilon_{rms}$ than the nominal "4d+2d" waterbag is not critical in the transverse planes, while in general it will produce some filamentation and contribute to halo formation in the longitudinal plane. These effects can however be reduced by a careful

choice of the input Twiss parameters (matching) and of the rms emittance; they do not represent a major concern for the main linac beam dynamics.

CHAPTER 6

EFFECT OF ERRORS ON PARTICLE DYNAMICS

Any disruption of the periodic linac structure will cause an increase of the longitudinal oscillation of the particles in phase and momentum. In a DTL the main sources of <u>longitudinal</u> random small perturbations (oscillations) are the following [Kap85]:

- amplitude and phase instabilities of the rf electric field (dominant effect),
- non-ideal lattice periodicity (also determined by acceleration),
- minor misalignments randomly distributed in each period of the structure,
- random errors in the longitudinal position of the accelerating gap centres,
- injection offset errors (longitudinal mismatch),
- current fluctuations.

The main sources of <u>transverse</u> random small perturbations (oscillations) in a non-ideal quadrupole channel are the following:

- deviation of the focusing field gradient from the nominal value,
- injection errors (transverse on- and off-axis mismatch),
- parallel displacement of the magnetic axis of the lens relative to the channel axis,
- slope of the magnetic axis of the lens relative to the channel axis,
- rotation of the median axes of the lens around the longitudinal axis of the channel.

The effect of longitudinal displacement of the lenses relative to the standard position is insignificant (normally orders of magnitude smaller).

The effects of some of these different sources of error have been studied, since they may play a significant role on the beam dynamics of the accelerated beam. Namely, the effect of errors in amplitude and phase of the rf electric field [Par98], the errors in the quadrupole gradient, and the mismatch [Dei98c][Dei98e] were investigated. At first

some results were obtained for each of the above effects separately; in a second step they were put one on top of another [Par99].

6.1 Amplitude and phase errors of the RF electric field

For the rf electric field amplitude an error $|\Delta E/E| < 1\%$ is commonly assumed, i.e. the real accelerating field may differ from the nominal one by a random amount ΔE uniformly distributed between $-0.01\,E$ and $+0.01\,E$ (rms variance $0.005\,E$) from tank to tank, where "tank" denotes a portion of linac fed by the same rf power amplifier.

The DTL was divided into 1600 tanks, of about 2 m length, since the required rf power per length unit is $P_{rf} = P_b + P_s = 1.0$ MW/m, including chopping (see Table 5.1), and some 2 MW amplifiers were assumed. There will be 10 cells/tank at the beginning of the linac and 5 at the end, due to the increasing cell length (21.8 cm $< \beta\lambda < 47.1$ cm).

For the phase a conventional random error $|\Delta\phi| < 1^{\mathrm{o}}$ may be assumed, again with uniform distribution (rms variance 0.5^{o}) from tank to tank, and the same for all the cells within a given tank; for a synchronous phase ϕ_s around 30°, this correspond approximately to a further 1% amplitude error, as $\cos(\phi_s \pm 1^{\mathrm{o}})/\cos\phi_s \cong 1 \pm \mathrm{tg}\,\phi_s \sin 1^{\mathrm{o}} \cong 1 \pm 0.01$.

These <u>uncorrelated</u> amplitude and phase errors will affect mainly the longitudinal motion of the bunch centre around the synchronous energy, since (in first approximation) the space-charge forces will remain the same within the bunch, referred to its centre. The theoretical expectation at the linac end is $\Delta W/W = \pm\,\Delta E/E \times N_t^{-\frac{1}{2}}$, where N_t is the number of used rf power amplifiers; in this case, $\Delta W/W = \pm\,1\,\% \times 1600^{-\frac{1}{2}} = 2.5 \times 10^{-4} = 0.025\%$.

The MAPRO input files containing the rf field amplitudes and phases were modified in order to include a $\pm 1\%$ and $\pm 1^{\mathrm{o}}$ error respectively, randomly different from tank to tank but equal for all the cells in a given one. Then a 400 mA beam, represented by 5000 macroparticles, was tracked all along the linac.

In the <u>transverse planes</u> there is no remarkable effect, as expected: both the beam shape and the transverse emittance growth are almost identical as in the error-free case. The full beam radius always stays below 8.5 mm, compared to an aperture of 16 mm.

Longitudinally the output distribution has approximately the same shape: the bunch itself stays confined and moves as a whole, without any additional filamentation or emittance growth. However, the bunch centre oscillates with respect to the nominal position, with a maximum amplitude of about $\pm 0.02\%$ in energy and $\pm 2^o$ in phase, slightly smaller than expected (see Fig. 6.1).
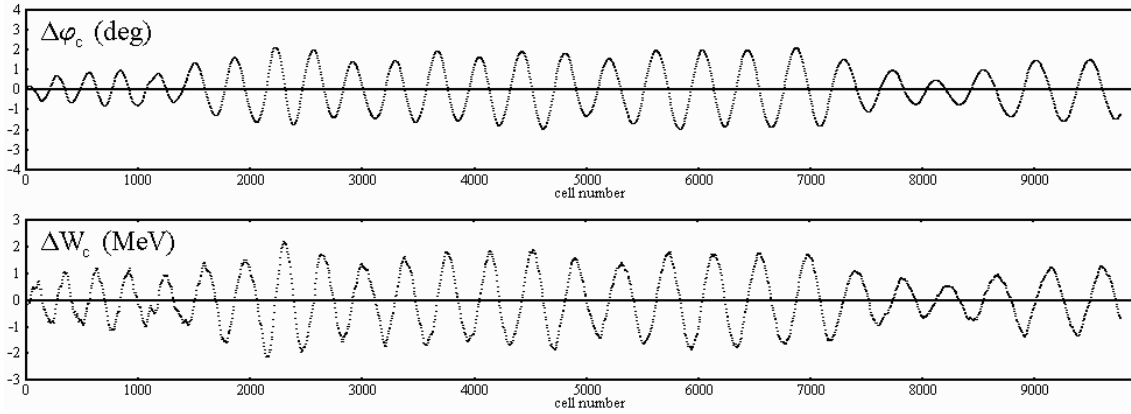
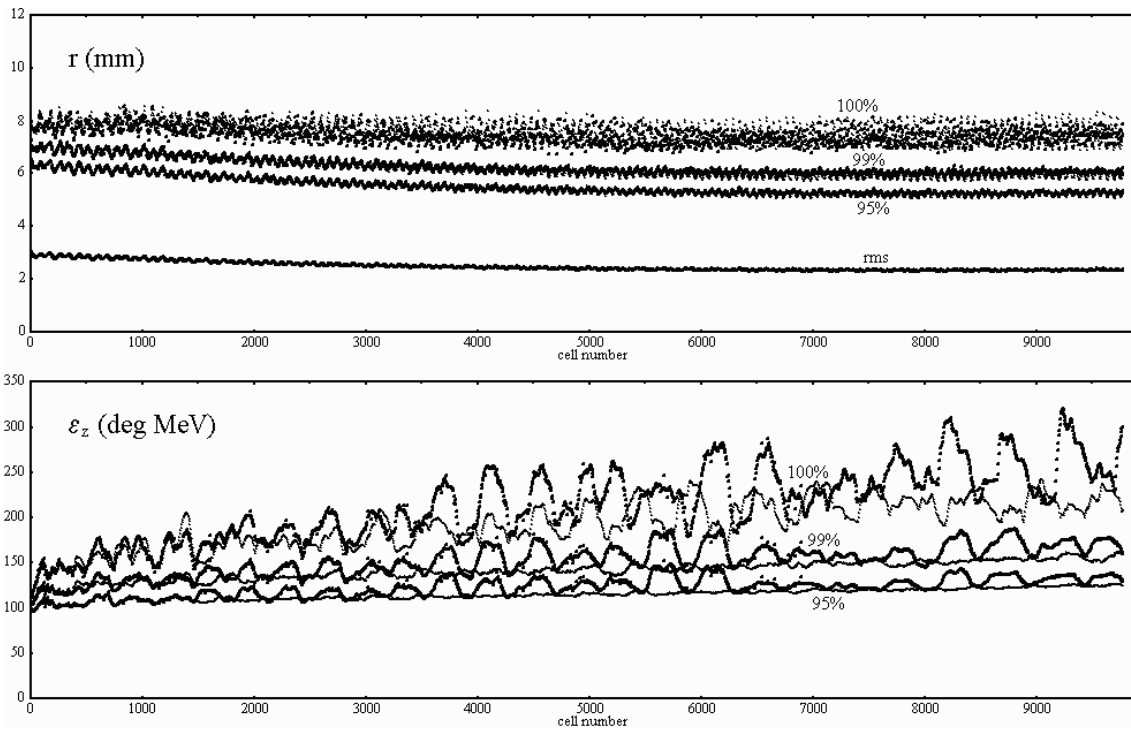Figure 6.1: Position of the bunch centre with uncorrelated amplitude and phase errors.

Figure 6.2: Development of the full (100%, 99% and 95%) radius and emittance along the nominal linac (thin line) and with 1% amplitude and 1° phase error in the rf field (bold line) for 5000 macroparticles. The thin and bold curves for the radius are almost identical.

There is however an increase of the emittance growth, if calculated with respect to the nominal synchronous phase and energy. The MAPRO code was then modified in order to compute the full emittance with respect to the phase and energy of the bunch centre, i.e. to subtract the oscillation. In this way the resulting curves are almost identical to those obtained in a linac without errors; but of course, as long as the bunch centre movement is not corrected, a larger area of longitudinal phase space may be filled by the shifting output beam, which has to be kept into account for the layout of the bunch rotation system (see Chapter 8). For this reason in Figure 6.2 the "virtual" full emittance is shown (the oscillation is not subtracted).

The effects of amplitude and phase errors were also evaluated separately, using the same sequence of random numbers. It was found that the phase errors produce smaller oscillations of the bunch centre than expected ($\pm 0.01\%$, $\pm 1^o$ versus $\pm 0.02\%$, $\pm 2^o$). When both kinds of errors (uncorrelated) are included, the global effect is not larger: the bunch centre is again displaced up to about $\pm 2^o$ in phase and $\pm 0.02\%$ in energy.

Having demonstrated that the distribution does not change significantly due to the rf amplitude and phase errors (because the space-charge forces are "internal" and the phase oscillations are small enough that nonlinearities of the rf field may be neglected), it is then possible to study the effect of errors for zero current, which increases enormously the computation speed. In a following step, this tracking was then repeated without including space-charge for a large number of different sets of errors; of course, new input matching conditions had to be found, in order to run with $I = 0$.

Running MAPRO for 100 different sets of errors, the average position of the bunch centre at the end of the linac results to be quite close to the nominal 0 value ($\langle \Delta \phi \rangle$ = 0.11^o, $\langle \Delta W/W \rangle = -0.0012\%$), while its rms variance is equal to $\Delta \phi_{rms} = 1.28^o$ in phase and $(\Delta W/W)_{rms} = 0.011\%$ in energy (see Fig. 6.3). Assuming this distribution to be Gaussian, this means that −with a probability of 95% (respectively 99.7%)− the final position of the bunch centre will differ from the design one by less than 2.56^o (respectively 3.84^o) in phase and 0.022% (respectively 0.033%) in energy.

For time-dependent rf errors the longitudinal position of the bunch will not be stable. Consequently, for proper injection into the following storage rings, the bunch rotation system at the end of the transfer line should be synchronized in phase with the incoming bunch position or a larger emittance should be taken into account (see Chapter 8).

Figure 6.4 shows the output distributions at the end of the linac for the nominal design, including rf phase and amplitude errors. In the real transverse space there is only a negligible increase of the beam size; in the longitudinal phase space the bunch centre is displaced by -1.3° in phase and $+1.2 \times 10^{-4}$ (=1.2 MeV) in energy. The assumed statistically distributed rf field errors do not contribute to additional filamentation nor to halo

development in the beam and are therefore acceptable for the beam dynamics in the linac.
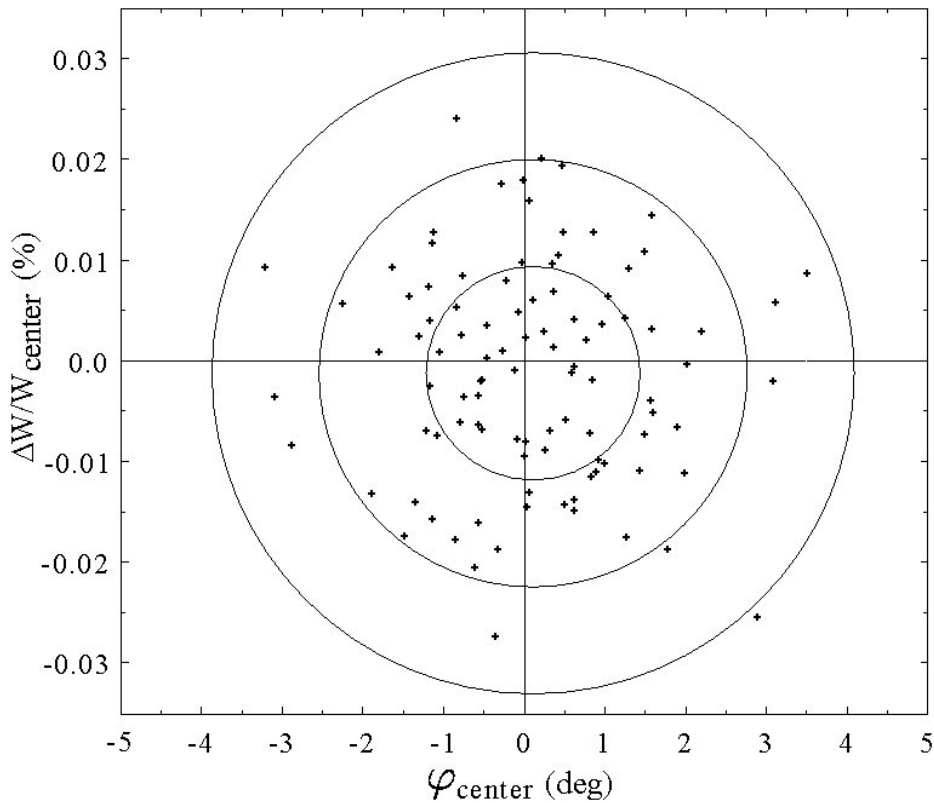
Figure 6.3: Position of the bunch centre at the output of the linac with uncorrelated 1% amplitude and 1° phase errors for 5000 macroparticles, without space-charge (statistics over 100 different sets of errors).
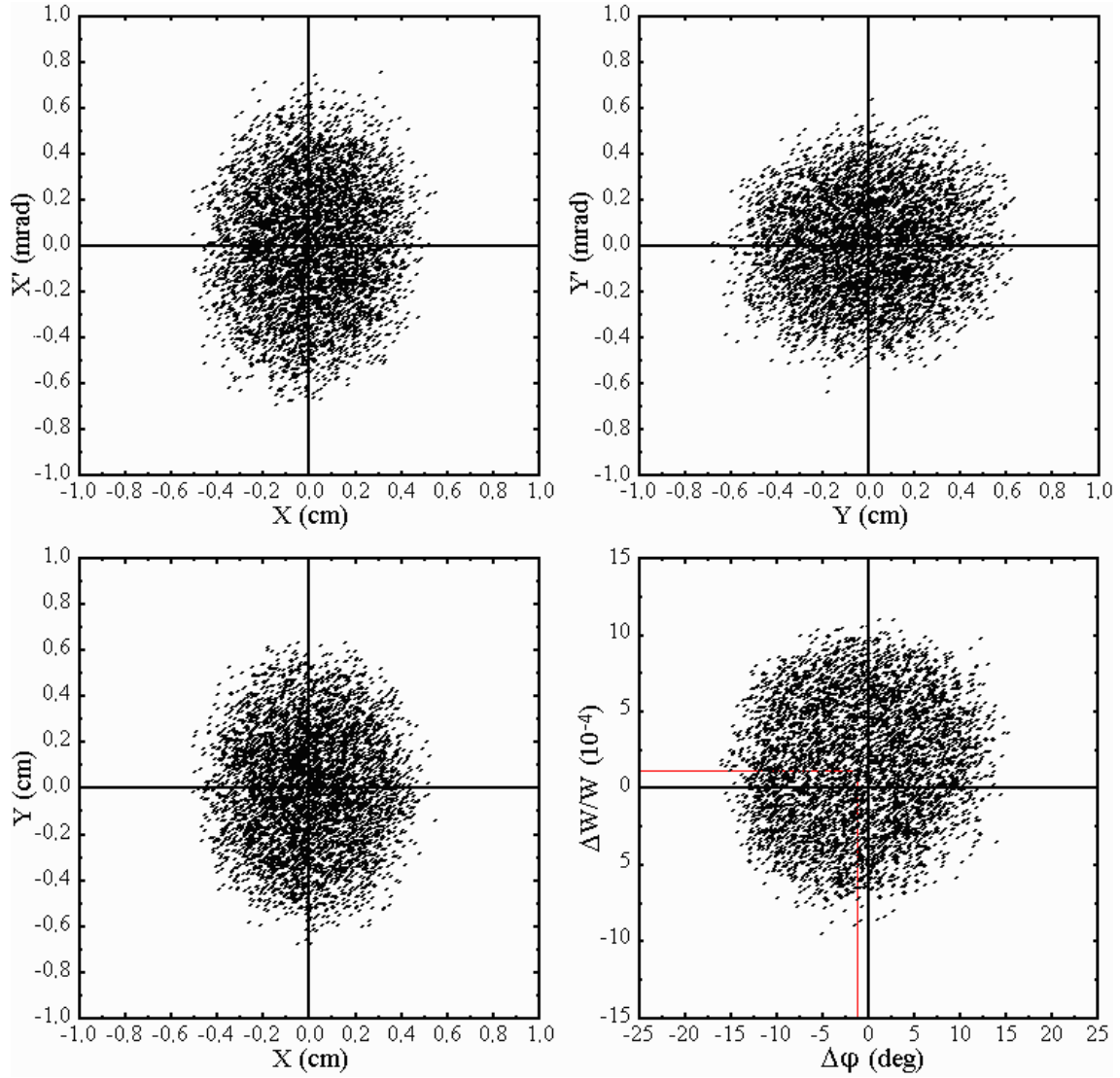
Figure 6.4: Output distribution at the end of the linac for 5000 macroparticles, with uncorrelated 1% amplitude and 1° phase errors.

6.2 Gradient errors of the quadrupolar magnetic field

As the quadrupolar magnetic field is concerned, a gradient error with amplitude $|\Delta G/G| < 1\%$ was initially assumed, due to current fluctuations of the power supplies.

This means that the effective focusing gradient can differ from the nominal one by a random amount ΔG which is uniformly distributed between $-0.01\,G$ and $+0.01\,G$ from each group of five lenses to another (rms variance $0.005\,|G|$). Since one power supply will feed the five quadrupoles of a kind in a period, the same error is assumed for all of them, which means a set of $N_c/5 = 1955$ different errors was used.

When 5000 macroparticles are accelerated along the linac, without any correction, this gives a surprisingly (at first glance) large emittance growth and halo formation: the $\pm 1\%$ errors are statistically adding up as $(N_c\,/\,5)^{\frac{1}{2}}$, with $N_c = 9775$ quadrupoles, as follows from the very long linac. The transverse rms emittances has already increased by about 20% after 1/3 of the total length, while the 99% emittances has almost doubled. By the end of the linac, the outermost particle reaches a distance of 15.5 mm from the axis, versus a beam pipe radius of 16 mm.

In order to cope with such an error, one would have to rematch the beam. If this is not possible, then the error size has to be reduced until a reasonable emittance growth is obtained. A much smaller amplitude error was then assumed, namely $|\Delta G/G| < 0.1\%$ (notice that, in practice, this can be a very strong limitation). At the same time, however, a small fraction of the power supplies (10 of them on a total of $N_c/5 = 1955$) were allowed to have an additional amplitude error 25 times higher, i.e. $|\Delta G/G| < 2.5\%$.

When 5000 macroparticles are accelerated along the whole linac, the transverse rms emittances increases by about 5% at the output (it was $\cong 4\%$ in absence of errors); also the full emittances (for both 100% and 99% of the beam) are not much larger than the old ones; the outermost particles remain well away from the beam pipe wall. Similar results were obtained assuming a gradient error $|\Delta G/G| < 0.2\%$ for <u>all</u> the quadrupoles.

Figure 6.5 shows the full beam radius and the longitudinal emittance for 100%, 99% and 95% of the beam, with $\pm 1\%$ and $\pm 0.2\%$ quadrupole gradient errors. Notice that, with $\pm 1\%$ errors, the full beam radius approaches the pipe aperture and the full longitudinal emittance is 60% larger than with $\pm 0.2\%$ errors, because in high intensity bunched beams a transverse mismatch produce a longitudinal halo, as described in Chapter 6.5.

The errors on the quadrupole gradients must therefore be limited at $\pm 0.2\%$ in order to have negligible effects on beam dynamics, provided that such a small tolerance can be obtained also in practice.

Up to now only much shorter linacs have been investigated and built; therefore this effect, which was not known before, must be taken into account for the design of the HIDIF linac.
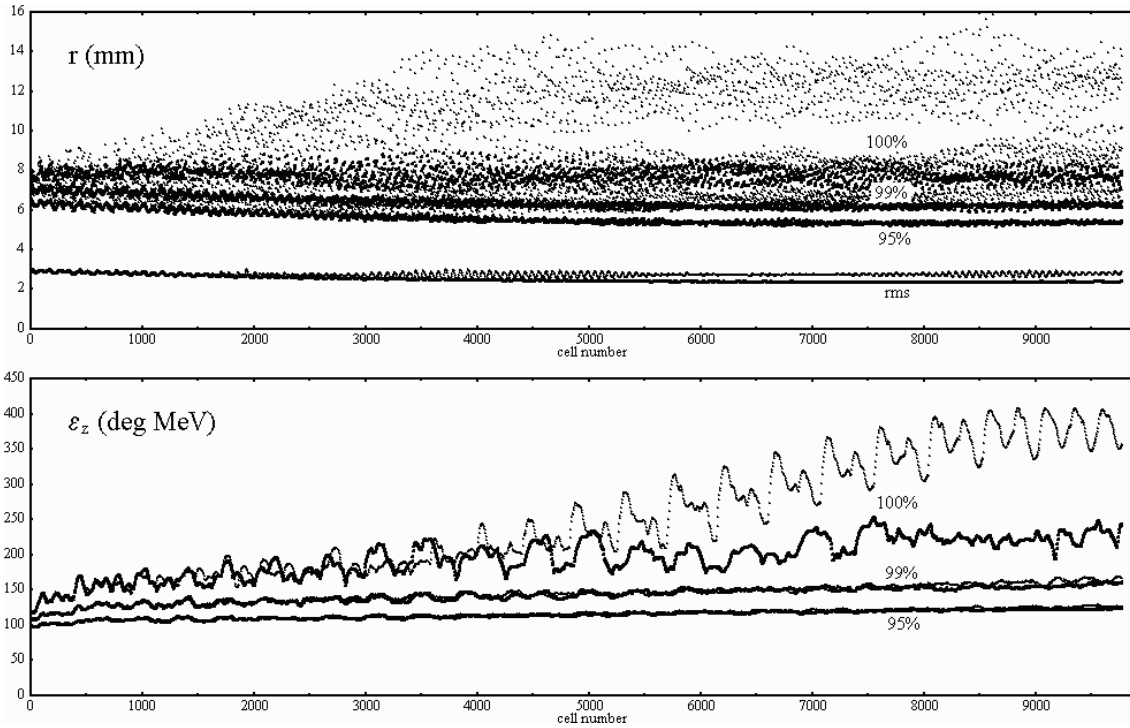

Figure 6.5: Development of the full (100%, 99% and 95%) radius and emittance along the nominal linac with quadrupole gradient errors of ±1% (thin line) and ±0.2% (bold line) for 5000 macroparticles.

6.3 Current fluctuations

Since the beams from 16 different ion sources have to be merged together to produce the 400 mA beam which is requested in the main linac, the question arises of the effects on particle dynamics of possible current fluctuations in the DTL. As the beam current stability is concerned, a maximum variation of ±10% with respect to the nominal current has been assumed, i.e. numerical calculations with 5000 macroparticles have been done
for the two cases of 360 and 440 mA.

71

Results show a slightly larger transversal emittance growth (from 5.5% to 6% for lower current and to 6.5% for higher current), mainly due to the mismatched input. The full radius of the beam increases to about 9 mm, always well below the beampipe aperture of 16 mm. No major effects are observed in the longitudinal plane for the case of 440 mA, that goes towards the current limit, but a smaller emittance growth (from 12% to 11%) for the case of 360 mA is observed. These effects are therefore uncritical.

Figure 6.6 shows the rms emittance along the nominal linac without any other error, for the reference beam current and for the assumed fluctuation of ±10%.
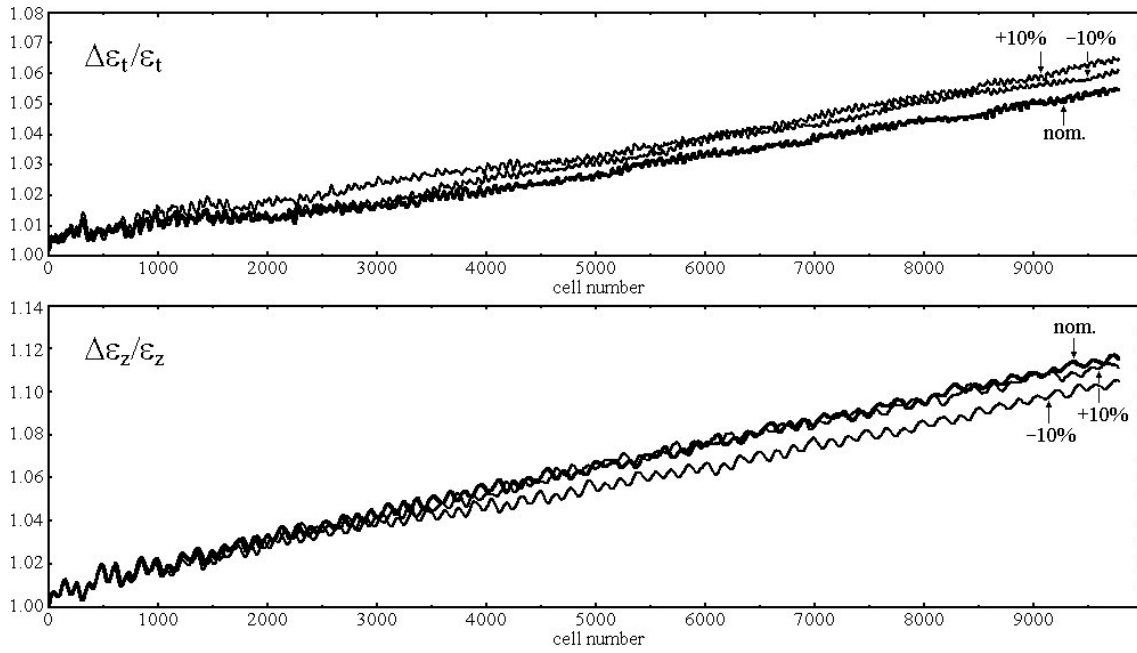
Figure 6.6: Behaviour of the rms emittance along the nominal linac for nominal current (bold line) and for ±10% variations (thin lines).

6.4 Other statistical errors

Random misalignments: If a lens is displaced transversely by the amount dr, then the beam will pass through an additional magnetic field $B = G\,dr$, which will deflect the particles from their normal path. For a thin lens, the change of slope is given by $(S/L_q)k^2 dr$, where S and L_q are the period and the quadrupole length, $k = qG/p$ [Kap95].

This effect is common to all particles, leading to coherent oscillations of the whole bunch about the

axis (a similar effect, due to off-axis input mismatch, is described in Chapter 6.5).

An important fact is that the beam emittance does not increase in a linear force field, when the amplitude of transverse oscillations increases due to these misalignment errors; oscillations can therefore be suppressed, in principle, by an automatic control system. If there is a good safety margin between the beam and the pipe radius, this effect can be neglected, because the oscillation amplitude can be simply measured and corrected with some steering device, that must necessarily be present in a 3 km long linac. A quadrupole lens misalignment of $\beta\lambda/1000$ (i.e. 0.2÷0.5 mm) is conventionally assumed.

Parametric perturbations are due to a <u>tilt</u> (rotation around the lens axis) to a rotation angle of the median axes and to errors in the gradient; these effects, which manifest themselves in the distortion of the beam emittance, are incoherent perturbations.

If incoherent perturbations are missing, then the increase of the effective emittance is simply equal to the displacement of the centre of the bunch squared (mismatched centre).

Halo formation due to Coulomb elastic <u>scattering</u> of the beam particles on residual gas can normally be neglected in a linac, where particles travel across a relatively short distance only once, assuming that the vacuum system is good enough that the mean free path of the particles is about equal to the acceleration length ($p < 10^{-7}$ torr).

6.5 Mismatch

In order to verify the effects of mismatch on the beam dynamics of the DTL for HIDIF, it is possible to increase one of the bunch dimensions (*x*, *y* or *z*) at the linac input and to observe the changes in the beam behaviour along the linac; any arbitrary input mismatch can be expressed as a combination of these three input conditions.

The horizontal size of the bunch $(\beta_x \varepsilon_x)^{\frac{1}{2}}$ can for instance be increased by 20% by keeping ε_x and multiplying β_x by $1.2^2 = 1.44$. In the same way, the vertical or the longitudinal dimensions can be increased by 20%. A few runs with a "4d+2d" waterbag

input distribution for 1000 macroparticles show some differences in the transverse and longitudinal rms emittance with respect to the nominal matched case, together with some halo formation (the maximum full radius of the beam grows up to 11.0 mm).

In the above cases the initial mismatch in one of the three space phase plane propagates to the other two, thus making it difficult to separate the effects of each kind of perturbation. For this reason it was preferred to follow the approach described in Chapter 3.4, where three independent "pure" eigenmodes can be clearly identified. Although this model has been developed for a transport line, it is possible to recognize the eigenmodes also in the presence of acceleration for the HIDIF linac.

Quadrupolar mode

For exciting the "quadrupolar" mode $(+-0)$ a 20% transverse size variation was assumed:

$$\Delta a_x/a_x = -\Delta a_y/a_y = +0.2 \qquad \text{and} \qquad \Delta b/b = 0$$

then:

$$\beta_x^{\text{mis}} = (1 + \Delta a_x/a_x)^2\, \beta_x^{\text{o}} = 1.44\, \beta_x^{\text{o}}$$
$$\beta_y^{\text{mis}} = (1 - \Delta a_x/a_x)^2\, \beta_y^{\text{o}} = 0.64\, \beta_y^{\text{o}}$$
$$\beta_z^{\text{mis}} = \beta_z^{\text{o}}$$

where β_x^{o}, β_y^{o} and β_z^{o} are the matched betatron functions.

A preliminary run with "4d+2d" waterbag input distribution for 1000 macroparticles shows some increase of the transverse rms emittance (from 4% for the nominal matched case to 10% for the mismatched one) and of the full ones ($\varepsilon_{\text{full,100\%}}$ is 25% higher, while $\varepsilon_{\text{full,99\%}}$ increases by 10%, indicating a slight halo formation); the maximum full radius of the beam increases from 8.9 to 9.7 mm. The longitudinal direction is less affected. With 10% mismatch results are intermediate between the previous and the matched case.

The calculations were then repeated for 20% mismatch using 5000 macroparticles, obtaining the results which are summarized in Table 6.1.

The phase advance for the quadrupolar mode can be evaluated with the formula given in Chapter 3.4; it results to be $\sigma_Q = 2\,\sigma_t = 34^{\text{o}}$. The best fit on numerical calculations (see Fig. 6.7) comes up with $\sigma_Q = 38^{\text{o}}$, which is in fact larger than the

theoretical value, but smaller than the phase advance of $\sigma_1 = 39.3^o$ that one would obtain for the out-of-phase mode in a dc beam.

Notice that there is, in theory, a parametric resonance between the transverse envelope tune σ_t and the tune σ_Q of the mismatched envelope ($\sigma_t/\sigma_Q = 17^o/34^o = 1/2$): this would cause halo production in the radial direction. In the numerical results, on the other

hand, this resonance is avoided ($\sigma_t/\sigma_Q = 17^o/38^o \cong 0.447 \neq 1/2$).
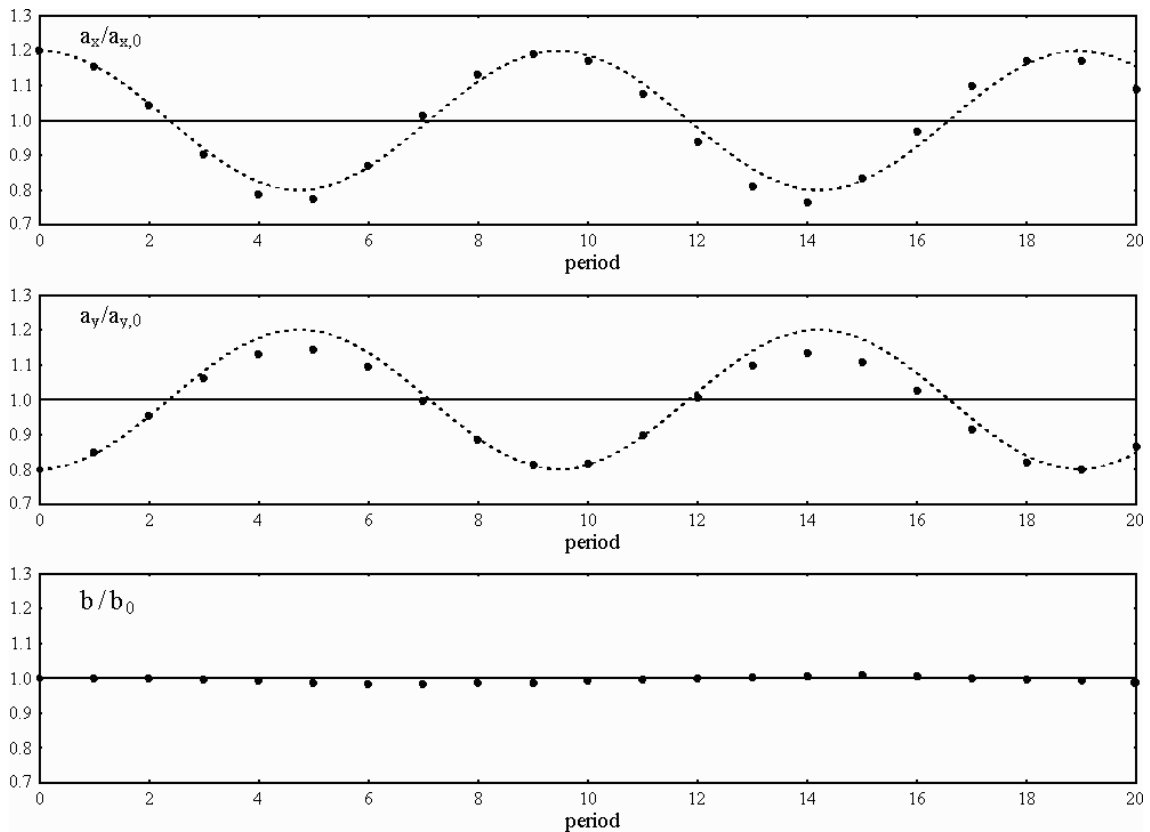
Figure 6.7: Excitation of the quadrupolar mode through 20% initial mismatch: rms bunch sizes with respect to the nominal (matched) one at the end of each period, for a "4d+2d" waterbag input distribution of 5000 macroparticles; the dotted line is the best fit.
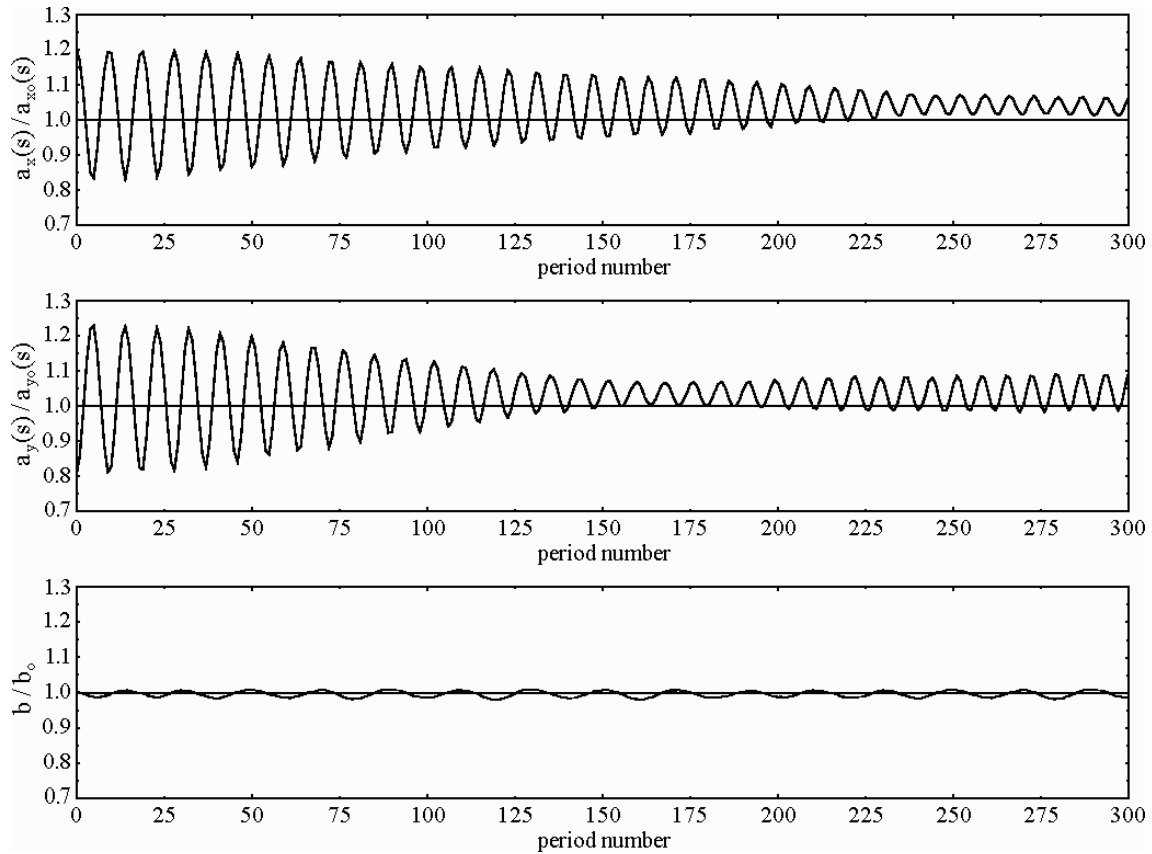
Figure 6.8: As previous Fig. 6.7; the oscillation is damped after about 1/3 of the linac length.

Figure 6.8 shows the effect of acceleration and nonlinear space-charge forces: the envelope oscillation is damped after about 300 periods (3000 cells), corresponding to about 1/3 of the linac length. This happens because, owing to the coupling, the coherent bunch oscillation in the quadrupolar mode evolves into an incoherent motion of the single particles, as can be observed from the increase in the average beam size.

Figure 6.9 shows the output distribution at the end of the linac. There is an immediate radial halo formation, but no axial one. The radial rms emittance increases,

since the local aspect ratio (and therefore the temperature ratio) is higher in the mismatched case:

$$a_x(s)/a_y(s) = 1.44\; a_{x,o}(s)/a_{y,o}(s)$$

and therefore the energy is continuously redistributed between the horizontal and the vertical plane, owing to equipartitioning.
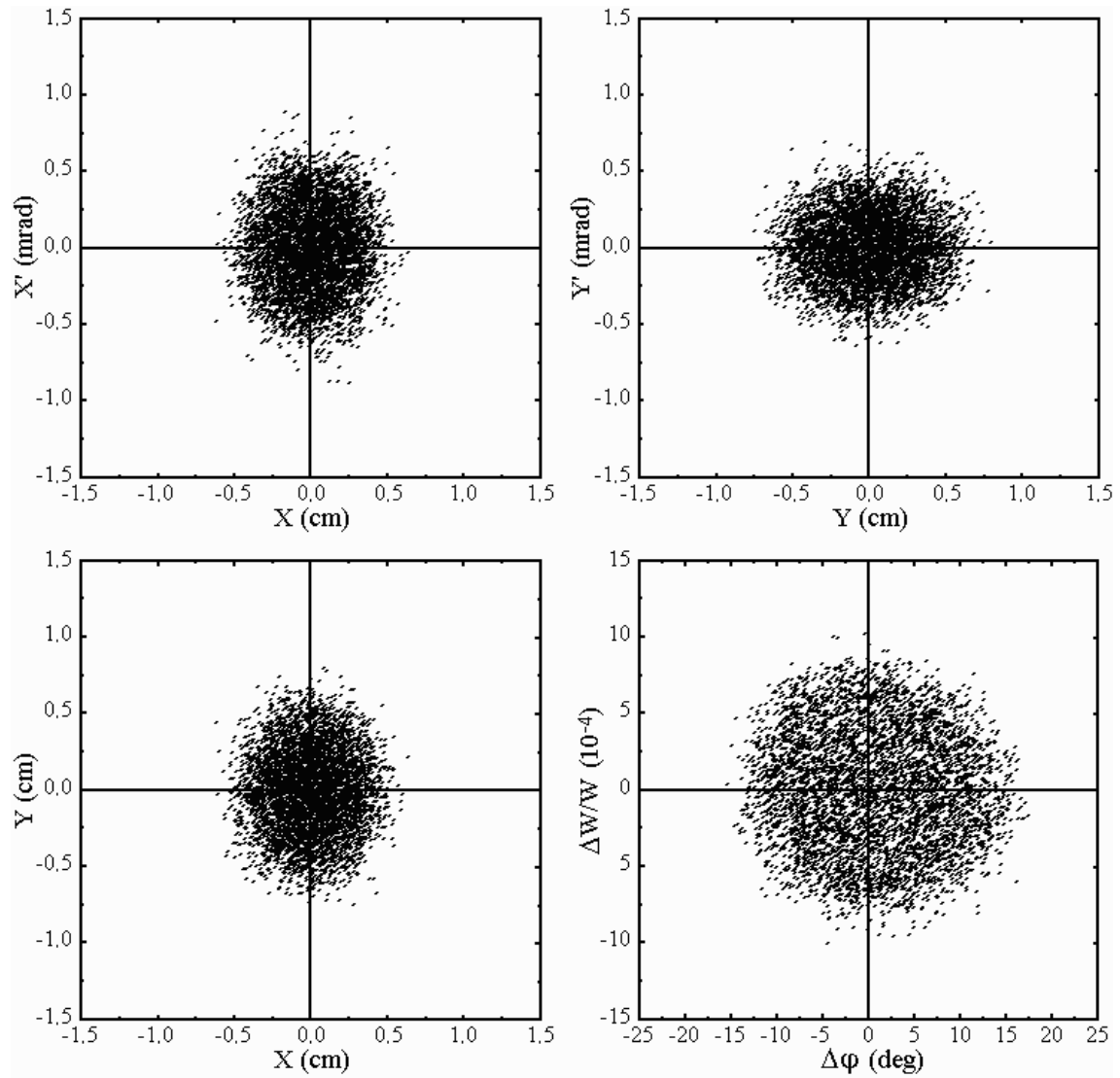
Figure 6.9: Quadrupolar mode: output distribution of 5000 macroparticles with maximum 20% initial mismatch error.

High mode

For exciting the "high" mode (+ + +) a 20% transverse size variation was assumed:

$$\Delta a_x/a_x = \Delta a_y/a_y = +0.2 \qquad \text{and} \qquad \Delta b/b = f_H \, \Delta a_x/a_x$$

For the HIDIF scenario the tunes at the DTL input are: $\sigma_t = 17^o$, $\sigma_l = 11^o$, $\sigma_{to} = 22.5^o$ and $\sigma_{lo} = 13.5^o$ (see Tab. 5.1). From these values and from the relations given in Chapter 3.4 one can calculate:

$$f_H = 0.093 \qquad \text{and} \qquad \sigma_H = 39.5^o$$

and finally one gets:

$$\beta_x^{mis} = (1 + \Delta a_x/a_x)^2 \, \beta_x^{o} = 1.44 \, \beta_x^{o}$$
$$\beta_y^{mis} = (1 + \Delta a_x/a_x)^2 \, \beta_y^{o} = 1.44 \, \beta_y^{o}$$
$$\beta_z^{mis} = (1 + 0.093 \, \Delta a_x/a_x)^2 \, \beta_z^{o} = 1.038 \, \beta_z^{o}$$

A preliminary run with "4d+2d" waterbag input distribution for 1000 macroparticles shows a larger increase in the transverse rms emittance (from 4% to 12÷13%); the full transverse emittance, both for 100% and 99% of the beam, is now higher by at least a factor 2, which indicates a strong halo formation; the maximum full radius of the beam increases in fact from 8.9 to 12.3 mm. Again, the longitudinal direction is less affected. With 10% mismatch results are intermediate between the previous and the matched case.
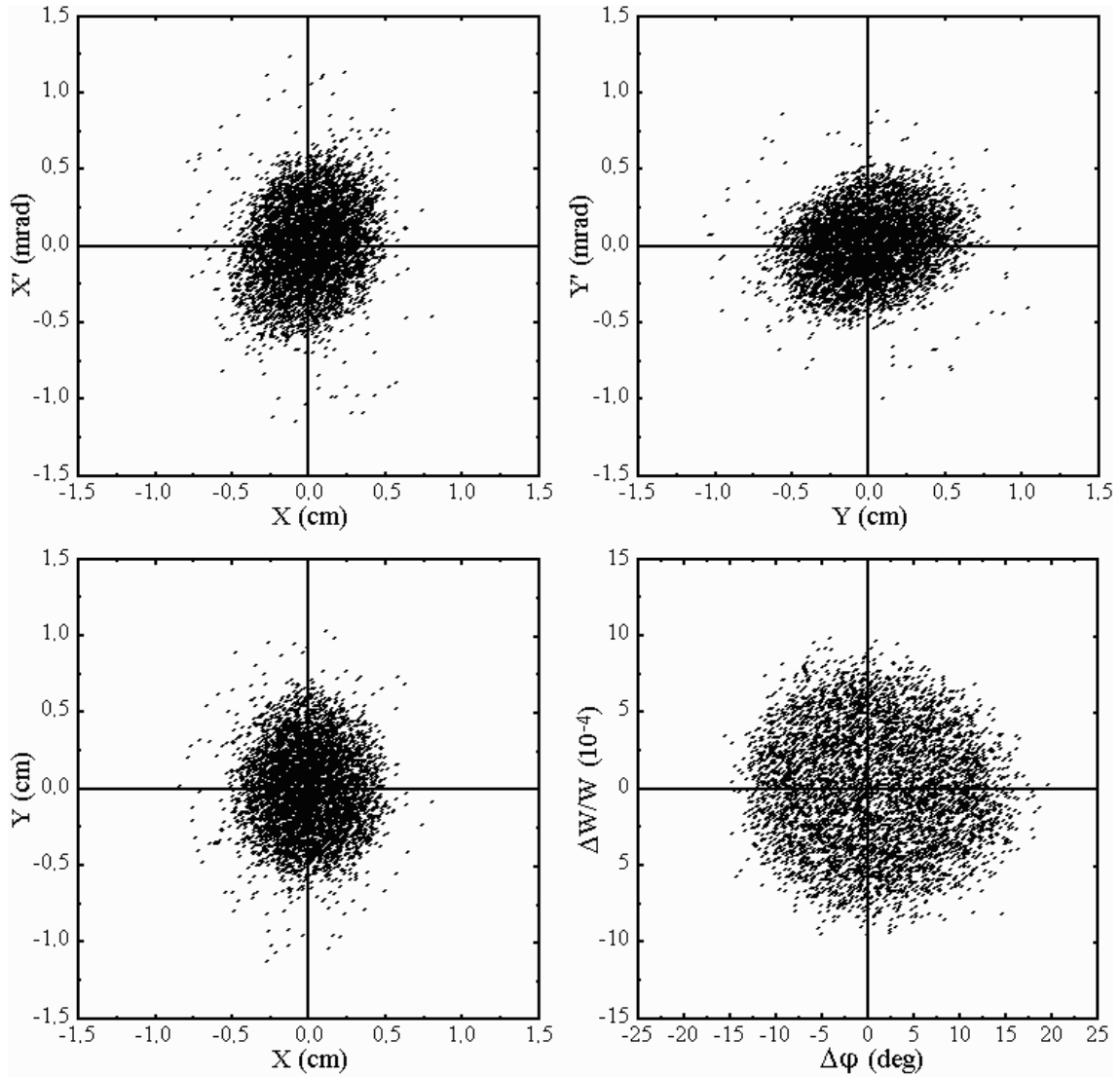
Figure 6.10: High mode: output distribution of 5000 macroparticles with maximum 20% initial mismatch error.

The calculations were then repeated for 20% mismatch using 5000 macroparticles, obtaining the results which are summarized in Table 6.1.

The numerical calculations come up with $\sigma_H = 41°$, which is in fact very close to the theoretical value of $\sigma_H = 39.5°$. Figure 6.10 shows the output distribution at the linac end.

There is a delayed <u>radial halo</u> formation, but no axial one. The radial rms emittance is only slightly increasing, since the aspect ratio is not changed by the mismatch:

$$a_x(s) \,/\, a_y(s) = a_{x,o}(s) \,/\, a_{y,o}(s)$$

79

Low mode

For exciting the "low" mode $(+ + -)$ a 20% longitudinal size variation was assumed:

$$\Delta b/b = +0.2 \qquad \text{and} \qquad \Delta a_x/a_x = \Delta a_y/a_y = (1/f_L)\, \Delta b/b$$

From the relations given in Chapter 3.4 one can calculate:

$$f_L = -5.29 \quad \text{and} \quad \sigma_L = 22.7^o$$

and finally one gets:

$$\beta_x^{mis} = (1 + (1/f_L)\Delta a_x/a_x)^2\, \beta_x^o = 0.926\, \beta_x^o$$
$$\beta_y^{mis} = (1 + (1/f_L)\Delta a_x/a_x)^2\, \beta_y^o = 0.926\, \beta_y^o$$
$$\beta_z^{mis} = (1 + \Delta b/b)^2\, \beta_z^o = 1.44\, \beta_z^o$$

A preliminary run with "4d+2d" waterbag input distribution for 1000 macroparticles shows the same increase of the transverse rms emittance as in the matched case and just slightly higher full emittances; the maximum full radius of the beam increases from 8.9 to 9.5 mm. The longitudinal direction is more affected: a larger increase of the rms emittance (from 10% to 13%) and of the full one (a factor 2) indicate halo formation. With 10% mismatch results are intermediate between the previous and the matched case.

The calculations were then repeated for 20% mismatch using 5000 macroparticles, obtaining the results which are summarized in Table 6.1.

The numerical calculations come up with $\sigma_L = 25^o$, compared to the theoretical value of $\sigma_H = 22.7^o$. There is now, in theory, a parametric resonance between the longitudinal envelope tune σ_l and the tune σ_L of the mismatched envelope ($\sigma_l / \sigma_L = 11^o/22.7^o \cong 0.485 \approx 1/2$): this would cause strong halo production in the axial direction. In the numerical results, on the other hand, this resonance is avoided ($\sigma_l / \sigma_L = 11^o/25^o \cong 0.440 \neq 1/2$).

Figure 6.11 shows the output distribution at the linac end. There is a delayed <u>axial halo</u> formation but no radial one, since the axial rms emittance increase is small and then also the coupling with the longitudinal motion does not increase [Pab97b]. Notice that the bunch shape is distorted in the longitudinal plane, owing to nonlinear rf forces.
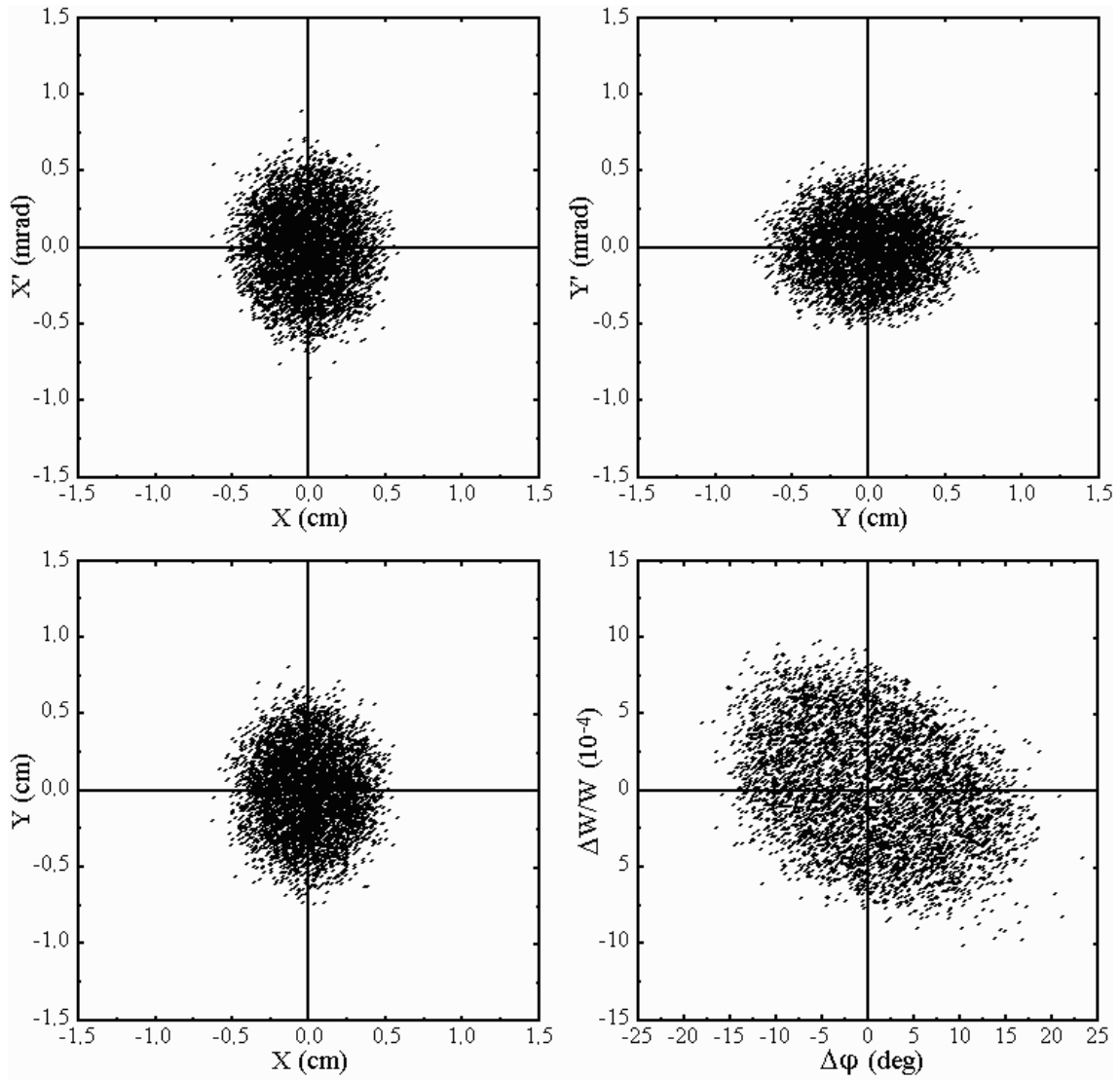
Figure 6.11: Low mode: output distribution of 5000 macroparticles with maximum 20% initial mismatch error.

Mixed mode

As a last test, a "mixed" mode was considered, given by a combination of all the three "pure" eigenmodes considered above. For exciting this mixed mode $(+ - +)$ a 20% transverse and longitudinal size variation was assumed:

$$\Delta a_x/a_x = -\Delta a_y/a_y = \Delta b/b = +0.2$$

A run with "4d+2d" waterbag input distribution for 5000 macroparticles shows both transverse and longitudinal halo formation, as could be expected from the superposition of the high and low modes. In Figure 6.12 the full emittance along the linac is illustrated for 100%, 99% and 95% of the beam. In the transverse planes it can be observed that the ratio full-to-rms emittance is almost everywhere larger than 10 (in fact, $\varepsilon_{rms} = 0.18$ and $\varepsilon_{full,100\%} = 2 \div 3 \pi$ mm mrad); this ratio is much smaller for 99% and 98% of the beam, as $\varepsilon_{full,99\%} = 1.5 \pi$ mm mrad and $\varepsilon_{full,98\%} = 1.2 \pi$ mm mrad, small enough for ring injection.

Figure 6.13 shows the output distribution at the linac end. Notice the longitudinally distorted bunch shape (as in the low mode) and the transverse halo (as in the high mode).
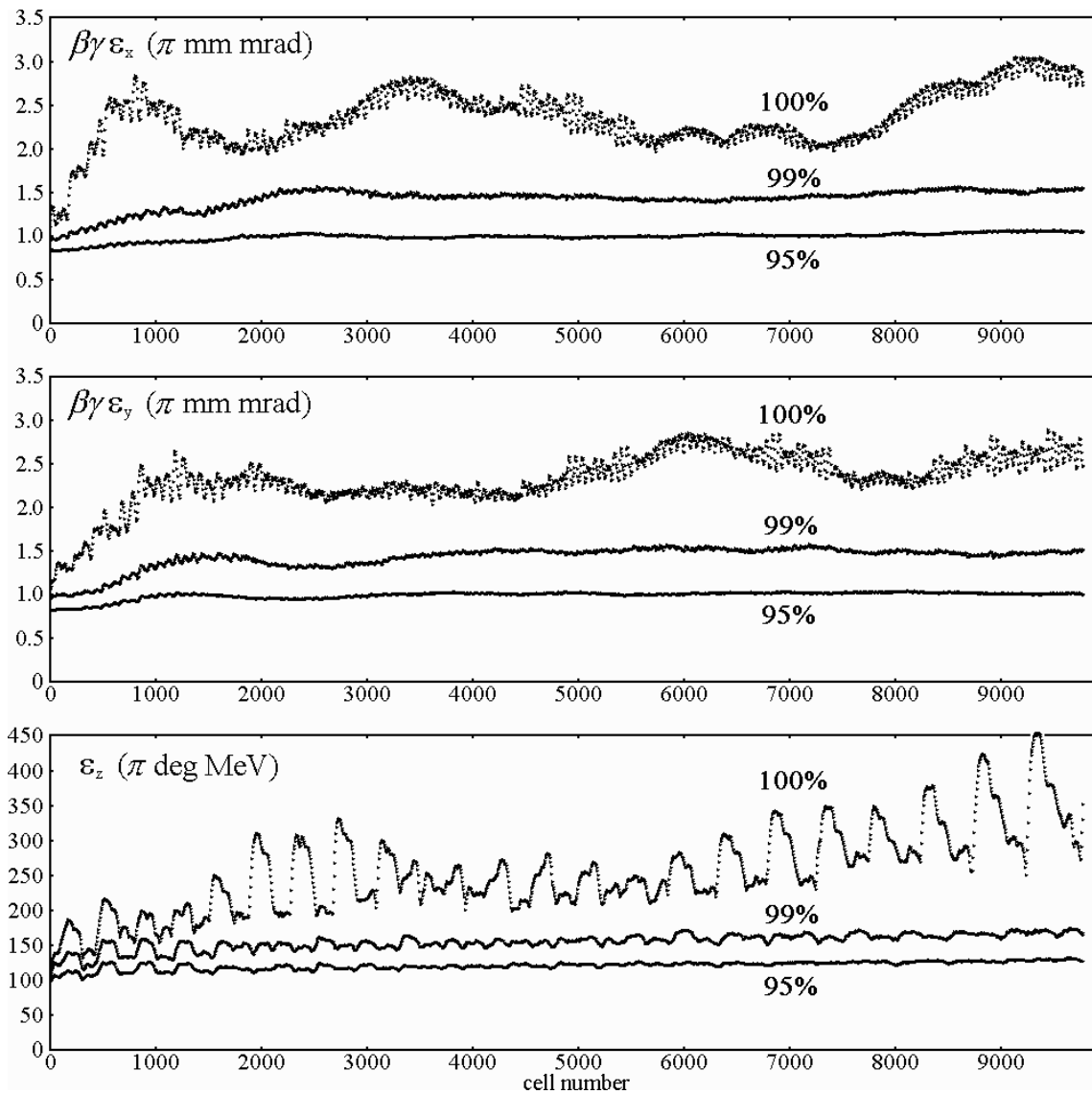
Figure 6.12: Mixed mode: development of the full (100%, 99%, 95%) emittance for 5000 macro-particles along the nominal linac with maximum 20% initial mismatch error.
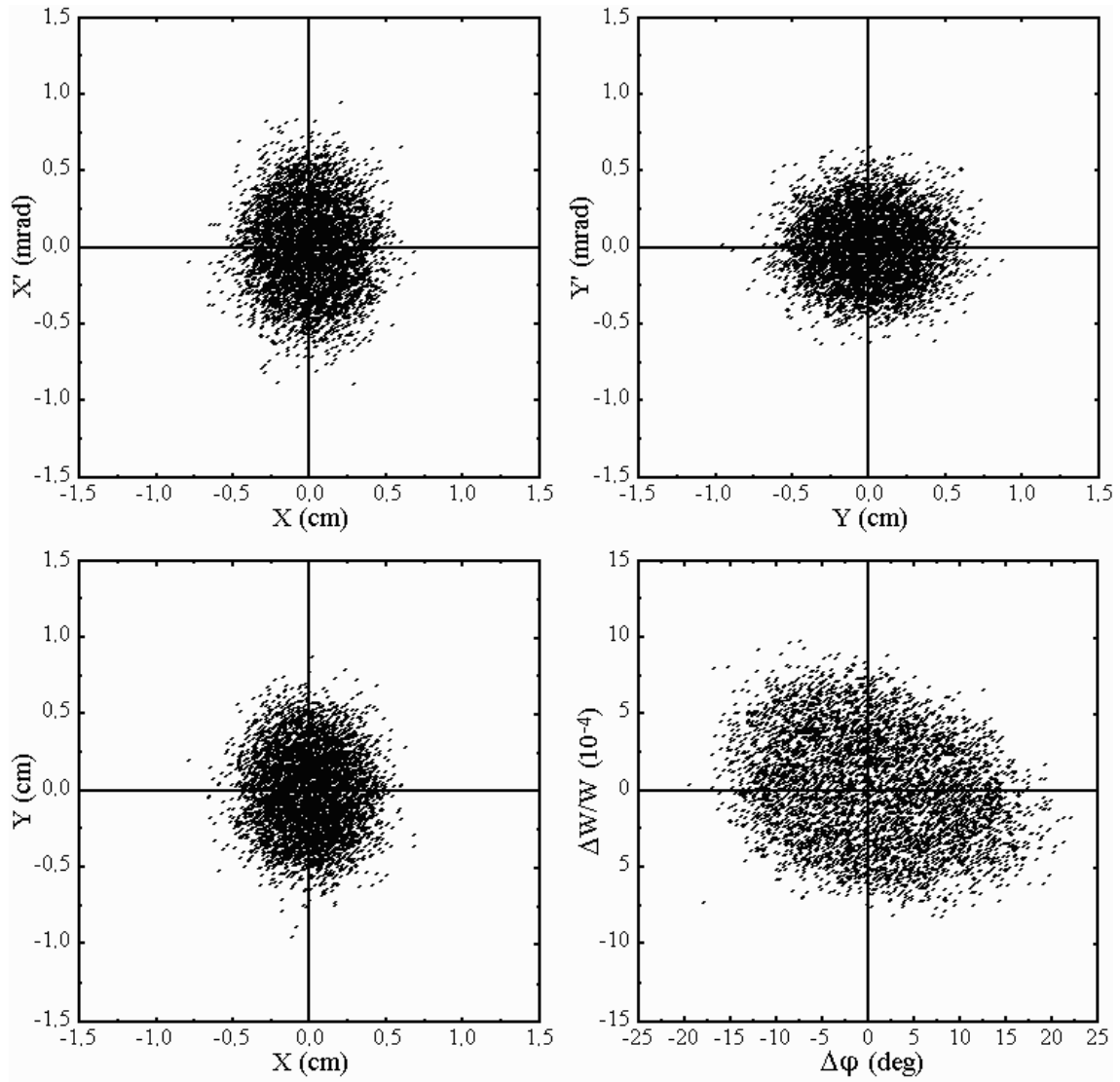
Figure 6.13: Mixed mode: output distribution of 5000 macroparticles with maximum 20% initial mismatch error.

Table 6.1: Summary of emittance and radius at linac end for different modes; 20% mismatch.

mode	transverse planes				longitudinal plane		
	$\varepsilon_{full,100\%}$ $/\varepsilon_{rms}$	$\varepsilon_{full,99\%}/\varepsilon_{rms}$	$\Delta\varepsilon_{rms}/\varepsilon_{rms}$	r_{max} (mm)	$\varepsilon_{full,100\%}$ $/\varepsilon_{rms}$	$\varepsilon_{full,99\%}$ $/\varepsilon_{rms}$	$\Delta\varepsilon_{rms}$ $/\varepsilon_{rms}$
0	9.0 ±0.5	6.3 ±0.2	≈ 4.0 %	8.2	7.6 ±0.5	5.8 ±0.2	≈ 10 %
quad	11.7 ±0.4	7.1 ±0.2	≈ 12.5 %	9.9	7.6 ±0.2	5.6 ±0.1	≈ 10 %
high	21.9 ±1.5	9.9 ±0.3	≈ 13 %	13.4	8.3 ±0.4	5.7 ±0.2	≈ 11 %

low	11.1 ±0.7	6.5 ±0.1	≈ 4.1 %	9.5	10.3 ±0.7	6.0 ±0.3	≈ 12.5 %
mixed	13.6 ±0.9	7.6 ±0.2	≈ 13.5 %	10.7	13 ±3	6.1 ±0.2	≈ 10 %

Results are summarized in Table 6.1, where the transverse values are calculated as the arithmetic average of the horizontal and vertical emittance, while the indetermination ($\pm x$) has been estimated from the width of the oscillation in the last few periods. The nominal matched case, indicated as 0, is shown for comparison.

It can be noticed that the <u>high mode</u> mismatch is the worst case for the transverse planes, since $\varepsilon_{full,100\%}/\varepsilon_{rms}$ is more than double than in the nominal case and $\varepsilon_{full,99\%}/\varepsilon_{rms}$ is also 50% larger; only 97% of the particles are within the required emittance. The beam radius is quite large as well: only 2.6 mm distance are left between the outermost particle and the wall of the beam pipe, which is not safe enough for beam losses, since any other error was absent in the above simulations. The <u>low and mixed mode</u> mismatch are the worst cases for the longitudinal plane, since $\varepsilon_{full,100\%}/\varepsilon_{rms}$ is much larger than in the nominal case; $\varepsilon_{full,99\%}/\varepsilon_{rms}$ is however only 5% larger.

In all cases, calculations with 1000 macroparticles showed that with 10% initial mismatch the effects on beam radius and emittance growth are proportionally reduced.

Off-axis mismatch

Another kind of mismatch may result from the beam being injected off-axis into the linac; in this case however, all the particles will be affected in the same way and in first approximation the bunch should move itself like a whole. The situation is similar to what happens in the case of a transverse displacements of <u>just one</u> quadrupole (or longitudinally in the case of <u>just one</u> amplitude or phase error in the rf field).

A simulation was made injecting a beam 3.0 mm off-axis, using the nominal "4d+2d" waterbag distribution for 5000 macroparticles. If the displacement lays in the horizontal or vertical plane only, then the bunch centre oscillates only in that plane (no coupling) with the same period as the betatron oscillation and the initial amplitude is only slightly reduced along the linac (it becomes 2.6 mm at the end), because the external forces are almost linear and $\beta\gamma$ increases very slowly along the DTL (see Fig. 6.14).

If the displacement lays in both the horizontal and the vertical plane ($dx = dy = +2.1$ mm was used in the simulation, to keep the 3.0 mm amplitude), then the bunch centre oscillates transversally always in the same plane, as the horizontal and vertical oscillation periods are identical (see Fig. 6.15).
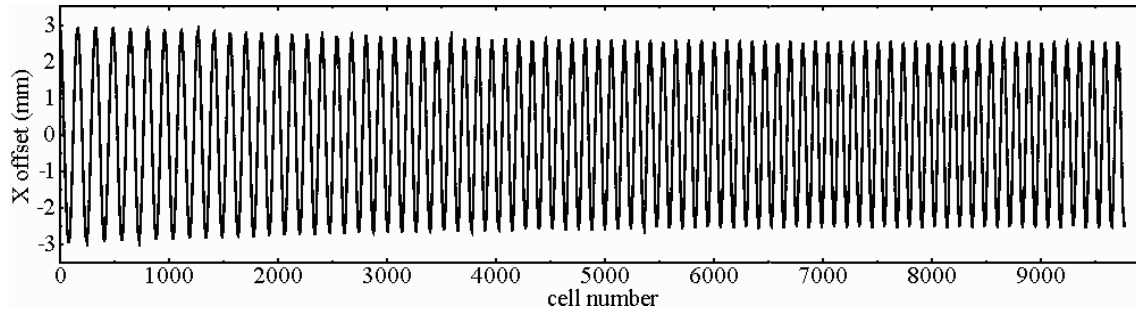

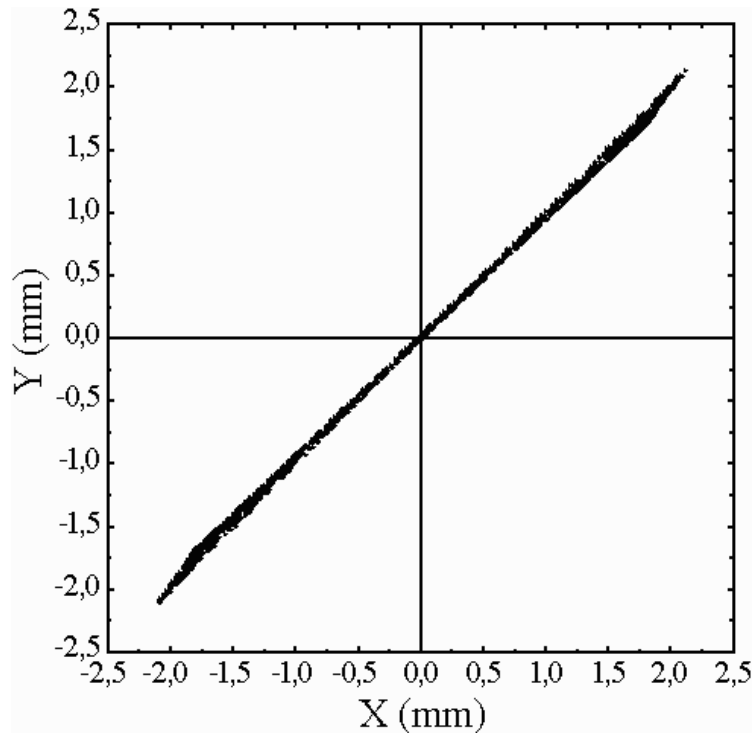Figure 6.14: Position of the bunch centre along the linac for an off-axis injection $dx = +3.0$ mm.

Figure 6.15: Position of the bunch centre along the linac for an off-axis injection $dx = dy = +2.1$ mm, i.e. $dr = 3$ mm.

The rms emittance growth stays constant in all planes, as foreseen. Since the full radius is computed with respect to the linac axis, the beam size increases and decreases periodically, with a period double than the bunch centre oscillation: the minimum value (the bunch centre crosses the axis) corresponds to the nominal radius; the maximum value to the nominal radius plus the oscillation amplitude. In this example, the maximum radius was 11.2 mm, which still fits well in the 16 mm aperture (see Fig. 6.16).
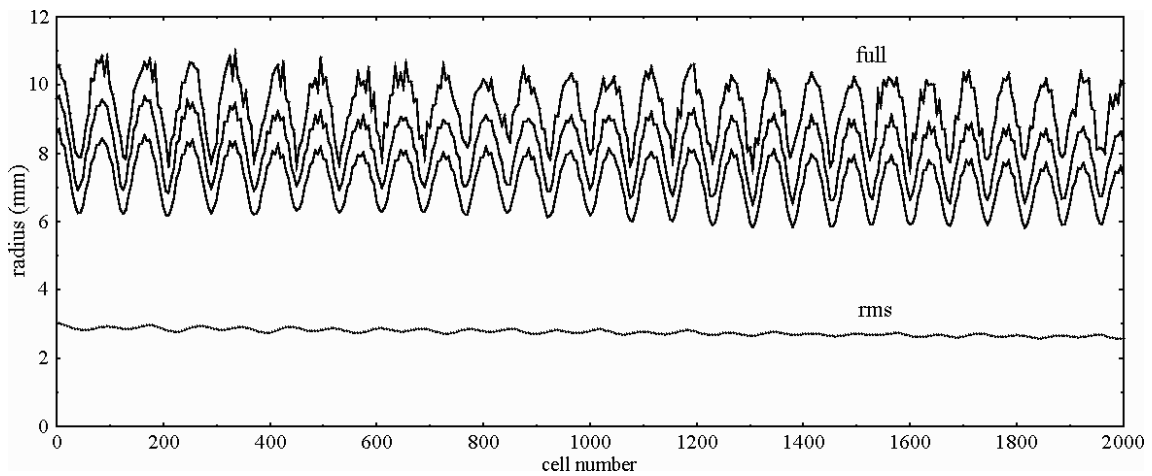
Figure 6.16: Full (100%, 99%, 95%) and rms radius along the first part of the linac for an initial off-axis injection $dx = dy = +2.1$ mm, i.e. $dr = 3$ mm.

The full transverse emittance is much increased, because it is computed with respect to the linac axis; if the bunch oscillation is subtracted (computing the emittance with respect to the bunch centre position), then results are almost identical to those obtained in the linac without errors. This is therefore only a "virtual" increase; nevertheless, as long as the bunch centre movement is not corrected, a larger area of transverse phase space may be filled by the shifting beam and the resulting output value at the end of the linac (in this case $\varepsilon_{full,99\%} = 1.90$ π mm mrad) will stay above the ring acceptance.

In summary, the excitation of one of the three eigenmodes through an initial 20% on-axis mismatch always yields halo formation: transversally for the "quadrupolar" mode (small) and for the "high" mode (stronger), longitudinally for the "low" mode. The combination of more modes may give even larger effects, then it would be recommended to reduce the tolerances for on-axis mismatch by a factor 2, to about

10%. Off-axis mismatch should be minimized as well, by a correction of the coherent bunch oscillations.

The result of this study is that mismatch is dangerous and must be carefully controlled.

6.6 Different input distributions

In Chapter 5.3 the impact of a 6-dim waterbag input distribution for the reference layout (no errors) has been studied. Now the effects of statistical errors of the rf electric field on the so-called case #3 are investigated, with a ratio full-to-rms emittance equal to 8.

As a first example (case #3a) 5000 macroparticles have been used, with the same input distribution as in case #3, i.e. the full emittance $\varepsilon_{full,100\%}$ is slightly larger than the ring acceptance (1.26 π mm mrad) already at the beginning of the linac.

The effects on the transverse planes are negligible, as expected: the output full emittance for 99% of the beam, $\varepsilon_{full,99\%}$, is within the requested acceptance for loss-free injection into the rings. Longitudinally, the output distribution has approximately the same shape as in case #3 but the bunch centre oscillates with an amplitude which reaches a maximum of about 2° in phase and 0.02% in energy, as it happened in the nominal case when errors were added. The emittance growth, if calculated with respect to the nominal synchronous phase and energy of the bunch centre, is almost identical to that obtained in a linac without errors. Results are summarized in Table 6.2.

With 20,000 macroparticles (case #3b) all curves become smoother (see Fig. 6.17), but no remarkable difference is observed with respect to the previous case. The output distribution at the linac end is shown in Figure 6.18; results are summarized in Table 6.2.

From the table it can be observed that adding rf errors to a 6-dim waterbag distribution has only a small effect transversally (compare case #3 with #3a); in particular, the full emittance for 99% of the beam, $\varepsilon_{full,99\%}$, is still acceptable for loss-free injection into the rings. Longitudinally a halo reduction is observed. Increasing the

number of macro-particles from 5000 to 20,000 yields similar or even smaller values and indeterminations.
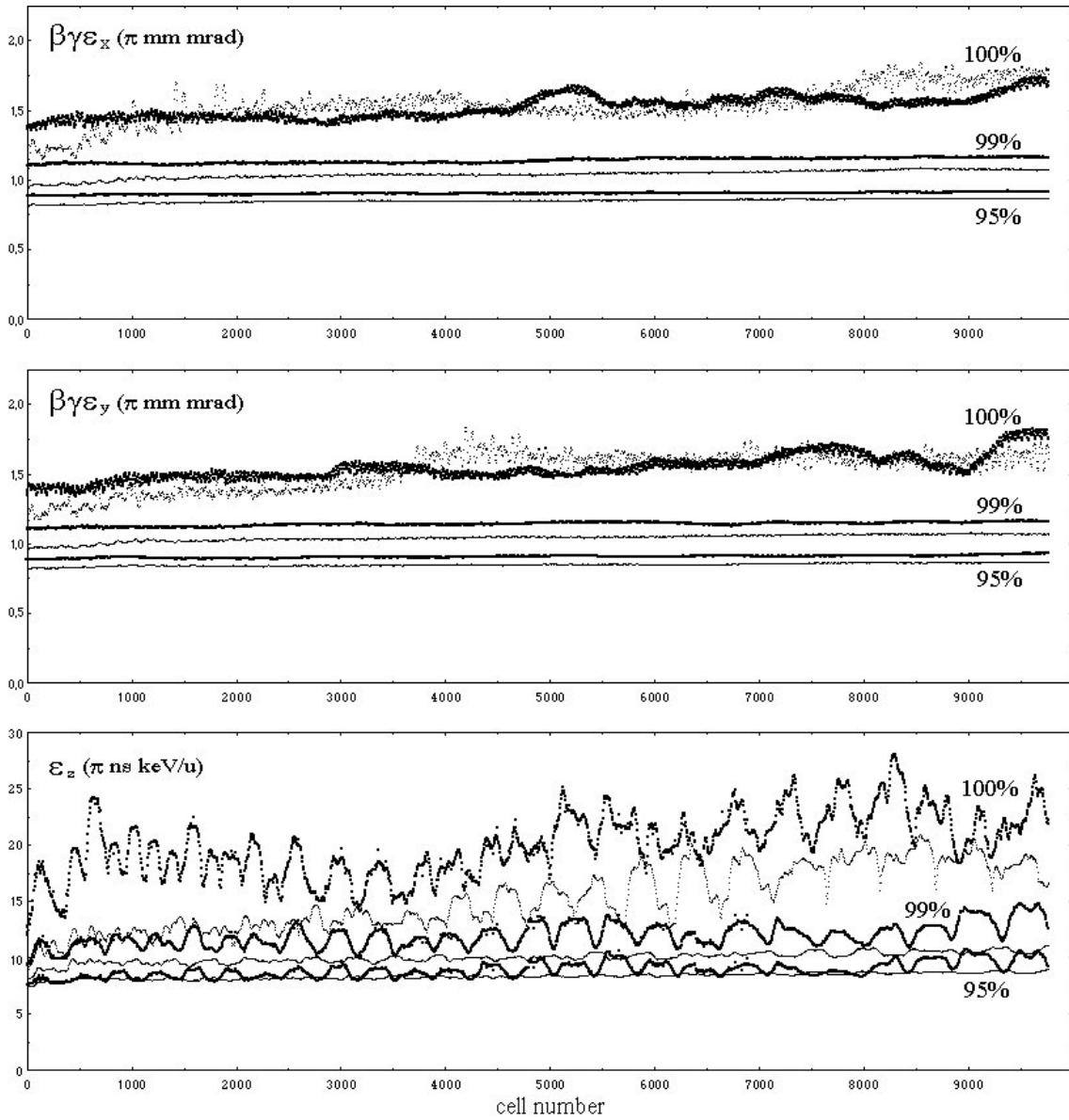

Figure 6.17: Development of the full (100%, 99% and 95%) emittance along the nominal linac (thin line) and with rf field amplitude and phase errors, for a 6-dim waterbag input distribution of 20,000 macroparticles (bold line).

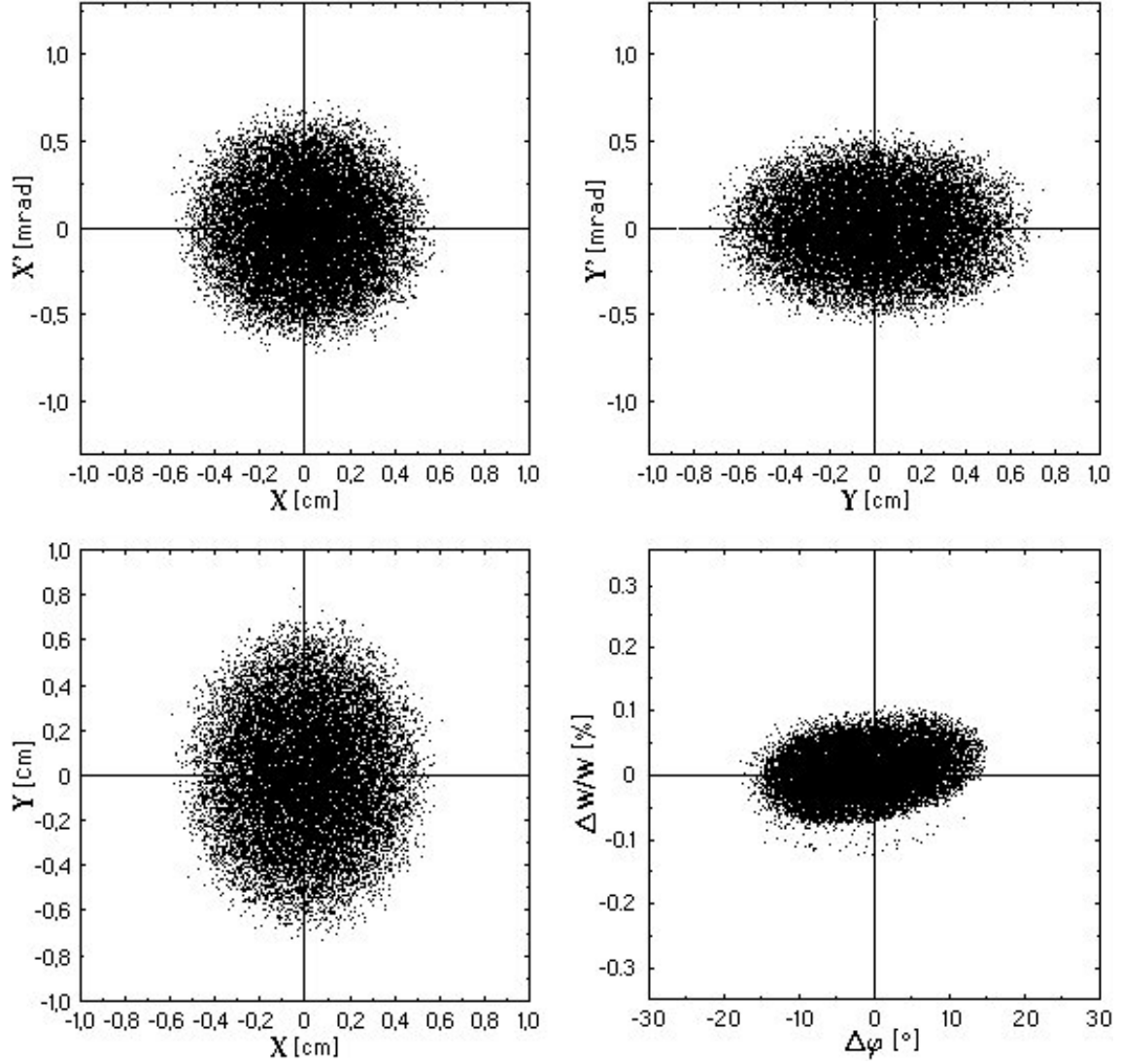In conclusion, the linac is again not very sensitive to statistic errors of the rf electric field, also in the case of a 6-dim waterbag input distribution.

Figure 6.18: Output distribution at the linac end for 20,000 macroparticles; 6-dim waterbag input; 1% amplitude and 1° phase error of th electric rf field.

Table 6.2: Summary of emittances at the end of the linac.

	transverse planes			longitudinal plane		
case	$\varepsilon_{full,100\%}/\varepsilon_{rms}$	$\varepsilon_{full,99\%}/\varepsilon_{rms}$	$\Delta\varepsilon_{rms}/\varepsilon_{rms}$	$\varepsilon_{full,100\%}/\varepsilon_{rms}$	$\varepsilon_{full,99\%}/\varepsilon_{rms}$	$\Delta\varepsilon_{rms}/\varepsilon_{rms}$
#0	9.0 ±0.5	6.3 ±0.2	≈4 %	7.6 ±0.5	5.8 ±0.2	≈10 %
#3	8.9 ±0.3	6.5 ±0.1	≈3 %	14.5 ±3	7.2 ±0.2	≈16 %
#3a	9.6 ±0.3	6.6 ±0.1	≈3 %	11.1 ±1.9	6.2 ±0.5	≈15 %
#3b	9.6 ±0.2	6.44 ±0.03	≈3 %	10.8 ±1.0	6.3 ±0.5	≈14 %

90

6.7 Combination of different sources of error

All the statistical errors discussed in Chapter 6.1 and 6.2 have been combined with the mismatch seen in Chapter 6.5, using the nominal "4d+2d" waterbag input distribution.

For the rf field the nominal errors of $\pm1\%$ in amplitude and $\pm1^{o}$ in phase were used, which have tolerable effects on the beam dynamics. For the quadrupole gradients the case of a uniformly distributed error of $\pm0.2\%$ was selected, which is about equivalent to the case of $\pm2.5\%$ for ten groups of quadrupoles and of $\pm0.1\%$ for the remaining ones.

Then three test cases were run, with 1000 macroparticles, for the quadrupolar, high and low mode mismatch, using an intermediate amplitude of 10% in order not to overwhelm the other sources of error. As before, the low mode mismatch resulted to affect the beam behaviour more than the other two modes, also in presence of other errors.

The last run with the 10% low mode mismatch (worst case) was then repeated, but using 5000 macroparticles, in order to improve the reliability of the calculations. The output distribution at the end of the linac is shown in Figure 6.19.
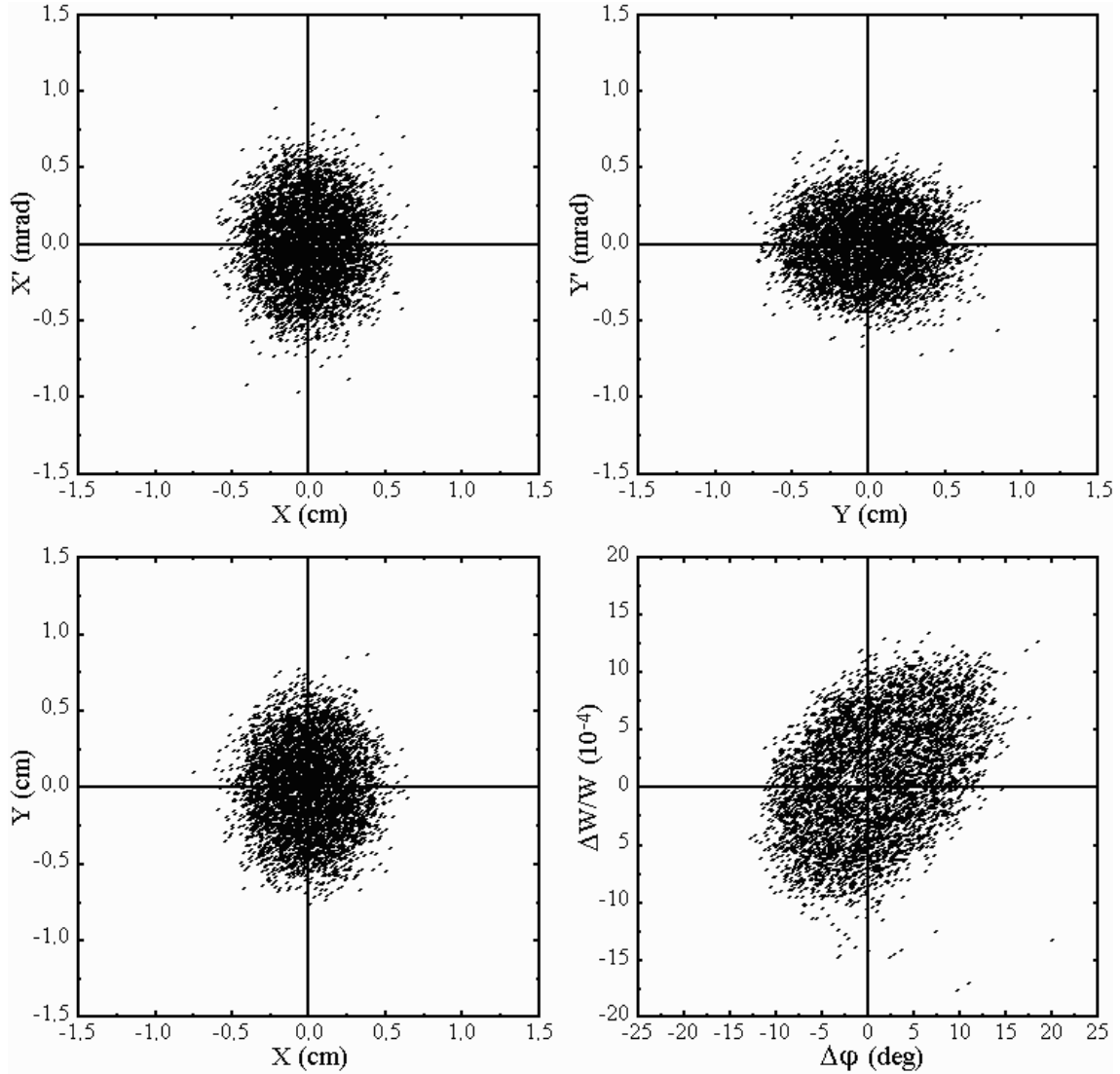
Figure 6.19: Output distribution at the end of the linac with "4d+2d" waterbag input for 5000 macroparticles; ±1% amplitude and ±1° phase error of the electric rf field, ±0.2% error of the quadrupole gradient, 10% low mode mismatch.

The transverse rms emittance growth is 8.5%; the full emittance for 99% of the beam, $\varepsilon_{full,99\%} = 1.38\ \pi$ mm mrad, is slightly larger than requested for ring injection; it should be noticed however that $\varepsilon_{full,98.5\%} = 1.26\ \pi$ mm mrad is just equal to the ring acceptance! The full beam size is 10.9 mm.

The longitudinal rms emittance grows by 12.5%; the ratio full-to-rms emittance for 99% of the beam is just slightly larger than in the nominal case.

In this chapter it has been demonstrated that conventional errors of $\pm 1\%$ in amplitude and $\pm 1^{\circ}$ in phase for the rf field are acceptable: while on the transverse planes their effect is negligible, in the longitudinal one the bunch oscillates in energy and phase with such an amplitude that does not represent a problem for the beam dynamics in the linac; however it has to be verified that the proper conditions for ring injection can be fulfilled after the transport in the transfer line and the bunch rotation.

The tolerance on the quadrupole gradients could not be fixed at a conventional $\pm 1\%$, unless a correction of the beam matching is assumed; only errors of $\pm 0.2\%$ are allowed instead (supposing they are feasible), or one has to look for some correction mechanism.

The effects of beam current fluctuations up to $\pm 10\%$ and the impact of different input distributions, having a larger full-to-rms ratio, are negligible.

It has been found that on-axis mismatch can be described as a superposition of three eigenmodes, with the "high" and the "low" mode mainly responsible for transverse and longitudinal halo formation respectively. In the worst case ("high" + "low" mode), an initial mismatch larger than 10% should be avoided, which will have a major impact on the design of the linac. In that case, even adding the effects of the statistical errors above, the beam has always a stable behaviour: no losses and emittance growth under control. Only 0.5% of the particles are outside the given limit in transverse emittance, but it should be noticed that 2÷3% losses are in any case foreseen in the present scheme for ring injection [Pri98].

Off-axis mismatch is not a problem if linear forces are assumed; the transverse misalignment of quadrupoles lenses (i.e. drift tubes) has a similar effect as off-axis mismatch and it can be neglected under the same assumption, as well as other statistical errors.

CHAPTER 7

TELESCOPING

7.1 Reference design of HIDIF study ($\Delta m/m = \pm 10\%$)

In the HIDIF scenario, the possibility of acceleration and transport of three different atomic species with different masses in the same DTL has been studied, in order to get a "telescoping" effect downstream (see Chapter 2).

The idea is to merge three bunches with identical momenta and hence different velocities, due to their mass differences (neglecting relativistic effects, from $p = mv$ one has $\Delta m/m = -\Delta v/v$). In this way the emittance is not increased, because each ion species is subject to Liouville's theorem only in its own phase space ("non-Liouvillean" merging).

After acceleration in the same main linac during three consecutive macropulses, they would be stored and bunched in separate storage rings, then bunched in induction linacs and finally deflected into a common beam line towards the target, with such a delay between them that they focus in time over the length of this transfer line (see Fig. 7.1).

The velocity difference should be about $\pm 10\%$ around the nominal one ($\beta c \cong 10^8$ m/s) to allow for the kicker rise time and to reduce the mutual space-charge effects during the longitudinal penetration of the bunches. Since $\Delta m/m = -\Delta v/v$, also the mass difference should be about $\pm 10\%$ around the nominal ^{209}Bi. The candidate ions are ^{187}Re and ^{232}Th.
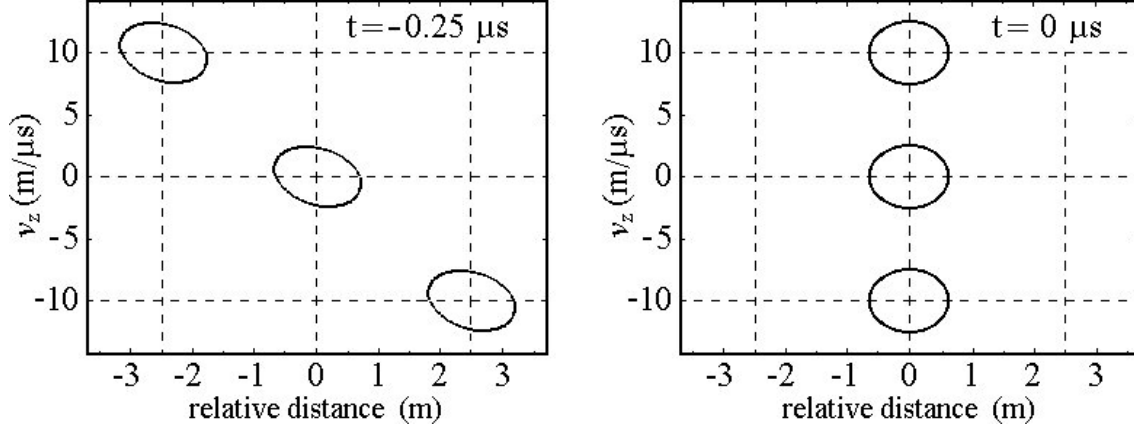
Figure 7.1: Final overlap of telescoping bunches in velocity space during the last 0.25 μs.

In order to satisfy the relation $\beta\lambda = L_c$ between the particle velocity β and the cell length L_c, the velocity β must be the same for the three species all along the linac (and also along all the structures in the funnelling section, which are rf linacs as well). This means that the specific kinetic energy must also be the same at any point. In particular, at the linac input, it is possible to calculate the parameters shown in Table 7.1 using simple relativistic relations.

Then the output momentum for the nominal mass ($A = 209$) can be calculated and the required output energy for the other two are found (see Tab. 7.2). The lighter species should have a <u>total</u> kinetic energy W_{out} about 10% higher than the nominal one; the heavier species about 10% smaller. Notice that the difference in the <u>specific</u> kinetic energy W_{out}/A is about ±20%.

Table 7.1: Available kinetic energy and momentum at the linac input.

A	W_{in}	W_{in}/A	$\gamma_{in} = W_{in}/mc^2+1$	$\beta_{in} = (1-\gamma_{in}^{-2})^{1/2}$	$\beta_{in}\gamma_{in}$	$p_{in} = \beta_{in}\gamma_{in}\,mc$
209	2.09 GeV	10.0 MeV/u	1.01066	0.1449	0.1464	28.70 GeV/c
187	1.87 GeV	10.0 MeV/u	1.01066	0.1449	0.1464	25.68 GeV/c
232	2.32 GeV	10.0 MeV/u	1.01066	0.1449	0.1464	31.86 GeV/c

Table 7.2: Required kinetic energy and momentum at the linac end.

A	W_{out}	W_{out}/A	$\gamma_{out} = W_{out}/mc^2+1$	$\beta_{out} = (1-\gamma_{out}^{-2})^{1/2}$	$\beta_{out}\gamma_{out}$	$p_{out} = \beta_{out}\gamma_{out}\,mc$
209	10.45 GeV	50.0 MeV/u	1.05330	0.3141	0.3308	64.86 GeV/c
187	11.61 GeV	62.1 MeV/u	1.06617	0.3468	0.3698	64.86 GeV/c
232	9.46 GeV	40.8 MeV/u	1.04347	0.2834	0.2980	64.86 GeV/c

Since the velocity gain must be identical for the three species, then the accelerating rf electric field has to be increased or decreased according to the mass number A, so that lighter ions experience a smaller force than heavier ones and get the same acceleration.

As can be seen from the last column of Table 7.1, the momentum p will be different for each species, therefore also the focusing has to be adjusted (the three ion species have the same charge $q = +1$ and therefore the beams have different rigidities p/q).

On the other hand, acting in this way, all the three species will have the same specific kinetic energy at the output of the linac, as summarized in Table 7.3.

Table 7.3: Actual kinetic energy and momentum at the linac end.

A	W_{out}	W_{out}/A	$\gamma_{out} = W_{out}/mc^2+1$	$\beta_{out} = (1-\gamma_{out}^{-2})^{1/2}$	$\beta_{out}\gamma_{out}$	$p_{out} = \beta_{out}\gamma_{out}\,mc$
209	10.45 GeV	50.0 MeV/u	1.05330	0.3141	0.3308	64.86 GeV/c
187	9.35 GeV	50.0 MeV/u	1.05330	0.3141	0.3308	58.03 GeV/c
232	11.60 GeV	50.0 MeV/u	1.05330	0.3141	0.3308	72.00 GeV/c

The proposed solution consists in extending the length of the linac by adding a new section, capable to accelerate the lighter ions from 50.0 to 62.1 MeV/u (see Fig. 7.2). This section must not be used for the ions with nominal mass, which will just be transported along it without acceleration (rf field switched off). The heavier ions need to be accelerated only up to 40.8 MeV/u, therefore also the last part of the nominal linac must not be used for them.
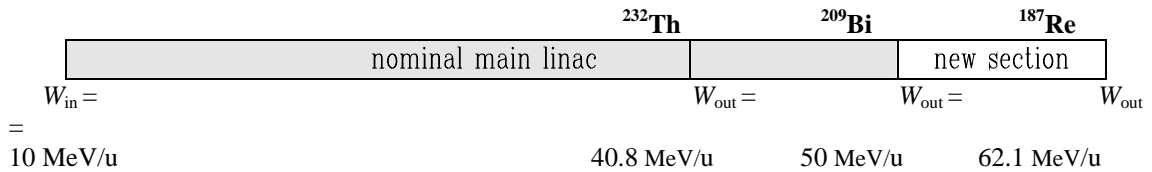

Figure 7.2: Main linac layout for $\Delta m/m = \pm 10\%$.

While there is no conceptual problem in extending the linac length (the new section would be however more than 800 m long), one has to investigate carefully what happens to the nominal and heavier ions which will have to be transported through a

very long drift line. Furthermore, an independently phased "rebuncher" cavity must be placed after every switched off "tank", which implies a completely new design of the last part of the linac. Finally, the rf electric field and the quadrupole gradients must be adapted to the ion mass, changing from macropulse to macropulse, which could imply technical problems.

The design procedure may be divided into the following four steps:

Step 1: The rf electric field is scaled with the mass ratio ($E_o = 3.00$ MV/m for ^{209}Bi, 2.68 MV/m for ^{187}Re and 3.33 MV/m for ^{232}Th) in order to fulfil the relation $\beta\lambda = L_c$ and get the same energy increase per cell as in the nominal linac, so that each species is accelerated from 10.0 to 50.0 MeV/u. The quadrupole gradients are also scaled with the same ratio, since the beam rigidity at fixed energy is proportional to the mass; for the heavier ion, this implies that a magnetic pole tip field of 1.28 Tesla is reached at the beginning of the linac, unless the aperture radius is slightly decreased (which seems not to be a problem at the beginning).

Step 2: The last part of the main linac, where the electric field is switched off for transporting ^{232}Th ions, is found to be 840 m long (1880 cells). To provide longitudinal focusing, a few cavities should however be used as "rebuncher", leaving them on but with -90° phase. Notice that the field in each "rebuncher" cavity must be independently phased in order to fit with the travelling bunch, since the cell length increases but the ^{232}Th beam has a constant energy (at the linac end, in a 5 cavity "tank" powered by a single rf power amplifier, there would be a phase shift of about 40° from a cavity to the next one); keeping the nominal field amplitude of 3.33 MV/m, a single-cavity "rebuncher" must be placed after every switched off "tank". The transverse focusing is kept constant, but the product of quadrupole length and gradient has to be slightly reduced with respect to the nominal linac, to compensate for the missing rf defocusing effect.

Step 3: The new section of the linac, to accelerate ^{187}Re ions from 50.0 to 62.1 MeV/u, is designed adopting the same procedure as in the main linac, going through the codes CLAS and GENLIN; a 5F05D0 focusing scheme is assumed and $E_o = 3.33$ MV/m is set (as for the heaviest ion species in order to make the new section as short as possible). With a constant synchronous phase of -30°, this yields a length of 760 m

(1540 cells). The quadrupole lengths and strengths are set according to the same principles than in the main part of the linac.

Step 4: The rf field of the rebuncher cavities (one every fourth cell) is set to 3.33 MV/m for the nominal ^{209}Bi, which is transported at 50.0 MeV/u along the new section. It has to be increased up to 3.63 MV/m for the heavier ^{232}Th, which is transported at 40.8 MeV/u along 1600 m, in order to achieve a good longitudinal focusing. For both species, the transverse focusing is kept constant, but slightly reduced with respect to the nominal linac.

A run with 1000 macroparticles was made for each of the three species in the new main linac, which total length is now 11,315 cells (corresponding to 4.14 km); the run had to be splitted into two parts, since only 9999 cells are allowed by MAPRO code. In all cases it was possible to accelerate the given ion mass to the requested momentum and to transport it up to the end of the linac without losses and preserving the beam size.

Transversally, the rms emittance remains quite small for ^{187}Re and ^{209}Bi, with a final growth around 4%. For the heavier ^{232}Th the growth is even smaller in the first part (7895 cells) but it grows then with a larger rate in the last part, reaching 6% after having been drifting along 3420 cells at a constant energy of 40.8 MeV/u (see Fig. 7.3).

Longitudinally, the rms emittance for all the three species looks quite similar all along the linac, reaching growth values between 15% and 18% at its end.
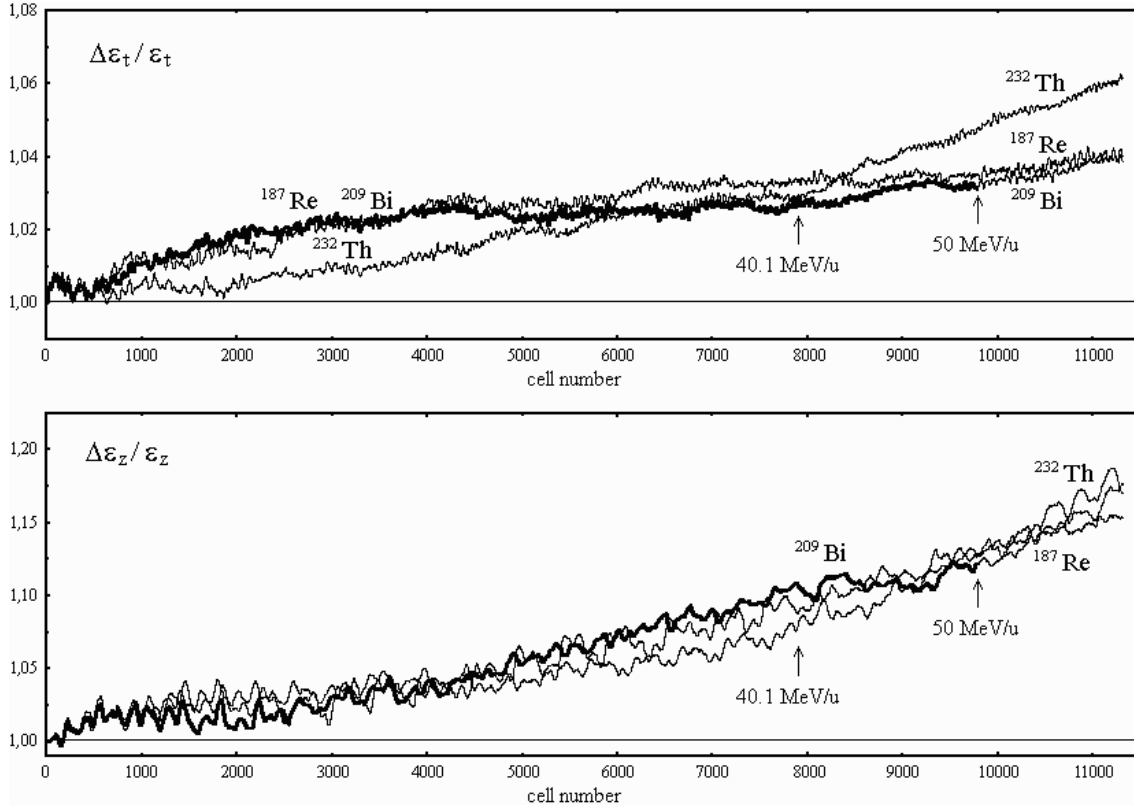
Figure 7.3: Rms emittance growth along the new linac for A = 187, 209, 232; nominal "4d+2d" waterbag input of 1000 macroparticles; no errors. The bold curve is the old nominal linac.

The full transverse emittance always increases during a drift; in particular $\varepsilon_{full,99\%}$ remains below the ring acceptance for the lighter species (which is always accelerated), it is slightly too large for the nominal one and becomes 15% too large for the heavier one. In spite of some transverse filamentation, the full radius is always below 9 mm.

The full longitudinal emittance is quite good for the lighter ^{187}Re and for the nominal ^{209}Bi, but it is quite distorted and filamented for the heavier ^{232}Th.

The calculations for the heavier species were repeated using 5000 macroparticles; results from simulations showed a big improvement in terms of longitudinal rms emittance growth ($\Delta\varepsilon_z / \varepsilon_z$ decreases from 18% to 12%), while transversally $\varepsilon_{full,99\%}$ = 1.26 π mm mrad is just at the limit for proper injection into the rings.

Nevertheless the beam dynamics design is not very robust for the heavier ^{232}Th ion; moreover the electric field of 3.63 MV/m and the magnetic field of 1.28 Tesla might be too large. For this reason new calculations have been performed, where the mass difference between species is reduced to $\Delta m/m = \pm 5\%$, in order to possibly simplify the linac design and to obtain more reliable results.

7.2 Calculations for a lower mass difference ($\Delta m/m = \pm 5\%$)

For a mass difference of about $\pm 5\%$ around the nominal one (^{209}Bi), two possible ions are ^{197}Au and ^{222}Rn. Then output momentum and energy have been re-calculated (see Tab. 7.4).

With the same assumptions as in Chapter 7.1, the length of the linac must be extended by adding a new section, which accelerates the lighter ions from 50.0 to 56.1 MeV/u only; this time it will be therefore about half long. The other two species will only be drifting in this new section; the heavier one will be drifting also in the last part of the nominal linac (see Fig. 7.4).

Table 7.4: Required kinetic energy and momentum at the linac end.

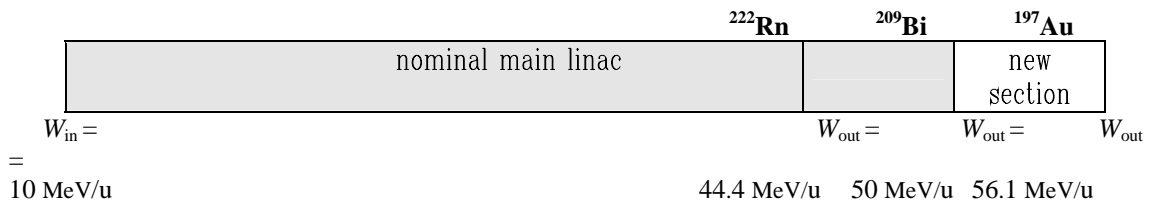| A	W_{out}	W_{out}/A	$\gamma_{out} = W_{out}/mc^2 + 1$	$\beta_{out} = (1-\gamma_{out}^{-2})^{\frac{1}{2}}$	$\beta_{out}\gamma_{out}$	$p_{out} = \beta_{out}\gamma_{out}\, mc$
209	10.45 GeV	50.0 MeV/u	1.05330	0.3141	0.3308	64.86 GeV/c
197	11.05 GeV	56.1 MeV/u	1.05981	0.3312	0.3510	64.86 GeV/c
222	9.87 GeV	44.4 MeV/u	1.04738	0.2974	0.3115	64.86 GeV/c

Figure 7.4: Main linac layout for $\Delta m/m = \pm 5\%$.

Following the same approach of Chapter 7.1, the beam behaviour of the three species was investigated along the new linac. In particular, electric fields of 2.83, 3.00 and 3.19 MV/m for the accelerating part and a maximum magnetic field of 1.22 Tesla

have been used. The last part of the main linac is 350 m long (760 cells); the new part has a length of 390 m (810 cells) and accelerates ^{197}Au ions from 50.0 to 56.1 MeV/u. The rebuncher cavities use an electric field of 3.19 MV/m for the nominal ^{209}Bi and the heavier ^{222}Rn.

Results are good for the nominal ^{209}Bi and the lighter ^{197}Au, but the heavier ^{222}Rn is still problematic. Figure 7.5 shows the rms emittance growth along the linac.

Yet a higher rebunching field has been used for the heavier species (values up to 4.0 MV/m have been tested), but without significant reduction of the longitudinal emittance.

In conclusion, this quick check for $\Delta m/m = \pm 5\%$ gave no improvement with respect to the nominal design ($\Delta m/m = \pm 10\%$), then calculations have been stopped.

The "telescoping" option is not recommended from the point of view of particle dynamics in the main linac and it adds problems and technical difficulties, not only to the DTL design but also to the funnelling section. A practical solution is not yet available.
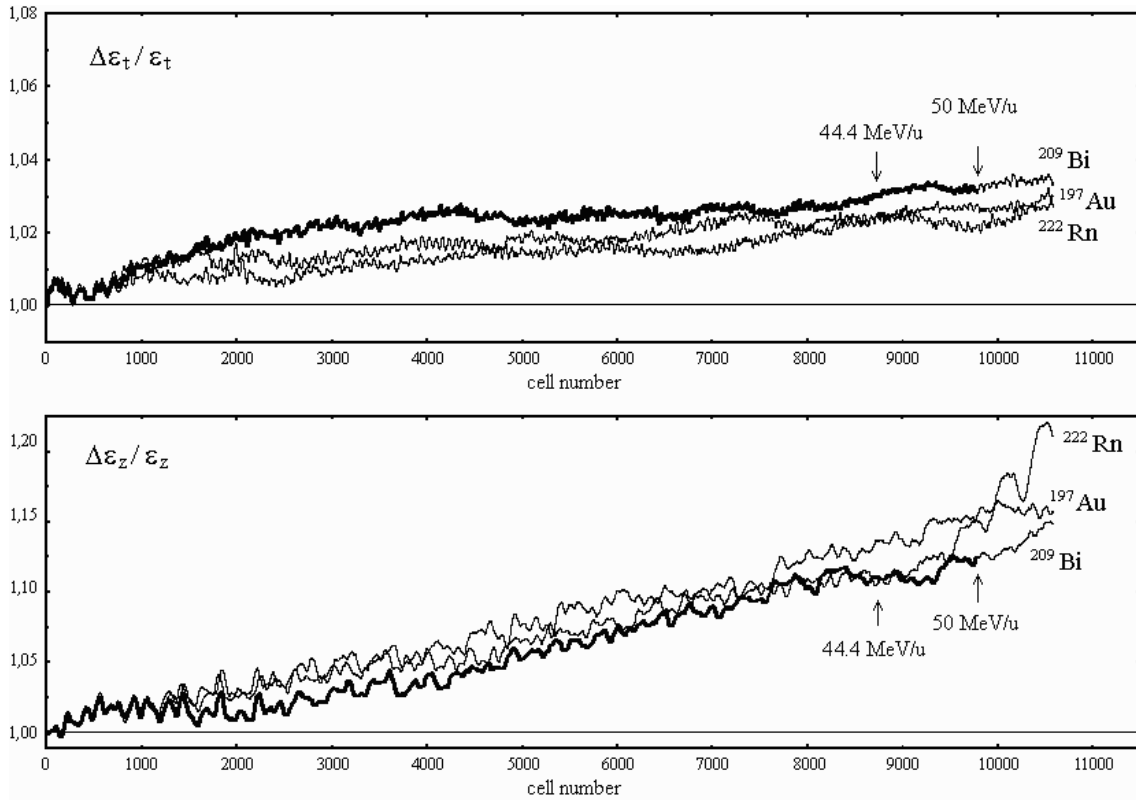
Figure 7.5: Rms emittance growth along the linac for A = 197, 209, 222; nominal "4d+2d" waterbag input for 1000 macroparticles; no errors. The bold curve is the old nominal linac.

CHAPTER 8

TRANSFER LINE BETWEEN DTL AND RINGS

The maximum momentum spread allowed in a ring is in general smaller than in a linac, since a change in momentum yields to a different orbit and this effect adds up during several turns. Therefore it is quite usual to "debunch" the beam at the end of a linac, i.e. to increase the bunch size in phase and then to "rotate" it in the longitudinal phase space in order to reduce its size in energy (the emittance should remain constant); in this way the required *dp/p* for the ring is provided from the injector linac.

The first step of this process can be performed by means of a transfer line, where the beam is drifting and the length of the bunch increases owing to the momentum spread and to space-charge forces; the second step by means of one or more rf cavities which provide a linear ramping voltage decelerating the particles with a higher momentum and accelerating those with a smaller one. The net result of this process is a reduction of the momentum spread at the expense of an increase of the bunch length.

For loss-free injection from the Alvarez type Drift Tube Linac discussed in this thesis to the following storage rings, a transverse emittance smaller than 4π mm mrad (full, geometrical) and a momentum spread smaller than $\pm 2 \times 10^{-4}$ are requested for 99% of the beam [Pla97].

The full geometrical emittance computed at the end of the nominal linac, without errors, is 3.5 π mm mrad in both transverse planes, which fulfils the first requirement; but the energy spread for 99% of the beam is $\pm 8 \times 10^{-4}$, corresponding to $dp/p = \pm 4 \times 10^{-4}$, which is too large [Dei98b]. When adding statistical errors and mismatch, the transverse limitation can still be fulfilled (see Chapter 6), but the momentum spread gets even larger.

Therefore a bunch rotation system should be foreseen: at first the beam drifts and gets longitudinally defocused, then one or more rf cavities have to be positioned

somewhere behind the linac. The needed length L_{tr} of this transfer line and the rotation voltage U_o are significantly affected by the space-charge forces.

As a first step, numerical simulations have been performed starting from the output distribution of the nominal error-free linac, for nominal "4d+2d" waterbag input [Dei98d] and for both the 6-dim waterbag and the "4d+2d" Gaussian input (see Chapter 5.3).

In a second step, "quasi-analytical" calculations have been performed in order to evaluate the effect of rf errors on the longitudinal emittance envelope along the transfer line and in the bunch rotator. Results have been compared to a numerical simulation starting from the output distribution of the nominal linac ("4d+2d" waterbag input) with mismatch (see Chapter 6.5), adding an artificial offset of the bunch centre to account for rf errors and considering a nonlinear voltage bunch rotation (combination of all errors).

Finally, the case of a 6-dim waterbag input for 20,000 macroparticle with rf errors (see Chapter 6.7) was considered [Par98a], extending the calculations up to a nonlinear voltage bunch rotator [Par99].

8.1 Numerical simulations for the reference layout

For simplicity, the same 5F05D0 focusing scheme as in the linac was adopted for the design of the 50 MeV/u transfer line, without accelerating gradient and keeping the same parameters as in the last cell of the linac; only the quadrupole strengths were slightly reduced, because of the missing rf defocusing effect. The beam behaviour along the transfer line has been examined performing particle dynamics calculations with MAPRO code, using as an input the 400 mA ^{209}Bi$^+$ ion beam distributions at the output of the linac.

The bunch rotation was initially simulated as a simple linear kick: a voltage U_o yields an energy variation $\Delta W_i = qU_o\Delta\phi_i$ for the i-th macroparticle. In a second step a more realistic system has been studied, based on the superposition of three harmonic components.

For the nominal case investigated in Chapter 5.2, the total bunch width at the end of the linac is $\Delta\phi_o^{max} = \pm 15^o$, corresponding to a rms bunch length $b = \pm 0.7$ cm; after a 170

m long drift, it is increased to $\Delta\phi_L^{max} = \pm 85^o$, corresponding to ± 4.9 cm rms; the radial dimensions stay constant (see Fig. 8.1).

In Figure 8.2 the rms energy spread along the transfer line is shown, together with the full one for 100%, 99% and 95% of the beam. Owing to the small, but not negligible, longitudinal space-charge forces over $L_{tr} = 170$ m, the rms energy spread increases from ± 3 to $\pm 6.7 \times 10^{-4}$, whereas the energy spread for 99% of the beam increases from ± 6.5 to $\pm 13 \times 10^{-4}$. The saturation value of the rms energy spread is consistent with the result of the analytical formula derived by applying linear space-charge forces only [Bon93].

Most of the energy spread increase occurs in the first 75 m, where the rms bunch length is less than $b = 2$ cm; in this part of the transfer line, image-charge effects can be neglected if the beam pipe radius is made large enough compared to b (about 5 cm). In principle, they cannot be neglected for the next 95 m, but they will only cause minor changes of the particle distribution, because the travelled path is short [Bon96].
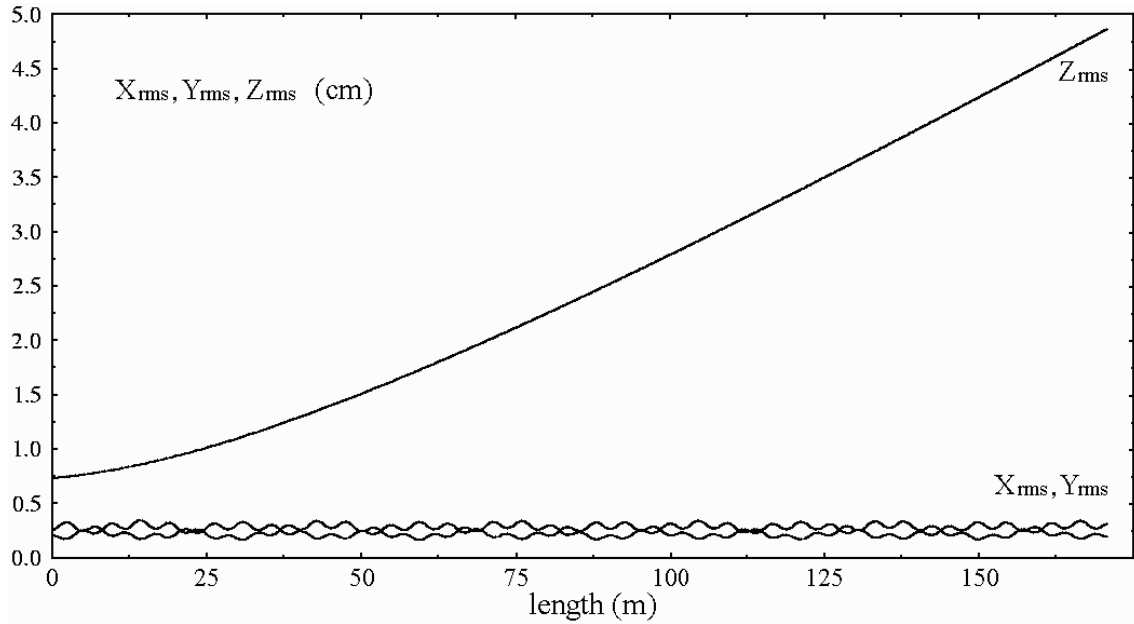
Figure 8.1: Bunch rms length and radius along the transfer line.
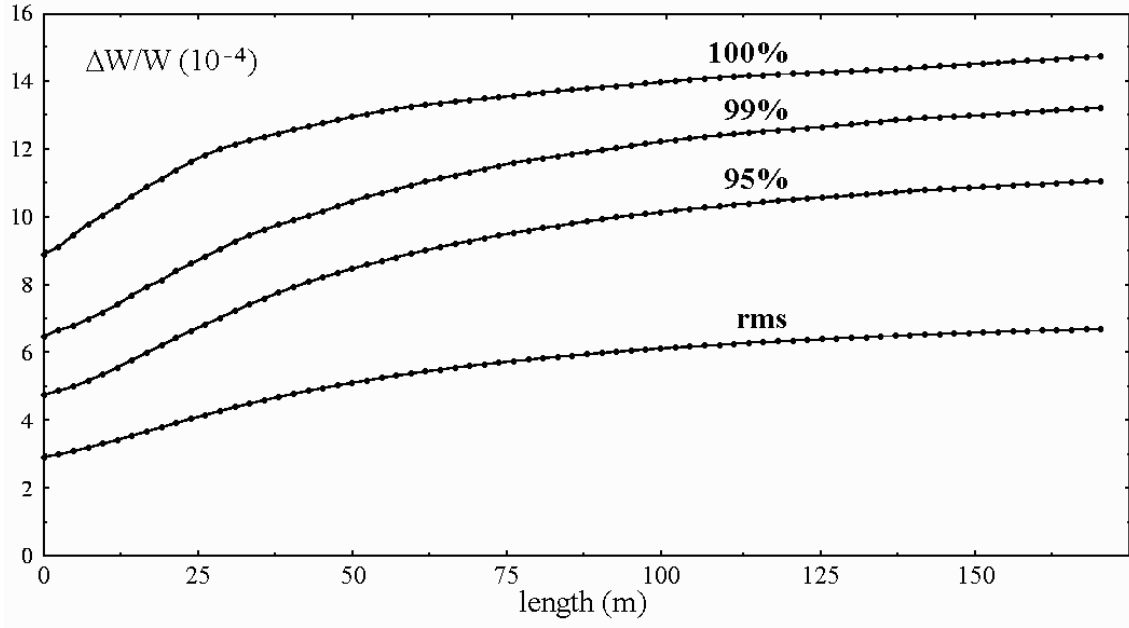
Figure 8.2: Full (100%, 99% and 95%) and rms energy spread along the transfer line.

The momentum spread can finally be reduced by placing a bunch rotation system at the end of the transfer line; for a first test a linear kick with $U_o = 11.2$ MV has been used [Par97]. In Figure 8.3 the longitudinal emittance is shown at the end of the linac and of the transfer line, before and after bunch rotation; the energy spread for 99% of the beam reduces from ± 13 to $\pm 1.8 \times 10^{-4}$, well below the limit for ring injection (dashed lines).
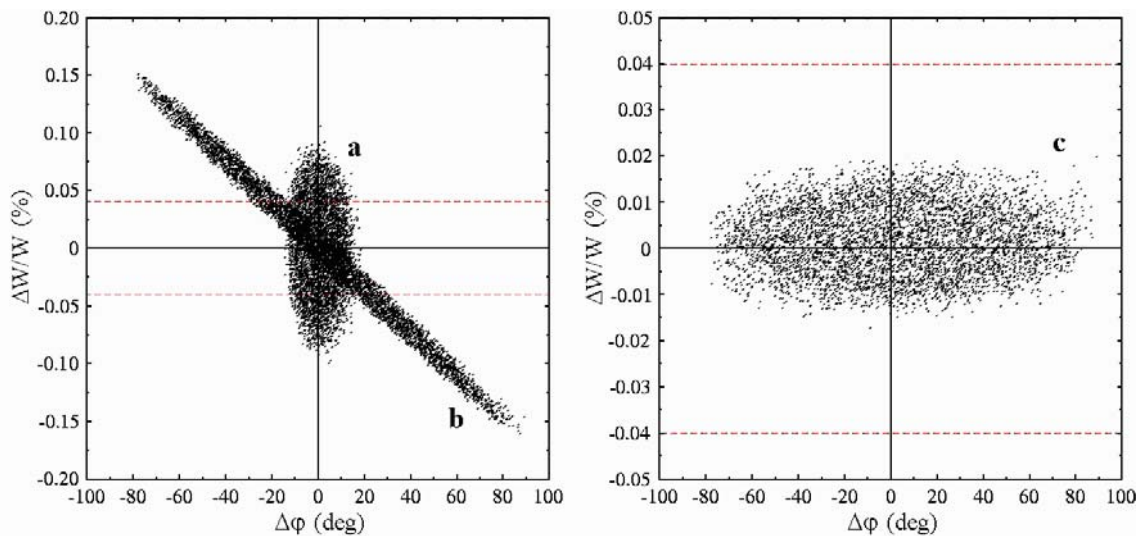
Figure 8.3: Output distribution of 5000 macroparticles for nominal error-free linac layout: at the end of the linac (a); at the end of the transfer line before rotation (b); after linear voltage bunch rotation (c).

98

In case that a 6-dim waterbag distribution or a "4d+2d" Gaussian distribution is used as a linac input, rather than the nominal "4d+2d" waterbag one, the longitudinal emittance after bunch rotation is more filamented and the energy spread is larger.

Figure 8.4 shows the results obtained for the six cases studied in Chapter 5.3. It can be observed that the bunch shape is more deformed than in the nominal case, owing to the larger initial size, but the whole bunch always stays within the allowed energy spread of $\pm 4 \times 10^{-4}$, apart from case #5, where however only one macroparticle is outside the allowed region (i.e. 99.98% of the beam fulfils the requirement). In absence of errors the impact of different input distributions is therefore negligible.

Nevertheless, since errors on the rf electric field amplitude ($\pm 1\%$) and phase ($\pm 1^{o}$) are expected to shift the position of the bunch centre by $\pm 3 \times 10^{-4}$ in energy (and mismatch may produce additional filamentation), it is necessary to check their influence on the beam behaviour along the transfer line.
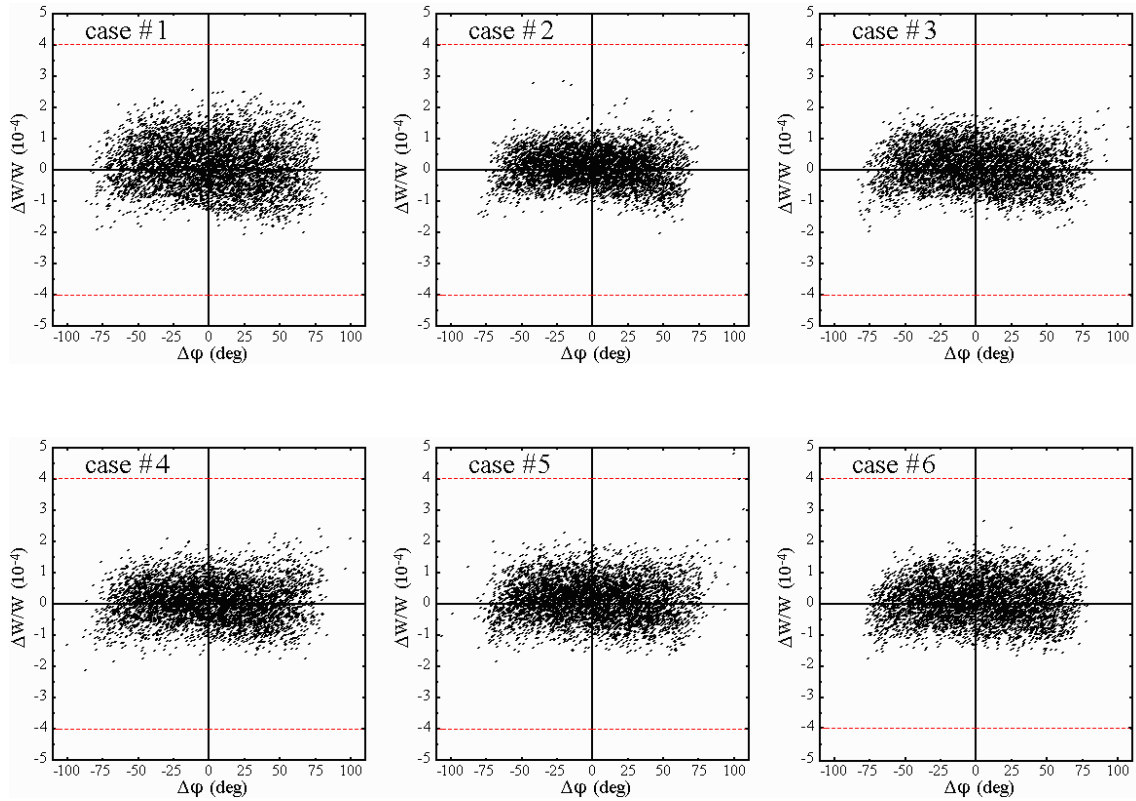

Figure 8.4: Output distribution in the longitudinal plane after linear voltage bunch rotation, for nominal error-free linac layout with 5000 macroparticles.

8.2 Effect of rf field errors on bunch trasport and rotation

The analytical representation of the beam ellipse in the longitudinal plane, using the full dimensions $\Delta\phi$ and ΔW, is given by:

$$\gamma\,(\Delta\phi)^2 + 2\alpha\,\Delta\phi\,\Delta W + \beta\,(\Delta W)^2 = \varepsilon_l^{\text{full}}$$

<u>At the linac end</u> (subscript 0) the ellipse is upright, i.e. $\alpha_0 = 0$ and $\beta_0\gamma_0 = 1$; from numerical simulations the maximum amplitudes $\Delta\phi_0^{\text{max}} = 15^{\text{o}}$ and $\Delta W_0^{\text{max}} = 10.5$ MeV are known (since $\Delta W/W = 10.5 \times 10^{-4}$ and $W = 10$ GeV); then from well-known relations (see Chapter 3.1):

$$\Delta\phi_0^{\text{max}} = (\beta_0\,\varepsilon_l^{\text{full}})^{\frac{1}{2}} = (\varepsilon_l^{\text{full}}/\gamma_0)^{\frac{1}{2}} \quad \rightarrow \quad \gamma_0 = \varepsilon_l^{\text{full}}/(\Delta\phi_0^{\text{max}})^2 = 0.70 \text{ MeV/deg}$$

$$\Delta W_0^{\text{max}} = (\gamma_0\,\varepsilon_l^{\text{full}})^{\frac{1}{2}} = (\varepsilon_l^{\text{full}}/\beta_0)^{\frac{1}{2}} \quad \rightarrow \quad \beta_0 = \varepsilon_l^{\text{full}}/(\Delta W_0^{\text{max}})^2 = 1.43 \text{ deg/MeV}$$

and the beam ellipse equation in the $\Delta\phi_0\,\Delta W_0$ co-ordinates may be re-written as:

$$\varepsilon_l^{\text{full}}\,(\Delta\phi_0/\Delta\phi_0^{\text{max}})^2 + \varepsilon_l^{\text{full}}\,(\Delta W_0/\Delta W_0^{\text{max}})^2 = \varepsilon_l^{\text{full}}$$

$$(\Delta\phi_0/15^{\text{o}})^2 + (\Delta W_0/10.5 \text{ MeV})^2 = 1 \qquad\qquad (8.1)$$

At the end of the transfer line, <u>before bunch rotation</u> (subscript L), the ellipse is tilted, i.e. $\alpha_L \neq 0$; from numerical simulations it is known that the emittance growth in the transfer line is negligible and the maximum amplitudes are $\Delta\phi_L^{\text{max}} = 80^{\text{o}}$ and $\Delta W_L^{\text{max}} = 16$ MeV; then:

$$\Delta\phi_L^{\text{max}} = (\beta_L\,\varepsilon_l^{\text{full}})^{\frac{1}{2}} \quad \rightarrow \quad \beta_L = (\Delta\phi_L^{\text{max}})^2/\varepsilon_l^{\text{full}} = 40 \text{ deg/MeV}$$

$$\Delta W_L^{\text{max}} = (\gamma_L\,\varepsilon_l^{\text{full}})^{\frac{1}{2}} \quad \rightarrow \quad \gamma_L = (\Delta W_L^{\text{max}})^2/\varepsilon_l^{\text{full}} = 1.6 \text{ MeV/deg}$$

$$\alpha_L = (\beta_L\gamma_L - 1)^{\frac{1}{2}} = 8.0$$

and the beam ellipse equation in the $\Delta\phi_L\,\Delta W_L$ co-ordinates may be re-written as:

$$1.6 \text{ MeV/deg } (\varDelta\phi_L)^2 + 2\times 8.0 \ \varDelta\phi_L \ \varDelta W_L + 40 \text{ deg/MeV } (\varDelta W_L)^2 = 160 \text{ deg MeV}$$

$$(\varDelta\phi_L / 10^o)^2 + 0.1 \ \varDelta\phi_L \ \varDelta W_L + (\varDelta W_0 / 2 \text{ MeV})^2 = 1 \tag{8.2}$$

<u>After bunch rotation</u> (subscript f), the phase of each point of the ellipse is equal to the previous one ($\varDelta\phi_f = \varDelta\phi_L$), while its energy changes by $qU_o\varDelta\phi_L$, with $U_o = 11.2$ MV:

$$\varDelta W_f = \varDelta W_L - 11.2 \text{ MeV} \times \varDelta\phi_L \times (2\pi/180^o) \tag{8.3}$$

Using Eq. (8.1), (8.2) and (8.3) one can plot the longitudinal beam ellipse, starting from the values given by numerical simulations for the HIDIF linac (see Fig. 8.5).

The condition for ring injection in the HIDIF scenario is that the longitudinal beam ellipse should lay within $\pm$ 4 MeV. As can be seen from the figure, this implies −at least− that the energy offset of the bunch centre <u>after rotation</u> is smaller than ± 2 MeV.

The bunch centre behaves like a single particle with zero current, then its energy offsets $\varDelta W_c$ does not change along the transfer line, while its phase offset is given by:

$$\varDelta\phi_{c,L} = \varDelta\phi_{c,0} + f_L \ \varDelta W_{c,0}$$
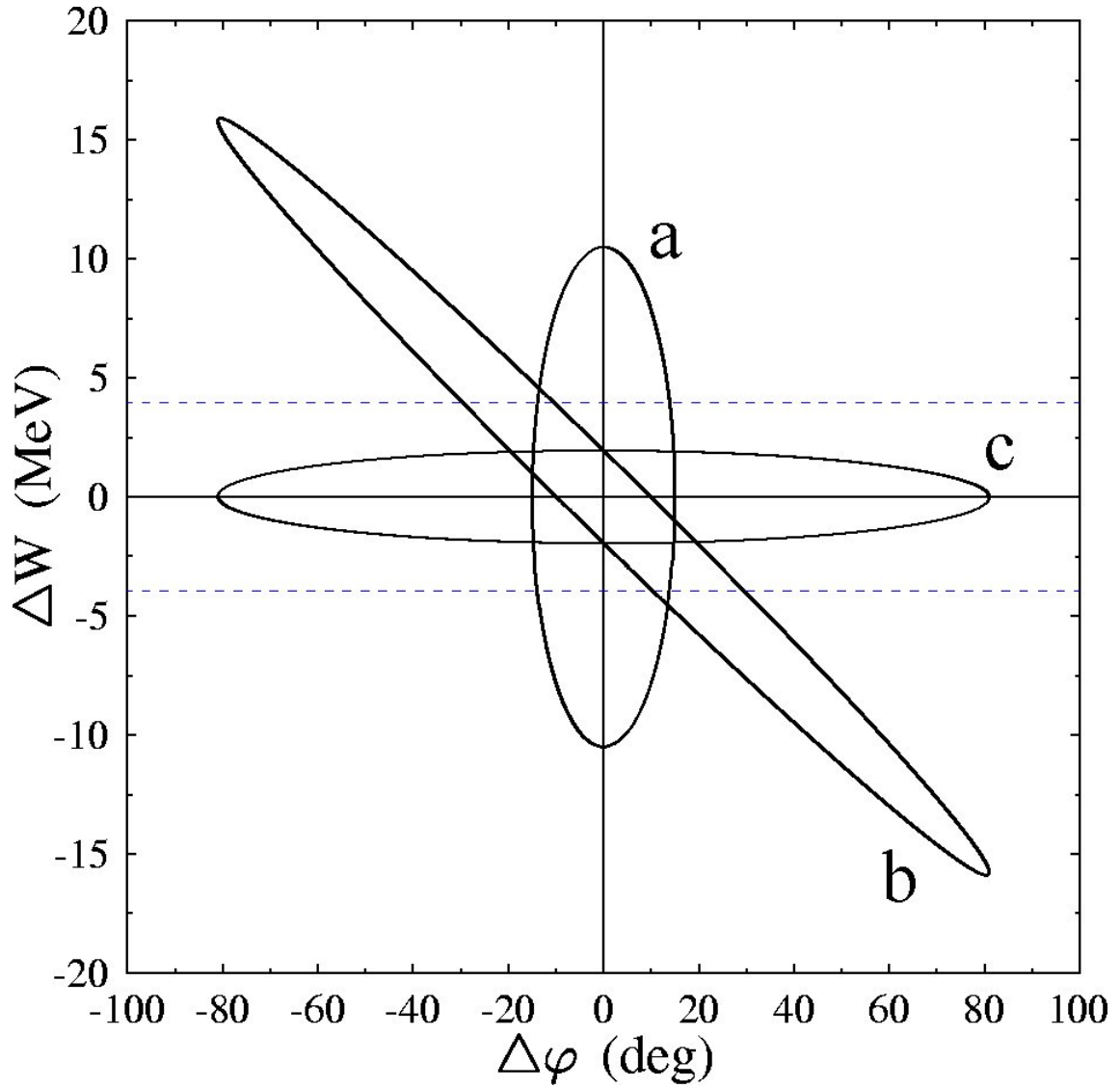
Figure 8.5: Quasi-analytical approach: output ellipse at the end of the linac (a), at the end of the transfer line before rotation (b) and after linear voltage bunch rotation (c).

where f_L is a geometric factor that can be computed from known parameters [Bon98c]:

$$f_L = 360^o\, L_{tr}\,/\,\lambda\,(\beta\gamma)^3\, m_0 c^2 = 360^o \times 170\,\text{m}\,/\,1.5\,\text{m} \times (0.33)^3 \times 209 \times 938\,\text{MeV} = 5.8^o/\text{MeV}$$

At the end of the transfer line, before bunch rotation, one will then have:

$$\Delta\phi_{c,L} = \Delta\phi_{c,0} + 5.8^o/\text{MeV}\ \Delta W_{c,0} \tag{8.4}$$

The bunch rotator will only change the energy offset of the bunch centre according to Eq. (8.3). Using the above Eq. (8.3) and (8.4), the centre offset after bunch rotation can be calculated for any initial configuration.

From numerical simulations it is known that, with 99.7% probability, the bunch centre offset lays within an ellipse with semiaxes $\Delta\phi_{c,0}{}^{max} = 4^o$ and $\Delta W_{c,0}{}^{max} = 3$ MeV (see Chapter 6.1). Two examples have been considered.

Example #1: with an energy offset $\Delta W_{c,0} = 3$ MeV of the beam centre at the linac end (no phase offset), one has at the output of the transfer line, after bunch rotation:

$\Delta\phi_{c,f} = \Delta\phi_{c,0} + f_L \Delta W_{c,0} = 5.8^o/\text{MeV} \times 3\,\text{MeV} = 17.4^o$

$\Delta W_{c,f} = \Delta W_{c,0} - e U_o \Delta\phi_{c,L} = 3\,\text{MeV} - 11.2\,\text{MeV} \times 17.4^o \times (2\pi/180^o) = -0.6\,\text{MeV}$

Example #2: with a phase offset $\Delta\phi_{c,0} = 4^o$ of the beam centre at the linac end (no energy offset), one has at the output of the transfer line, after bunch rotation:

$\Delta\phi_{c,f} = \Delta\phi_{c,0} + f_L \Delta W_{c,0} = 4^o$

$\Delta W_{c,f} = \Delta W_{c,0} - e U_o \Delta\phi_{c,L} = -11.2\,\text{MeV} \times 4^o \times (2\pi/180^o) = -0.9\,\text{MeV}$

In Figure 8.6 the evolution of the 99.7% probability boundary (see Fig. 6.3) is plotted along the transfer line, i.e. these ellipses limit the region where the bunch centre will lay, with a 99.7% probability. It is interesting to observe that the energy offset of the bunch centre after rotation is always smaller than the required ± 2 MeV, even when starting from a larger one! This is due to the intrinsic properties of the rotation system.
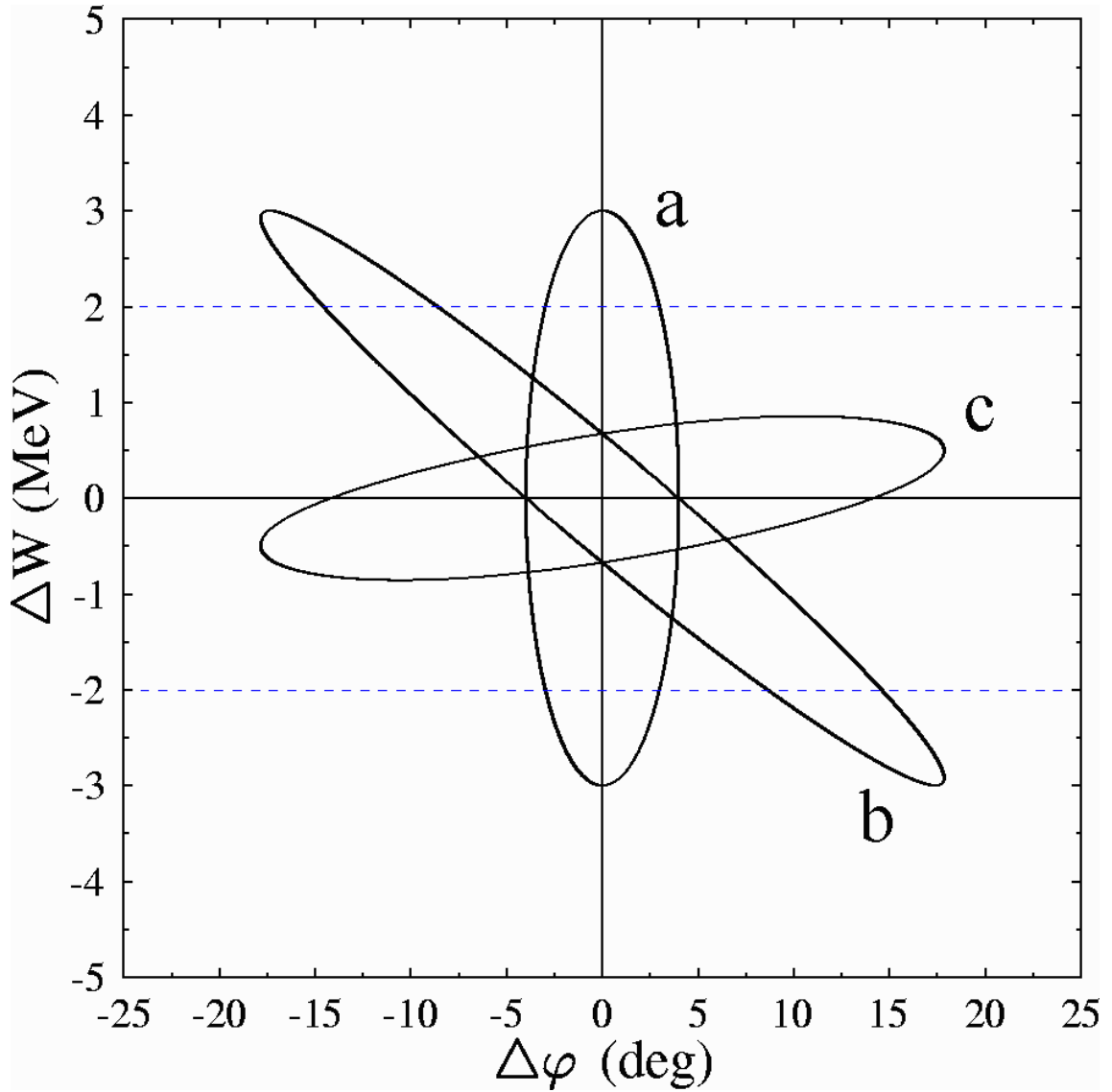
Figure 8.6: Quasi-analytical approach: maximum offset of the bunch centre at the end of the linac (a), at the end of the transfer line before rotation (b) and after linear voltage rotation (c).

Finally the beam ellipse is superposed to the phase-energy offset of the bunch centre, in order to calculate the rf error acceptance.

Eq. (8.1) is still used at the end of the linac, just substituting $(\Delta\phi_0+\Delta\phi_{c,0})$ to $\Delta\phi_0$, and $(\Delta W_0+\Delta W_{c,0})$ to ΔW_0. Eq. (8.2) is used at the output of the transfer line, with the substitution of $(\Delta\phi_L+\Delta\phi_{c,L})$ to $\Delta\phi_L$ and $(\Delta W_L+\Delta W_{c,L})$ to ΔW_L, and Eq. (8.3) after bunch rotation.

As examples, the two cases of a pure phase offset ($\Delta\phi_{c,0} = 4^\circ$) and a pure energy off-

set ($\Delta W_{c,0} = 3$ MeV) for the beam centre at the linac end are considered again. The longi-

tudinal beam ellipse for these two cases is shown in Figure 8.7; it always stays between
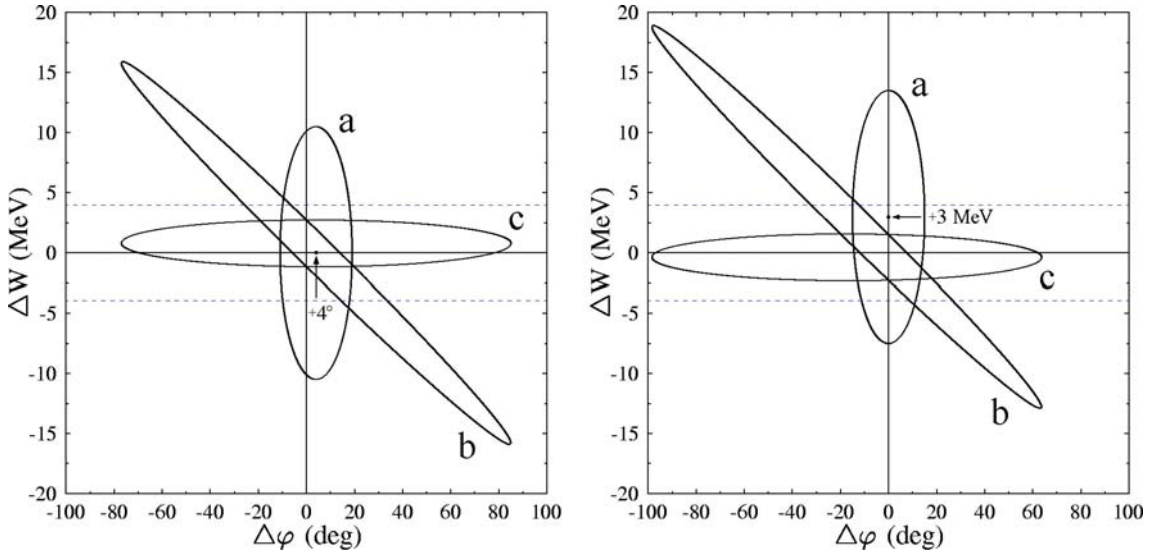
± 4 MeV after bunch rotation.

Figure 8.7: Quasi-analytical approach: output ellipse for an initial phase offset of $+4^\circ$ (left) and energy offset of $+3$ MeV (right) at the end of the linac (a), at the end of the transfer line before rotation (b), and after linear voltage bunch rotation (c).

For a more realistic simulation, a <u>nonlinear voltage</u> for the bunch rotation system was investigated. It was found that a quite good approximation of a linearly increasing voltage can be obtained using the first three odd harmonic components of the rf system, with an amplitude U_1 for the first one, $U_3 = -U_1/9$ for the second one and $U_5 = U_1/25$ for the third one; then the i-th macroparticle gets an energy variation:

$$\Delta W_i = qU_1 \sum_n (-1)^{n-1} (\sin{(2n-1)\phi_{n,i}}) / (2n-1)^2 \qquad \text{with } n = 1, 2, 3$$

and Eq. (8.3) should be substituted by:

$$\Delta W_f = \Delta W_L - 14.2 \text{ MeV} \times [\sin\Delta\phi_L - \sin(3\,\Delta\phi_L)/9 + \sin(5\,\Delta\phi_L)/25] \qquad (8.5)$$

As a further example, the effect of this 3-harmonic bunch rotator was tested for a combination of phase and energy offset ($\Delta\phi_{c,0} = 3^\circ$, $\Delta W_{c,0} = -2$ MeV) of the beam centre at the linac end. At first an analytical calculation was worked out, superposing the beam ellipse to the phase-energy offset of the bunch centre (see Fig. 8.8). Then a numerical simulation was made, starting from the output distribution of the nominal linac with 20% "mixed mode" mismatch (see Chapter 6.5) and adding artificially the above offset of the bunch centre. In this way a combination of the two main kinds of errors (statistic rf errors and mismatch) has been studied.

The results from MAPRO code, shown in Figure 8.9, look very similar to those from the analytical calculations and they show that, even in this case, the bunch stays within ± 4 MeV after bunch rotation.
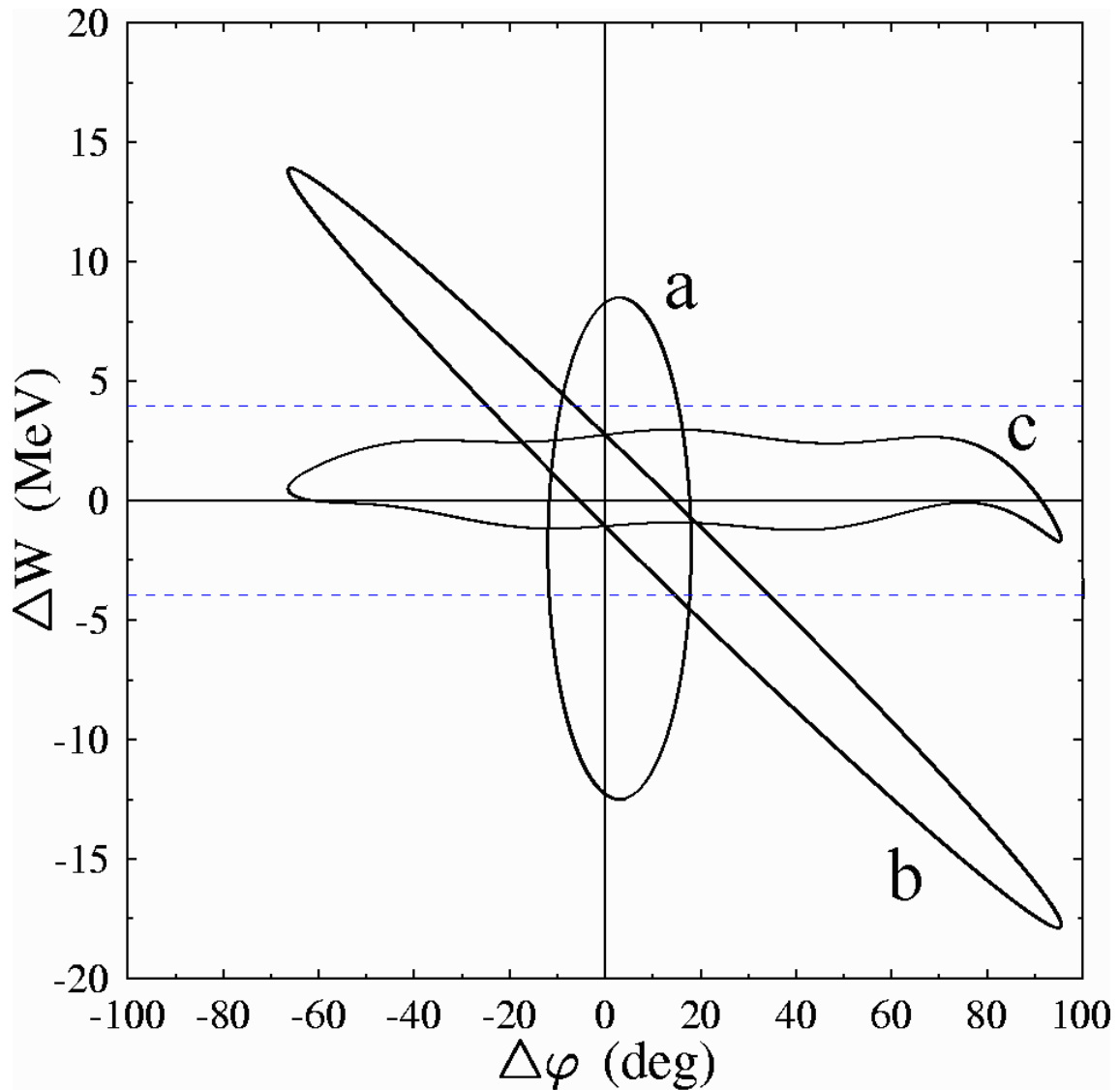
Figure 8.8: Quasi-analytical approach: output ellipse for an initial phase offset of $+3^\circ$ and energy offset of -2 MeV at the end of the linac (a), at the end of the transfer line before rotation (b), after rotation in a 3-harmonic system (c).
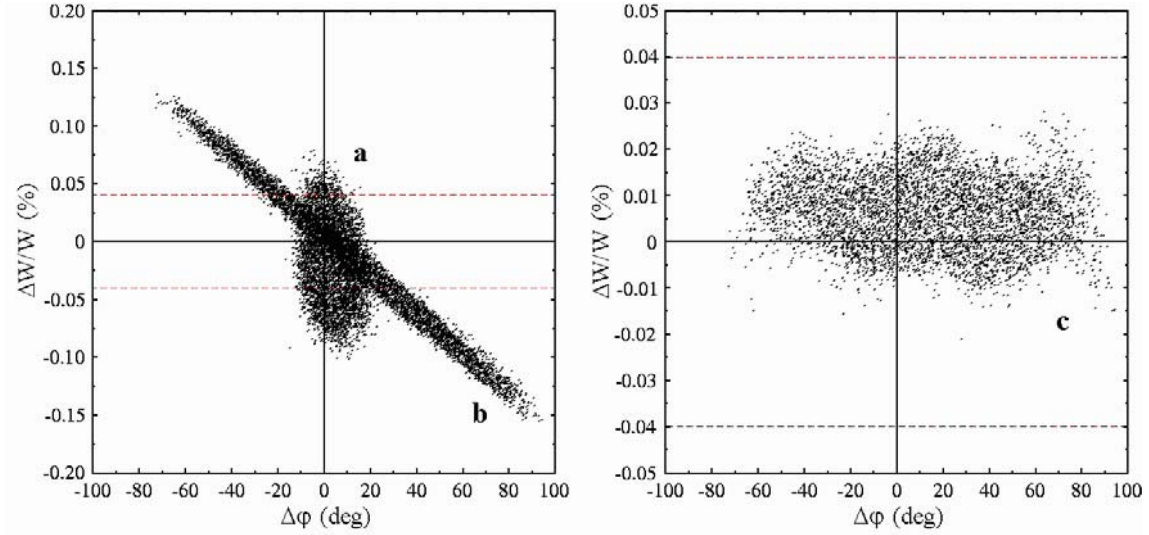
Figure 8.9: Output distribution of 5000 macroparticles for the nominal linac layout with 20% mixed mode mismatch and artificial bunch centre offset of $+3^\circ$ in phase and of -2 MeV in energy at the end of the linac (a), at the end of the transfer line before rotation (b), after rotation in a 3-harmonic system (c).

As a last example a numerical simulation was performed using as an input for the transfer line the output distribution obtained in Chapter 6.7 for the case of a 6-dim waterbag input for 20,000 macroparticles with rf errors; the calculations were continued up to a linear bunch rotator system. Results are shown in Figure 8.10.
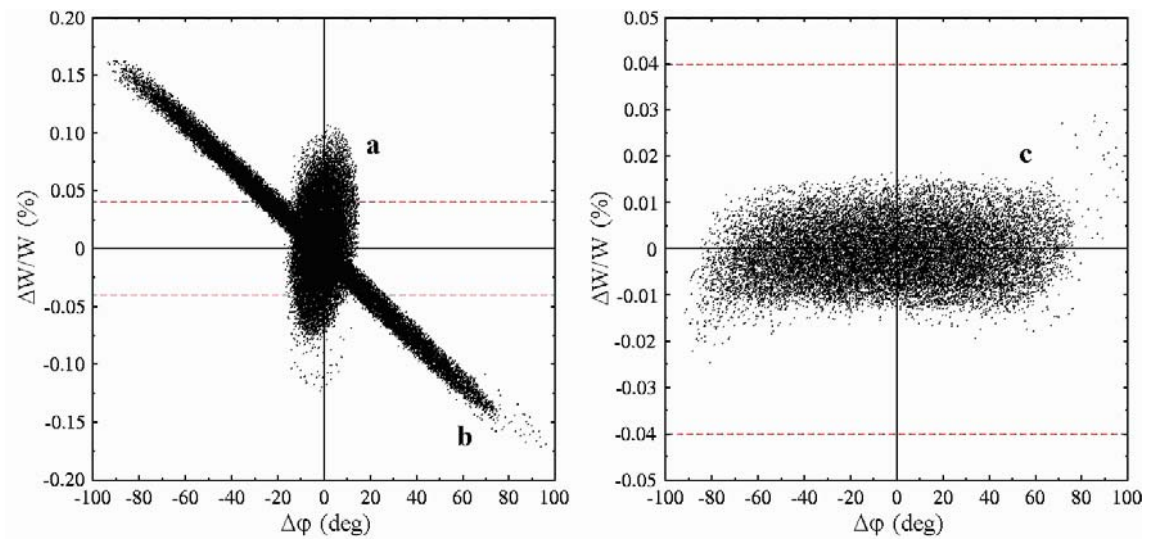
Figure 8.10: Output distribution of 20,000 macroparticles for the nominal linac layout with 6-dim waterbag input, 1% - 1° error in the rf field, at the end of the linac (a), at the end of the transfer line before rotation (b), after rotation in a linear system (c).

In this chapter it has been demonstrated that, even including uncorrelated phase and amplitude errors of the rf field and mismatch, all the particles lay in the requested range at ring injection.

A large energy offset of the bunch centre at the end of the linac will always be reduced after bunch rotation, at the expense of an increase of the phase offset; in the same way, a large phase offset will be reduced at the expense of an energy offset increase. When both energy and phase offset are present, the net effect is a smaller offset in energy and a larger one in phase.

The requirement on dp/p is then fulfilled, not only for the bunch centre, but for all particles, including those with a large phase difference, which adds up to the phase offset of the bunch centre. This is true even in the case of a nonlinear rotation voltage!

Notice however that the "reserve" in dp/p after bunch rotation for the error-free case is "eaten up" by statistical errors and mismatch.

CHAPTER 9

CONCLUSIONS AND OUTLOOK

The beam dynamics design for a high intensity heavy ion linac has been investigated and simultaneously tested in detail by numerical multi-particle calculations for the first time, in the framework of the HIDIF project.

The linac is a substantial component of the whole driver facility of an inertial fusion ignition facility; it has to provide a 400 mA, 10 GeV ^{209}Bi$^+$ beam with high beam quality for injection into the storage rings. It could be demonstrated that a 200 MHz drift tube linac of the Alvarez type, which is the "working horse" in nearly all big accelerator centres, is also a good possible solution for a fusion driver linac from the point of view of particle dynamics.

For this purpose the linac design was made in parallel with numerical simulations of the beam dynamics, allowing a proper choice of the accelerator parameters taking into account the HIDIF project requirements.

In spite of the high beam current, the proposed layout is not space-charge dominated, which turned out to be a big advantage in terms of emittance growth and halo formation.

In the ideal (i.e. error-free) case the emittance growth of the beam during acceleration is small and there is nearly no halo development. Therefore the input emittances ($\beta\gamma\varepsilon_{full} = 1.05 \ \pi$ mm mrad transversely, $\varepsilon_{full} = 100 \ \pi$ deg MeV longitudinally) could be chosen close to the allowed maximum output emittances, determined by the requirements for proper ring injection ($\beta\gamma\varepsilon_{full} = 1.26 \ \pi$ mm mrad, $dp/p < 10^{-4}$). In this way some space is left for probable emittance growth in the front-end part of the injector: assuming a transverse normalized input emittance of 0.15 π mm mrad at the first RFQ, a factor of about 8 can be tolerated, as long as the beam is not filamented in large parts.

Introducing statistically distributed errors of rf field amplitudes ($\pm 1\%$) and phases ($\pm 1^o$) into the calculations, the beam behaviour along the linac was very stable, resulting

in small oscillations of a well-confined bunch around its equilibrium position. Although a displaced beam in phase or energy will cover a larger longitudinal phase space area than the ideal beam at the linac output, this plays only a small role for ring injection, since the debunching and rotation system will reduce this effect.

A more severe restriction is the adjustment of the large amount of quadrupoles in the drift tubes and the stability of their fields: owing to this large number, the gradient errors should not exceed the quite small error of ±0.2%. If getting such a tolerance turned out to be problematic and a conventional error of ±1% has to be assumed, then some way to rematch the beam has to be foreseen in a few positions along the linac.

The influence on particle dynamics of beam current fluctuations up to ±10% is negligible. The effect of different input distributions, having a larger ratio full-to-rms emittance, is also marginal, as long as the beam is matched and the equivalent rms emittances are considered.

In the investigations of the behaviour of mismatched beams the model for a periodic focusing channel could be applied to the linac, due to the small acceleration rate: the predicted eigenmodes were identified with very good agreement. The beam behaviour changes only slightly for mismatch factors up to 20%, but some higher emittance growth (up to 15%) and in some cases halo development were observed; the longitudinal plane is especially affected. It is therefore recommended that the initial mismatch should not exceed ±10% for each of the three eigenmodes. Otherwise, a smaller rms emittance would be required at the input of the linac (and upstream in the funnel section) in order to allow this larger growth.

Off-axis mismatch leads again to stable oscillations around the axis: the beam is well confined, as long as the initial displacement is not too large. Nevertheless, the displaced beam in transverse position will cover a larger phase space area at the linac output; if such oscillations cannot be corrected, e.g. by steering mechanisms, the tolerances must be kept smaller than the 3 mm off-axis displacement which was assumed in the calculations.

In the error-free case the beam radius is about one half of the assumed bore radius of 16 mm. For the reasonable size of the errors discussed above, the outermost particles of the beam (which define the full beam radius) are never at a distance from the axis larger than 12 mm, as a maximum.

The modifications to the geometry and to the fields needed for "telescoping" have been investigated. This option still presents big technical problems and gives poor results in terms of beam behaviour, both for the nominal (±10%) and for a smaller (±5%) mass difference. This feature of the HIDIF project should be therefore further investigated, as no practical solution could be found up to now.

A transfer line between the DTL and the rings is needed to "debunch" the beam and "rotate" the bunch longitudinally in order to reduce its momentum spread. Analytical calculations and beam tracking have been made for the transport and the rotation part, demonstrating that it is possible to have all the particles inside the small required $dp/p = \pm 0.02\%$, even in presence of errors.

The calculations have been carried out with a maximum number of 20,000 macroparticles, due to the limited computational power available. In all the cases, even with combined effects of different errors and using the maximum allowed number of macroparticles, no losses occurred; this means that loss rates $< 5 \times 10^{-5}$ have been obtained.

For an ignition facility (low duty cycle) these results can be considered as a reliable guideline for the particle dynamics layout of such a high intensity linac: the amplitudes of the rf electric field and of the magnetic field in the quadrupoles are in fact reasonable, and the shunt impedance is good enough to give the overall linac efficiency necessary for HIDIF. Nevertheless, due e.g. to the long linac length and to the large number of drift tubes, the technical realization of this conventional Alvarez DTL remains an open problem, even if particle dynamics calculations indicate that it is feasible.

For an energy production facility a much higher average and peak beam power are discussed, with currents up to 600 mA and repetition rates of 10 to 30 Hz. In this case activation is a very strong concern and the tolerances will be much tighter: the loss rate should be kept smaller than 10^{-7}/m and at least one million or more macroparticles are necessary for numerical simulations. Moreover, for a final check of possible halo development, realistic emittances and distributions, including filamentation effects from the injector part, have to be used as an input to the main linac. But the results of this study for the ignition facility have already shown that an Alvarez type DTL could be a solution also in this case.

ACKNOWLEDGEMENTS

BIBLIOGRAPHY

[Acc98]   "AccApp'98 - 2nd International Topical Meeting on Nuclear Applications of Accelerator Technology", Gatlinburg, TN, USA, 20-23 September 1998, published by the American Nuclear Society.

[Alf39]   H. Alfvén: "On the Motion of Cosmic Rays in Interstellar Space", in: *Phys. Rev.*, <u>55</u> (1939), p. 425-429.

[Alv46]   L. Alvarez: "The design of a proton linear accelerator", in: *Phys. Rev.,* <u>70</u> (1946), p. 799-800.

[APT]   "Accelerator Production of Tritium Conceptual Design Report", Los Alamos National Lab. report LA-UR-97-1329, 15 April 1997, and [Acc98].

[ATW]   "Accelerator-Driven Transmutation of Waste (ADTW): Technical Review at MIT", Los Alamos National Lab. technical report LA-UR-98-608 (1998).

[Bad81]   R. Badger *et al.*: "HIBALL - A Conceptual Heavy Ion Beam Driven Fusion Reactor Study", KFK 3203, Karlsruhe, Germany and UWFDM-450 (1981).

[Bas97]   M. Basko, K.-J. Lutz, J. Maruhn, "On possible target design for a heavy ion ignition facility", in: *Nucl. Instr. & Meth. in Phys. Res. A,* Vol. 415/1-2 (1998), p. 85-92.

[Bnd93]   B.I. Bondarev, A.P. Durkin, B.P. Murin: "Halo Production in Charge-Dominated Beams Single-Particle Interactions", Moscow Radiotechnical Institute report to Los Alamos National Lab., 15 September 1993.

[Bnd94]   B.I. Bondarev, A.P. Durkin, B.P. Murin, R.A. Jameson: "Emittance Growth and Halo Formation in Charge-Dominated Beams", in: *Proc. 1994 Int. Conf. on Accelerator-Driven Transmutation Technologies and Applications*, 25-29 July 1994, Las Vegas, Nevada, LA-UR-94-2753, Los Alamos National Lab.

[Bon81]   K. Bongardt, D. Sanitz: "Funnelling of Heavy Ion Beams", KFK 3203, Karlsruhe, Germany and UWFDM-450 (1981).

[Bon93]   K. Bongardt: "Matching Problems between Linac and Compressor Ring", in: *Proc. of the 12th ICANS Meeting*, 24-28 May 1993, Abingdon, UK, RAL Rep. 94-025, p. A-115-123.

[Bon96]   K. Bongardt, M. Pabst, A.P. Letchford, V.G. Vaccaro, L. Verolino: "Filamentation effects and image charges in high β proton transfer lines", in: *Proc. of the 5th European Particle Acc. Conf., EPAC'96*, 10-14 June 1996, Sitges (Barcelona), Spain,   p. 1224-1226.

[Bon98]   K. Bongardt, M. Pabst, A.P. Letchford: "Halo Formation by Mismatch for the High Intensity Bunched Beams", in: *Proc. of the 19th Int. Linac Conf., LINAC'98*, 23-28 August 1998, Chicago, IL, p. 824-826.

[Bon98b]   K. Bongardt, R.W. Müller: "Linac Power Efficiency", in: [Hof98], p.69-72.

[Bon98c]   K. Bongardt, FZ Jülich, private communication.

[Con91]   M. Conte, W.W. McKay: *An Introduction to the Physics of Particle Accelerators*, Singapore: Singapore World Scientific, 1991.

[Cou58]   E.D. Courant, H.S. Snyder: "Theory of the Alternating-Gradient Synchrotron", in: *Annals of Physics* <u>3</u> (1958), p. 1-48.

[Dei96]   H. Deitinghoff, M. Pabst, **G. Parisi**, A. Sauer: "Beam Dynamics Calculations for the Acceleration of Different Ions in a Heavy Ion Linac", in: *Proc. of the 18th Int. Linac Conf., LINAC'96*, 26-30 August 1996, Geneva, Switzerland, p. 62-64.

[Dei97]   H. Deitinghoff, **G. Parisi**: "Particle Dynamics in a Heavy Ion DTL", in: *High Energy Density in Matter Produced by Heavy Ion Beams - Annual Report 1996*, GSI-97-08, Darmstadt, Germany, June 1997, p. 42.

[Dei97b] H. Deitinghoff, **G. Parisi**: "Considerations on Particle Dynamics in a Heavy Ion DTL", in: *Proc. of 1997 Particle Acc. Conf., PAC'97*, 12-16 May 1997, Vancouver, B.C., Canada, p. 1900-1901.

[Dei98]   H. Deitinghoff, H. Klein, **G. Parisi**, K. Bongardt, M. Pabst: "Beam Dynamics in an Alvarez Heavy Ion DTL", in: [Hof98], p. 46-53.

[Dei98b] H. Deitinghoff, **G. Parisi**, K. Bongardt, M. Pabst: "Particle Dynamics in a Heavy Ion DTL for HIDIF", in: *High Energy Density in Matter Produced by Heavy Ion Beams - Annual Report 1998*, GSI-99-04, Darmstadt, Germany, May 1999, p. 35.

[Dei98c] H. Deitinghoff, **G. Parisi**, K. Bongardt, M. Pabst: "Effect of Statistical Errors on Particle Dynamics in a Heavy Ion DTL for HIDIF", in: *High Energy Density in Matter Produced by Heavy Ion Beams - Annual Report 1998*, GSI-99-04, Darmstadt, Germany, May 1999, p. 36.

[Dei98d] H. Deitinghoff, **G. Parisi**, K. Bongardt, M. Pabst: "Particle Dynamics in the HIDIF Transfer Line between DTL and Rings", in: *High Energy Density in Matter Produced by Heavy Ion Beams - Annual Report 1998*, GSI-99-04, Darmstadt, Germany, May 1999, p. 37.

[Dei98e] H. Deitinghoff, **G. Parisi**, K. Bongardt, M. Pabst: "Effect of Mismatch on Particle Dynamics in a Heavy Ion DTL for HIDIF ", in: *High Energy Density in Matter Produced by Heavy Ion Beams - Annual Report 1998*, GSI-99-04, Darmstadt, Germany, May 1999, p. 38.

[ESS]   "ESS - A Next Generation Neutron Source for Europe. Volume III, The ESS Technical Study", ESS-96-53-M, November 1996, and [Acc98].

[Glu70]   R.L. Gluckstern: "Oscillation Modes in Two-dimensional Beams", in: *Proc. of the 1970 Proton Linac Conf.*, Fermi National Acc. Lab., Batavia, IL, 1970, Vol. 2,   p. 811-822.

[Hof81]   I. Hofmann, in: *IEEE Trans. Nucl. Sci*. NS-28 (1981), p. 2399.

[Hof82]   I. Hofmann: *Lecture Notes on High-Current Beam Dynamics*, INS-NUMA-45, Univ. of Tokyo, Japan, December 1982.

[Hof96]   I. Hofmann: "Inertial Fusion with Accelerators", in: *Proc. of the 5th European Particle Acc. Conf., EPAC'96*, 10-14 June 1996, Sitges (Barcelona), Spain, p. 255-259.

[Hof97]   I. Hofmann: "HIDIF - An approach to high repetition rate inertial fusion with heavy ions", 12th Int. Symp. on Heavy Ion Inertial Fusion, HIIF 97, 24-27 September 1997, Heidelberg, Germany, in: *Nucl. Instr. & Meth. in Phys. Res. Sect. A*, Vol. 415/1-2 (1998), p. 11-19.

[Hof98]   I. Hofmann, G. Plass (Ed.): *The HIDIF Study - Report of the European Study Group on Heavy Ion Driven Inertial Fusion for the period 1995-1998*, GSI-98-06 REP, Darmstadt, Germany, August 1998.

[IFM]   M. Martone (Ed.): *IFMIF, International Fusion Materials Irradiation Facility Conceptual Design Activity, Final Report*, ENEA Frascati report RT/ERG/FUS/96/11, Frascati, Italy, December 1996, and [Acc98].

[Jam81]   R.A. Jameson: "Beam intensity limitations in linear accelerators", in: *Proc. of the 1981 Particle Acc. Conf., PAC'81*, in: *IEEE Trans. Nucl. Sci,* Vol. NS-28, No. 3,   p. 2408.

[Jam94]   R.A. Jameson: "Self-consistent Beam Halo Studies & Halo Diagnostic Development in a Continuous Linear Focusing Channel", in: *AIP Proc. of the 1994 Joint US-CERN-Japan International School on Frontiers of Accelerator Technology*, Maui, Hawaii, 3-9 November 1994, p. 530-560 and LA-UR-94-3753, Los Alamos National Lab.

[Jun83]   P. Junior: "Space-Charge Limits in Heavy-Ion RFQ Linacs", in: *Part. Acc.,* 13 (1983), p. 231-247.

[Kap59]   I.M. Kapchinskij, V.V. Vladimirskij: "Limitations of proton beam current in a strong focusing linear accelerator associated with the beam space charge", in: *Proc. of the*

Int. Conf. on High Energy Accelerators, 14-19 September 1959, CERN, Geneva, Switzerland, p. 274-288.

[Kap70]   I.M. Kapchinskij, V.A. Teplyakov: "Linear Ion Accelerator with Spatially Homogeneous Strong Focusing", in: *Prib. i Tekhn. Eksp.,* 2 (1970), p. 12-20.

[Kap85]   I.M. Kapchinskij: *Theory of Resonance Linear Accelerators*, London: Harwood Academic Publisher, 1985.

[Kle68]   H.Klein: "Die Beschleunigung Schwerer Ionen mit der Wendelstruktur", Habilitation thesis, Frankfurt, 1968.

[Kos96]   D.G. Koshkarev, I.L. Korenev, L.A. Yudin: "Conceptual design of linac for power HIF driver", in: *Proc. of the 18th Int. Linac Conf., LINAC'96,* 26-30 August 1996, Geneva, Switzerland, p. 423-425.

[Lag96]   J.-M. Lagniel: "Halos and Chaos in Space-charge Dominated Beams", in: *Proc. of the 5th European Particle Acc. Conf., EPAC'96*, 10-14 June 1996, Sitges (Barcelona), Spain, p. 163-167.

[Lap71]   P.M. Lapostolle, in: *IEEE Trans. Nucl. Sci.,* NS-18 (1971), p. 1101.

[Lap87]   P. Lapostolle, "Introduction à la théorie des accélérateurs linéaires", CERN 87-09, Geneva, July 1987.

[Lap99]   P. Lapostolle, M. Weiss: "Formulae and Procedures useful for the Design of Linear Accelerators", CERN draft, to be published.

[Law58]   J.D. Lawson: "Perveance and the Bennett Pinch Relation in Partially Neutralized Electron Beams", in: *J. Electron. Control,* 5 (1958), p. 146-151.

[Law88]   J.D. Lawson, *The Physics of Charged-Particle Beams*, Oxford: Clarendon Press, 1988.

[Lut97]   K.J. Lutz, F. Illenberger, J.A. Maruhn, "Three-dimensional viewfactor simulations of an ignition scale target for heavy ion fusion", in: *Nucl. Instr. & Meth. in Phys. Res. A,* Vol. 415/1-2 (1998), p. 133-138.

[Mar68]   M. Martini, D.J. Warner: "Numerical Calculations of Linear Accelerator Cavities", CERN 68-11, Geneva, Switzerland, March 1968.

[Mar71]   M. Martini, M. Promé: "Computer Studies of Beam Dynamics in a Proton Linear Accelerator with Space Charge", in: *Part. Accel.,* 2 (1971), p. 289-299.

[Mit78]   K. Mittag: "On parameter optimisation for a linear accelerator", KFK-255, Karlsruhe, Germany, (1978).

[Oef97]   U. Oeftiger *et al*.: "Longitudinal particle dynamics in the HIDIF driver accelerator", 12th Int. Symp. on Heavy Ion Inertial Fusion, HIIF 97, 24-27 September 1997, Heidelberg, Germany, in: *Nucl. Instr. & Meth. in Phys. Res. A,* Vol. 415/1-2 (1998), p. 444-449.

[Pab96]   M. Pabst, K. Bongardt, A. Letchford: "Critical Beam Dynamical Issues in Neutron Spallation Source", ESS 96-38-L, Jülich, Germany, April 1996.

[Pab97]   M. Pabst, K. Bongardt: "Analytical Approximation of the Three Mismatch Modes for Bunched Beams", ESS 97-85-L, Jülich, Germany, August 1997.

[Pab97b] M. Pabst, K. Bongardt, A. Letchford: "Core and Halo Particle Dynamics of High Intensity Proton Beams", in: *Proc. of 1997 Particle Acc. Conf., PAC'97*, 12-16 May 1997, Vancouver, B.C., Canada, p. 1846-1848.

[Pab98]   M. Pabst, K. Bongardt, A. Letchford: "Progress on intense proton beam dynamics and halo formation", in: *Proc. of the 6th European Particle Acc. Conf., EPAC'98*, 22-26 June 1998, Stockholm, Sweden, p. 146-150.

[Par96]   **G. Parisi**: "Installation of CLAS, GENLIN, MAPRO on the IAP cluster and their application to the DESY linac", IAP Int.-Rep. 96-3, Frankfurt, Germany, April 1996.

[Par97]   **G. Parisi**, H. Deitinghoff, K. Bongardt, M. Pabst: "A heavy ion DTL design for HIDIF", 12th Int. Symp. on Heavy Ion Inertial Fusion, HIIF 97, 24-27 September 1997, Heidelberg, Germany, in: *Nucl. Instr. & Meth. in Phys. Res. Sect. A*, Vol. 415/1-2 (1998), p. 332-338.

[Par98]   **G. Parisi**, H. Deitinghoff, K. Bongardt, M. Pabst: "Error Effects and Parameter Analysis for a HIDIF DTL", in: *Proc. of the 6th European Particle Acc. Conf., EPAC'98*, 22-26 June 1998, Stockholm, Sweden, p. 1121-1123.

[Par98b]   **G. Parisi**, A. Sauer, H. Deitinghoff, H. Klein: "Parameter Study for a High Current Heavy Ion Linac", in: *Proc. of the 19th Int. Linac Conf., LINAC'98*, 23-28 August 1998, Chicago, IL, p. 79-81.

[Par99]   **G. Parisi**, H. Deitinghoff, K. Bongardt, M. Pabst: "Particle Dynamics in a DTL for High Intensity Heavy Ion Beams for Inertial Fusion", Workshop on space-charge dominated beam physics for heavy ion fusion, 10-12 December 1998, Saitama (Tokyo), Japan, in: Y.K. Batygin (Ed): *AIP Conf. Proc.* <u>480</u> (1999), p.158-172.

[Pic96]   N. Pichoff, G. Haouat, P.Y. Beauvais: "Halo Formation from Beam Coulomb Scattering on Residual Gas", in: *Proc. of the 5th European Particle Acc. Conf., EPAC'96*, 10-14 June 1996, Sitges (Barcelona), Spain, p. 1209-1211.

[Pla97]   G. Plass: "The status of the HIDIF study", 12th Int. Symp. on Heavy Ion Inertial Fusion, HIIF 97, 24-27 September 1997, Heidelberg, Germany, in: *Nucl. Instr. & Meth. in Phys. Res. Sect. A, Vol.* 415/1-2 (1998), p. 204-208.

[Poz98]   J. Pozimski, A. Jakob, H. Klein: "Investigations on Space Charge Neutralized Low Energy Beam Transport", in: [Hof98], p. 26-37.

[Pri98]   C.R. Prior: "HIDIF Horizontal-Vertical Multi-Turn Injection", in: [Hof98], p. 80-93.

[Pro71]   M. Promé, in: LA-TR-79-33, Los Alamos, 1979 (previously published as Ph.D. thesis, CEA-N-1457, 1971).

[Ram97]   R. Ramis *et al.*: "A 3 MJ optimized hohlraum target for heavy ion inertial confinement fusion", 12th Int. Symp. on Heavy Ion Inertial Fusion, HIIF 97, 24-27 September 1997, Heidelberg, Germany, in: *Nucl. Instr. & Meth. in Phys. Res. Sect. A, Vol.* 415/1-2 (1998), p. 93-97.

[Rat97]   U. Ratzinger, R. Tiede: "Status of the HIIF RF linac study based on H-mode cavities", 12th Int. Symp. on Heavy Ion Inertial Fusion, HIIF 97, 24-27 September 1997, Heidelberg, Germany, in: *Nucl. Instr. & Meth. in Phys. Res. Sect. A,* Vol. 415/1-2 (1998), p. 229-235.

[Rei78]   M. Reiser: "Periodic Focusing of Intense Beams", in: *Part. Acc.,* <u>8</u> (1978), p. 167-182.

[Rei81]   M. Reiser: "Current limits in linear accelerators", in: *J. Appl. Phys.*, <u>52</u>(2) (1981), p. 555-563.

[Rei91]   M. Reiser: "Free energy and emittance growth in nonstationary charged particle beams", in: *J. Appl. Phys.*, <u>70</u> (1991), p. 1919-1923.

[Rei94]   M. Reiser: *Theory and Design of Charged Particle Beams*, New York: J. Wiley & Sons, 1994.

[Sac71]   F.J. Sacherer: "RMS envelope equations with space charge", in: *IEEE Trans. Nucl. Sci.*, <u>NS-18</u> (1971), p. 1105, and CERN/SI/Int.DL/70-12, Geneva, Switzerland, November 1970.

[Sch97]   A. Schempp: "The injector for the HIDIF driver linac", 12th Int. Symp. on Heavy Ion Inertial Fusion, HIIF 97, 24-27 September 1997, Heidelberg, Germany, in: *Nucl. Instr. & Meth. in Phys. Res. Sect. A, Vol.* 415/1-2 (1998), p. 209-217.

[Sch98]   A. Schempp: "Design Issues of the Linac", in: [Hof98], p. 11-17.

[SNS]   "Spallation Neutron Source Conceptual Design Report", Oak Ridge National Lab. report SNS/CDR-2, Oak Ridge, TN, May 1997, and J.R. Alonso: "Status Report on the Spallation Neutron Source (SNS) Project", in: *Proc. of the 6th European Particle Acc. Conf., EPAC'98,* 22-26 June 1998, Stockholm, Sweden, p. 493-495.

[Sto96]   J.E. Stovall *et al.*, in *Proc. of the 18th Int. Linac Conf., LINAC'96*, 26-30 August 1996, Geneva, Switzerland, p. 680-691, 710-712, and LA-UR-96-2968.

[Str83]   J. Struckmeier, M. Reiser: "Theoretical Studies of Envelope Oscillations and Instabilities of Mismatched Intense Charged Particle Beams in Periodic Focusing Channels", GSI-83-11, Darmstadt, Germany, April 1983.

[Str88]   J. Struckmeier: "Bedienungsanleitung für das PARMILA Programm", GSI, Darmstadt, Germany, Januar 1988.

[Str96]   M. Stroetzel, P. Heeg, P. Strehl: "Induced radioactivity, required shielding", in: *Minutes of the 4th HIDIF Workshop*, 22-23 February 1996, GSI-Darmstadt, Germany.

[Sym1]   Proceedings of the *Symposium on Accelerator Aspects of Heavy Ion Fusion*, 29 March - 2 April 1981, GSI-82-8, Darmstadt, Germany.

[Sym2]   Proceedings of the *Int. Symposium on Heavy Ion Inertial Fusion*, 25-28 May 1993, Frascati, Italy, in: *Il Nuovo Cimento*, 106 A, Nr. 11 (1993), p. 1429-1755.

[Sym3]   Proceedings of *Int. Symposium on Heavy Ion Inertial Fusion*, 6-9 September 1995, Princeton, USA, in *Fusion Engineering and Design*, 32-33 (1996).

[Sym4]   Proceedings of *Space Charge in Linear Accelerators Workshop*, May 1978, LA-7265-C, Los Alamos Scientific Lab.

[Web97]   M. Weber *et al*.: "Development of a Bi^+ source for a heavy-ion-driven ignition facility", 12th Int. Symp. on Heavy Ion Inertial Fusion, HIIF 97, 24-27 September 1997, Heidelberg, Germany, in: *Nucl. Instr. & Meth. in Phys. Res. Sect. A,* Vol. 415/1-2 (1998), p. 339-344.

[Wid28]   R. Wideröe, in: *Archiv für Electrotechnik* 21 (1928), p. 387.

CURRICULUM VITAE

Name:		Giovanni Parisi
geboren am:	03. Mai '64	in Genua (Italien)
Eltern:		Santo Parisi[†], Elektriker Antonia Laquidara, Angestellte
Staatsangehörigkeit:		Italienisch
Schulbildung:	Okt. '70 - Jun. '75	Grundschule in Genua
	Okt. '75 - Jun. '78	Mittelschule in Genua
	Okt. '78 - Jun. '83	Naturwissenschaftliches Gymnasium in Genua
	Juli '83	Abitur
Studium:	Oktober '83	Beginn des Physikstudiums an der Universität Genua
	Dezember '88	Beginn der Diplomarbeit, Thema: "Aufbau der Magneten für den Elettra Synchrotron Booster"
	21. März '90	Diplom-Hauptprüfung
Wehrdienst:	Jul. '90 - Jun. '91	in Novara (Italien)
wiss. Tätigkeit:	Jul. '91 - Jul. '93	Anstellung als post-doc am Legnaro Landes-labor von INFN bei Padua (Italien)
	Sep. '93 - Dez. '95	Anstellung als Stipendiat am CERN in Genf (Schweiz)
	Feb. '96 - Nov. '96	Anstellung als wissenschaftlicher Mitarbeiter (TMR) am Institut für Angewandte Physik
Promotion:	Dezember '96	Beginn der Arbeiten zur vorliegenden Dissertation

Akademische Lehrer (Universität Genua und Frankfurt):

A. Blasi, G. Boato, A. Borsese, G. Caviglia, M. Conte, G. Gallinaro, E. Gamba,

V. Gracco, I. Hofmann, H. Klein, G. Luzzatto, M.G. Marinari, M. Marinelli, G. Morpurgo, P. Ottonello, G. Passatore, A. Schempp, S. Squarcia, V. Torre, U. Valbusa.